Petrology and Diagenesis of the Middle and Lower Santa Fe Group in the Northern Albuquerque Basin, New Mexico

by

John Michael Gillentine
New Mexico Institute of Mining and Technology
Socorro, New Mexico

Submitted in Partial Fulfillment of the Requirement for the Degree of Master of Science in Geology

January, 1996

ABSTRACT

Santa Fe Group sediments within the northern Albuquerque Basin mirror the basin's complex geologic setting and tectonic history, containing fragments of Precambrian plutonic and metamorphic rocks, Paleozoic and Mesozoic sedimentary rocks, and Cenozoic volcanic rocks shed from surrounding uplands. Sidewall-core samples of basin-fill deposits obtained from four Albuquerque municipal wells located in basin areas both west and east of the Rio Grande Valley classify as feldsarenite, lithic arkose or feldspathic litharenite. Differences in grain composition across the basin indicate dissimilar provenance. Plutonic and metamorphic sediments were probably derived from the northwest, whereas volcaniclastic sediments originated in the Jemez, Espinosa or Latir volcanic fields to the north. Abundant quartz (some grains with recycled overgrowths) in West Mesa cores were possibly derived from Cretaceous rocks that crop out to the west. Differences in the primary composition of cores were found not to control authigenesis because soluble detrital minerals are present in quantities more than adequate to provide the chemical species necessary for secondary mineral precipitation. Authigenic minerals are zeolite and calcite cements, and smectite or illite/smectite occurring as pore-fillings and alterations of framework aluminosilicates. Not all phases are present in all wells, and no systematic occurrence of any one phase is discernable in any given well. Changes in pore-water chemistry and mineral mass during the formation of the authigenic minerals were modeled using the program PHREEQE. Results of simulations using City of Albuquerque water quality data indicate that water at

the well head is not in equilibrium with authigenic minerals observed in thin section. Precipitation of individual model phases or combinations of phases required pore waters of distinctly different chemistry, suggesting the aquifer system is compartmentalized into discrete chemical zones. Available data does not allow definition of zone boundaries, but it is apparent from the sample set that they may be very small, perhaps on the order of cubic meters.

TABLE OF CONTENTS

Introduction 1

Geologic Setting 4
- Regional Tectonics 4
- Structural Style 4

Previous Work 7
- Stratigraphy and Stratigraphic Nomenclature 7
- Basin Evolution 10
- Basin-Fill Diagenesis 11

Methods 13
- Sampling Method 13
- Thin-Section Preparation 13
- Sandstone Petrography 14
  - Point-Count Parameters 14
  - Point-Count Error 15
- Scanning Electron Microscopy 15
- Electron Microprobe Analysis 16
- X-Ray Diffraction Analyses 17
- Cathodoluminescence Microscopy 18

Sandstone Petrology 19
- Primary Composition 19
  - Quartz 19
  - Feldspar 21
  - Little Fragments 22
  - Allogenic Clay 25

Diagenesis 27
- Authigenic Composition 27
  - Smectite, Illite, and Interlayed Illite/Smectite 27
  - Kaolinite 30
  - Zeolites 31
  - Calcite 34
- Core Depth and Secondary Mineralization 35
- Influence of Primary Mineralogy and Sedimentary Textures 37
- Porosity and Framework Grain Dissolution 41
- Compaction 49

Lithofacies and Indicators of Provenance 53

Geochemical Modeling 60
Methods 60
Results 61
Charles Wells 6 62
Cerro Colorado 1 63
Soil Amendment Facility 1 64
Discussion of Modeling Results 64

Conclusions 69
Provenance 69
Dissolution 70
Cementation and Alteration 70

References 72

Appendix A A-1
Definitions of Counted and Recalculated Parameters A-1
Table A-1: Counted and Recalculated Parameters A-2
Table A-2: Visual Estimates of Grain Size and Sorting A-6

Appendix B B-1
Definition of Porosity Terms B-1
Table B-1a: Porosity Distribution within CC1 ..... B-3
Table B-1b: Porosity Distribution within CW5 ..... B-4
Table B-1c: Porosity Distribution within CW6 ..... B-5
Table B-1d: Porosity Distribution within SAF1 ..... B-6
Table B-2a: Host Mineralogy of Intragranular Pore Space: individual wells .. B-7
Table B-2b: Host Mineralogy of Intragranular Pore Space: all wells B-11

Appendix C C-1
Abundance and Distribution of Authigenic Mineral Cements C-1

Appendix D D-1
Table D-1: Microprobe Results for representative feldspars D-1
Table D-2: Microprobe Results for representative clays D-5

LIST OF TABLES

Table 1. Correlation coefficients calculated for authigenic mineral abundance and primary sedimentologic parameters 40

Table 2. Average skeletal grain content (all mineralogies for each well; percent of 300 point counts 45

Table 3. Pore fluid composition and saturation state in the K_2O-Na_2O-CaO system: results of geochemical simulation using PHREEQE (Parkhurst et al., 1993) and a pure-water starting composition 50

Table 4. Pore-fluid composition, saturation state and mineral mass transfer in the K_2O-Na_2O-CaO system upon equilibration with authigenic mineral phases: results of geochemical simulation using PHREEQE (Parkhurst et al., 1993) and water quality data supplied by Albuquerque Water Utilities Division. 67

LIST OF FIGURES

Figure 1. Index map of Albuquerque Basin 2

Figure 2. Ternary diagram of detrital modes 20

Figure 3. Mineral cements by depth of occurrence 36

Figure 4. Mineral cement assemblages by texture of host 39

Figure 5. Macroporosity of core samples by core depth 42

Figure 6. Secondary porosity of core samples by core depth 43

Figure 7. Minus-cement porosity and total cement 50

Figure 8. Relative abundance of framework grains by core depth: CC1 56

Figure 9. Relative abundance of framework grains by core depth: SAF 57

Figure 10. Relative abundance of framework grains by core depth: CW5 58

Figure 11. Relative abundance of framework grains by core depth: CW6 59

LIST OF PLATES

Plate 1. Thin-section and SEM photomicrographs of core samples from CW6 81

Plate 2. Thin-section and SEM photomicrographs of core samples from CW5 83

Plate 3. Thin-section and SEM photomicrographs of core samples from CC1 and SAF1 85

Plate 4. Thin-section and SEM photomicrographs of core samples from CW5, CW6 and SAF1 87

INTRODUCTION

Recent concern over the quality and long-term availability of groundwater within the Albuquerque Basin, and the growing realization that groundwater resources within Bernalillo County are more limited than previously thought, has sparked interest for new research into the character of Santa Fe Group deposits that comprise the aquifer (Thorn, et al., 1993; Kernodle et al., 1995; Hawley and Haase, 1992; Hawley et al., 1995). As shallower aquifer zones in the Albuquerque-Rio Rancho Metropolitan area are depleted, progressively deeper groundwater reserves will be developed, where factors controlling transmissivity, conductivity and water quality are less well understood.

This study expands on earlier work characterizing the hydrogeologic framework of the northern Albuquerque Basin (Section IV in Hawley and Haase, 1992) by exploring in greater detail the sedimentary petrology and diagenesis of aquifer zones in the Middle and Lower Santa Fe Hydrostratigraphic Units (MSF and LSF). The approach was to examine the primary and secondary mineralogical components of basin fill, and from the results of this examination infer the geochemical environment that would account for the observed alterations. Data for the study were obtained from sidewall core samples of four Albuquerque municipal wells located in both the West Mesa (Llano de Alburquerque) and East Mesa (NE Heights) areas of the basin (Figure 1). Specific questions addressed in this study are:

1. Can systematic changes in the physical or chemical character of sediments be recognized in progressively older deposits penetrated by deep wells?

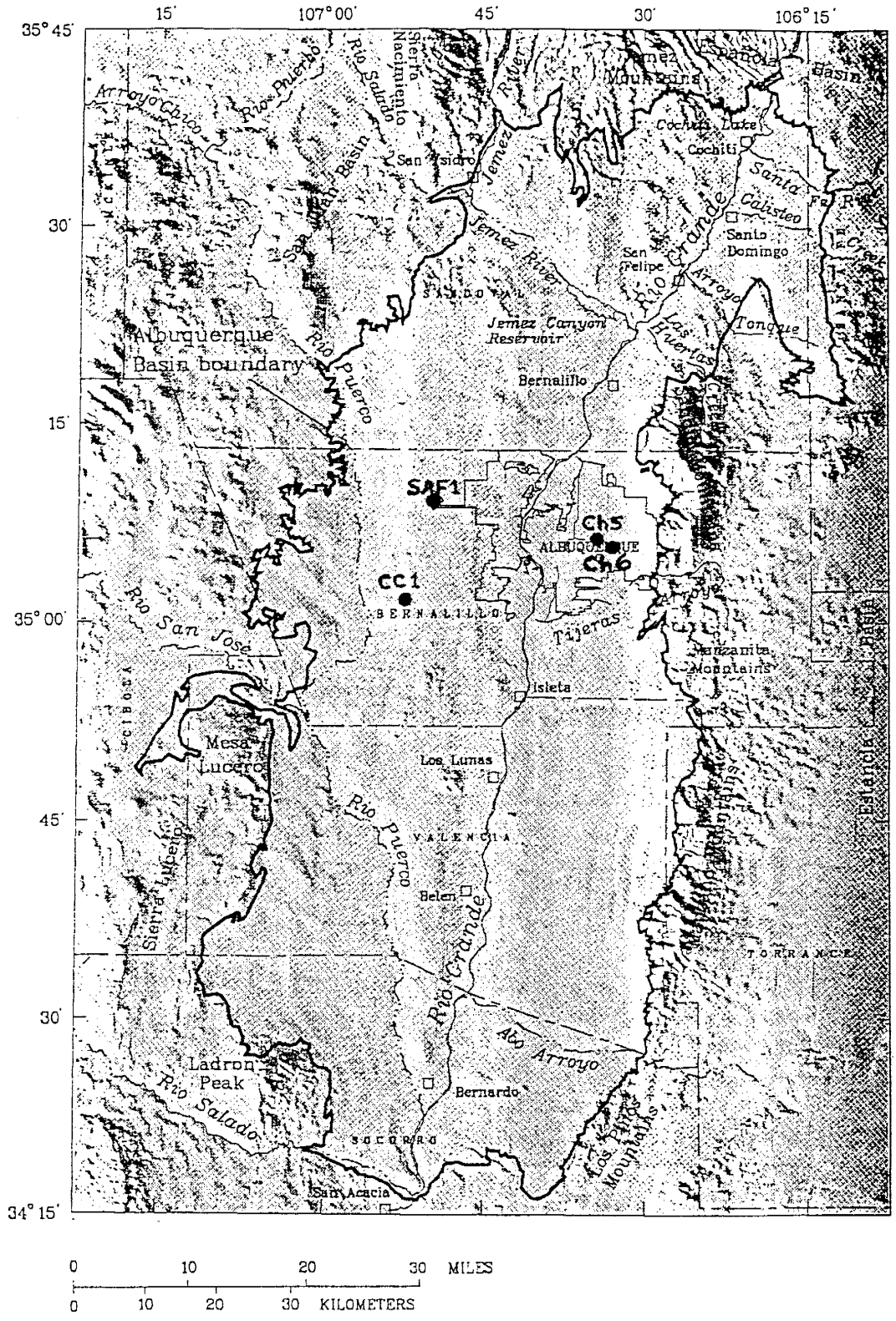

Figure 1. Index map of Albuquerque Basin area showing location of Albuquerque Municipal Wells: Charles Wells 5 and 6 (Ch5 & 6), Cerro Colorado 1 (CC1) and Soil Amendment Facility 1 (SAF1). Shaded-relief map base from Thorn et al. (1993, Fig. 13)

2. Can distinct diagenetic zones or facies be identified that represent differing chemical conditions in various depth and stratigraphic intervals?

3. Is authigenesis linked to primary mineralogy and depositional fabric (lithofacies), to an evolving pore-fluid chemistry, or both?

Diagenesis refers to the collective physical and chemical changes in sediments as they are progressively buried by younger deposits. Its impact on Albuquerque Basin groundwater resources comes about not only through alterations to the original mineralogical composition of the Santa Fe Group basin fill, but through modifications to the porosity and permeability of these sediments as well. Chemical reactions between groundwater and aquifer minerals result in the release of certain ionic species into solution, and the fixing by precipitation of certain other species into secondary or authigenic minerals.

GEOLOGIC SETTING

Regional Tectonics

The Rio Grande rift extends for nearly 600 miles (1000 km) from Leadville, Colorado, to Chihuahua, Mexico, and shares scale and geophysical characteristics with such systems as the Rhinegraben and East African rifts (Olsen et al., 1987; Ingersoll et al., 1990). The northern portion of the north-south trending rift consists of four linked axial basins: the upper Arkansas, San Luis, Espanola and Albuquerque Basins from north to south, respectively. The rift bifurcates near Socorro, New Mexico and widens toward the south into smaller, sub-parallel basins in basin-and-range style extension (Chapin, 1988).

Located within the central part of the rift zone, the Albuquerque Basin is physiographically distinct from adjacent basins because of its scale. It covers an area of approximately 4250 square miles (Kelley, 1977), and has structural blocks vertically offset by as much as 35,000 ft. (May and Russel, 1994). The basin is bounded on the east by the Sandia, Manzano and Los Pinos uplifts and on the west and northwest by the Lucero and Nacimiento uplifts.

Structural Style

Geological and geophysical investigations of the deep subsurface, (including oil and gas exploration wells, gravity surveys, and seismic profiling) have shown that the internal geometry of the basin consists of at least two groups of down-faulted basins

(grabens) dominated by an eastward-dipping half-graben complex north of the Tijeras (transverse) structural trend, and a westward-dipping half-graben to the south (Lozinsky, 1994; Russell and Snelson, 1994; Hawley et al., 1995). This style of linked half-graben architecture, where the polarity of down-dropped margins alternates along the length of the rift, is typical of Rio Grande basins (Chapin, 1988), as well as of other continental rifts systems worldwide (e.g., Rosendahl et al., 1986). Structural linkages between parallel, right-stepping rift segments are thought to occur at transfer, or accommodation zones of nested fault systems that conserve the regional extensional strain, and "accommodate" changes in graben polarity (Rosendahl et al., 1986). Alternatively, rift segments may be linked by offset, or "dogleg" segments that propagate in a direction oblique to the regional extensional direction (Nelson et al., 1992). According to these workers, rift-offsets are characterized by a bimodal fault pattern, with a dip-slip component in the normal segment and an oblique-slip component in the offset segment. Non-plane strain in Albuquerque Basin offsets may have resulted in lesser dip-slip displacement relative to the normal, north-south trending basin segments, and produced inter-graben structural saddles that separate the Santo Domingo, Central Albuquerque, and Belen subbasins. Differential displacement would coincide with significant rotation of structural blocks (Nelson et al., 1992). The length of subbasin segments and the position of rift-segment joins are thought to be inherited from pre-existing (Laramide to Precambrian), northeast-trending lineaments (Chapin and Cather, 1994).

The asymmetric geometry of the Albuquerque Basin has exerted an important influence on diagenesis by controlling the distribution of sedimentary facies within the

basin. Geometry controls not only the original composition of the basin-fill by determining clastic input from various source-terranes, but also has a significant influence on sediment transport energy and burial rate, sedimentary texture and degree of compaction (Allen and Allen, 1990).

Evidence for the timing of rift initiation comes from (1) radiometric ages of basalts, basaltic andesites and dacites interbedded with basal coarse clastics of the Popotosa Formation (Bachman and Mehnert, 1978; Osburn and Chapin, 1983), (2) ages of rift-related dike intrusions (Aldrich et al., 1986; Henry and Price, 1986), and (3) ages of the youngest mid-Tertiary ignimbrites of the northwest Mogollon-Datil volcanic field that sheeted across the pre-rift topography near Lemitar, New Mexico (Chamberlin, 1983; Osburn and Chapin, 1983; McIntosh et al., 1986). The combined evidence points toward a 28-27 Ma. age for the onset of rifting, which is supported by the shift in regional magmatism from intermediate, caldera-related lavas to predominantly basaltic, rift-related lavas by 26-24 Ma. (Dungan et al., 1989).

PREVIOUS WORK

Stratigraphy And Stratigraphic Nomenclature

Excellent summaries of previous stratigraphic work are given by Spiegel and Baldwin (1963), Galusha and Blick (1971), Kelley (1977) and Tedford (1982). The original term used by Hayden (1869) to describe the unconsolidated alluvium near the City of Santa Fe was "Santa Fe marls." This was modified to "Santa Fe Formation" by Darton (1922), who surveyed the region in a very general way during a statewide reconnaissance into the oil and gas and economic minerals potential of New Mexico. He mapped the entire Albuquerque Basin as QT -- alluvium (Recent) and Santa Fe Formation (Miocene and Pliocene), reporting an average thickness of the Santa Fe as ±450 ft. Although it was generally understood that the "Santa Fe Formation" comprised most of the unconsolidated deposits within the Rio Grande Depression from Colorado to Texas (Bryan, 1938), no formal type locality or unit subdivisions were specified until Denny (1940) published a map of the Pojoaque-Nambe area north of Santa Fe. He limited the Santa Fe Formation to "those deformed and predominantly fluviatile deposits of the Santa Fe region that contain the [mammalian] vertebrate fauna" (p.680); he placed the Santa Fe in the mid-Miocene to upper Pliocene.

In the Albuquerque area, some of the earliest detailed work was done by Bryan and McCann (1937, 1938), who preserved the definition of the Santa Fe as a regional unit, but recognized also the individuality of adjacent structural basins along the length of the rift. Despite discontinuity of outcrop, shifts in provenance and fragmentary fossil

evidence, they were able to trace the Santa Fe Formation from Hayden's generalized type locality into the northwest Albuquerque Basin on the basis of similar faunal ages and depositional style between basins. Bryan and McCann (1937) informally named three sandstone members along the north-west flank of the Llano de Albuquerque (i.e., Ceja Mesa), the lower gray, middle red, and upper buff, that underlie Pleistocene pediment and terrace gravels (the "Ortiz gravels" first described by Ogilvie, 1905). However, this broad, three-fold subdivision has not been adopted by all workers. Galusha (1966) formally introduced the Zia Sand Formation, which is roughly equivalent to the lower gray member of Bryan and McCann, but placed it below the Santa Fe Formation. Galusha and Blick (1971) stated that the three divisions are "not applicable to beds of the type area of the Santa Fe Group." Bailey et al. (1969) also departed from the three-member subdivision, describing and naming the Cochiti Formation in the southeastern Jemez Mountains. This unit, consisting of volcanic detritus derived from the Keres Group, was mapped to where it grades into coarse red granitic sands beneath Santa Ana Mesa. They narrowly defined the Santa Fe Formation, bounding it below by the Zia Sand Formation of Galusha (1966), and above by the Cochiti Formation. The fact that the Cochiti grades into beds of the Santa Fe Formation and is time-equivalent to the Santa Fe led Kelley (1977) to assert that it is equivalent to the middle red member and thus only a facies of the Santa Fe.

Kottlowski (1953) first proposed raising the Santa Fe to group status, a practice followed by Spiegel and Baldwin (1963), who used the term "Santa Fe Group" to describe a section of basin fill that included basal "mid Miocene (?)" volcanic flows and

"Pleistocene (?)" Ortiz gravels. They subdivided the basin-fill of the La Cienega-Seton Village area near Santa Fe into the Tesuque and Ancha Formations, and extended the Santa Fe Group to include areas adjacent to, but outside of the Rio Grande trough itself. Galusha and Blick (1971) originally suggested restricting the use of the term Santa Fe Group to the Espanola Basin type-locality, but subsequent workers have tended to use the much broader stratigraphic concept formally introduced by Bryan in 1938 (Hawley, 1978; Tedford, 1981; Chapin, 1988).

In a comprehensive study of the Albuquerque Basin, Kelley (1977) did not subscribe to group status for the Santa Fe, believing that mappable units were too indistinct to be elevated above member status. However, he did further define Bryan and McCann's (1937) three broad subdivisions, formally renaming two of the units Zia ("lower gray") and Ceja ("upper buff") members. Kelley argued that pervasive lateral and vertical interfingering of units precludes finer stratigraphic subdivision.

This complex interfingering and gradation of units, combined with relatively rapid changes in unit thickness, compositional variability and incomplete exposure, have made stratigraphic correlation difficult. Consequently, there has been considerable inconsistency in the stratigraphic nomenclature. Despite arguments that favor a limited definition of the Santa Fe (splitting as opposed to lumping), current practice is to consider the syn-rift basin-fill in a regional context by using the group terminology and by making allowance for local variability (e.g., Chapin, 1988; Ingersoll et al., 1990).

Hawley and Haase (1992) subdivided the entire basin-fill into three units: 1) pre-Santa Fe Tertiary deposits, 2) Santa Fe Group deposits, and 3) post Santa Fe Group

Quaternary deposits. In their conceptual model of basin hydrogeology, Santa Fe Group deposits were subdivided into Lower, Middle and Upper hydrostratigraphic units on the basis of shifts in depositional style over time, and roughly correspond to Bryan and McCann's (1937) and Kelley's (1977) formational subdivisions. Pre-Santa Fe units include the Galisteo and Baca Formations and consist primarily of sandstones, siltstones and mudstones of non-volcanic origin. A third pre-Santa Fe unit was identified in the southern Albuquerque basin by Lozinsky (1988, 1994) and referred to informally as the "unit of Isleta Well No. 2." It differs from the underlying pre-Santa Fe units in that it is mostly volcanogenic, correlating with Datil Group volcanic and volcanic-related sequences. Post Santa Fe Quaternary deposits consist of Pleistocene-Holocene valley-fill, inset stream terraces and alluvial fan deposits.

Basin Evolution

Current concepts of the basin's tectonic and depositional history are reviewed by Chapin and Cather (1994), Lozinsky (1994), May and Russell (1994), Russell and Snelson (1994), and Hawley et al. (1995). Lower Santa Fe Group units deposited from about 28-15 Ma. indicate an internal drainage system, and consist of fine-grained, playa-type mudstones and siltstones in the basin floor that intertongue laterally with eolian and basin-margin piedmont units. Increased tectonism and rapid sedimentation from about 15-5 Ma. deposited units of the Middle Santa Fe Group, which is the thickest sequence in the section and is marked by the appearance of fluvial deposition in the basin floor. After about 5 Ma., infilling of the basin's half graben segments had progressed to where the

ancestral Rio Grande became a through-going system, integrating the sediments of adjacent basins. Upper Santa Fe Group deposits are thus comprised of axial river sands and overbank fines in the deeper, central basin that intertonque laterally with poorly sorted sands and conglomerates of coalescing piedmont aprons at the uplifted basin margins. After about 1 Ma. the ancestral Rio Grande and Rio Puerco river systems began to incise the Santa Fe Group valley fill, leaving the Llano de Alburquerque geomorphic surface between the two river valleys. Post-Santa Fe Group Quaternary units are mostly backfill sequences that consist of coarse and poorly sorted fluvial-terrace deposits and the modern floodplain sediments of the Rio Grande and Puerco Valleys (Lambert, 1968; Lambert et al., 1982; Machette, 1985; Hawley and Love, 1991).

Basin-Fill Diagenesis

Walker et al. (1978), in their overview paper on diagenesis of first-cycle alluvium in the desert southwest, found that Santa Fe Group outcrops sampled along the Rio Grande rift share textural and mineralogical similarities with outcrop samples of Pliocene (?) fanglomerates from Baja, California, and with core samples of Plio-Pleistocene Gila Group deposits near Tucson, Arizona. These workers maintained that arkosic sediments of arid-region basins characteristically exhibit a decrease in textural maturity following the onset of diagenesis through precipitation of authigenic clay minerals, and an increase in mineralogical maturity through dissolution and replacement of framework grains. Disequilibrium between granitic and volcaniclastic detritus and circulating groundwater were believed to result in geologically rapid post-depositional alteration. Unless ions

released by intrastratal dissolution are later precipitated as cementing agents, groundwaters may remove these ions completely from interstitial pore spaces.

Groundwater removal of dissolved constituents was apparently not a major factor in Santa Fe Group diagenesis at San Diego Mountain near Las Cruces, New Mexico (Mack and Grigsby, 1985). Early precipitation of hematite as a grain-rimming cement was succeeded by pore-filling calcite cements of progressively higher Fe^{2+}/Mn^{2+} ratios, suggesting that pore waters became progressively reducing over time. Persistence throughout the section of mechanically infiltrated clays and authigenic calcium smectite void-filling cements further suggests that diagenetic reactions were controlled by an essentially closed-system pore fluid evolution. The conspicuous absence of authigenic zeolite and feldspar was attributed by the authors to the stability of early calcite cements, which inhibited later chemical interaction between detrital grains and pore solutions. Calcite cementation was also linked to the absence of any well-defined trend in compaction, despite the 3000 ft (950 m) thickness of section.

An earlier diagenetic survey of the Albuquerque Basin was made by Mozley et al. (1992). Calcite and zeolite cements were identified in thin-sectioned sidewall cores, and grain-rimming authigenic smectite was detected in SEM. Intragranular porosity (from dissolution of soluble framework grains) was defined by insoluble clay coatings surrounding "ghost grains," and by preferentially dissolved feldspars and volcanic rock fragments.

METHODS

Sampling

Four wells drilled within the last ten years by the City of Albuquerque provided the basic data for the present study (Figure 1). Charles Wells 5 and Charles Wells 6 are Water Utility Division production wells located east of the Rio Grande in the Albuquerque Northeast Heights. Cerro Colorado 1 and Soil Amendment Facility 1 (SAF 1) are Solid Waste and Public Works Department exploratory wells located on the west mesa. These four wells are unique among city wells because they were sidewall-cored in selected sandy intervals. Sidewall cores more successfully preserve the character of sediments than do rotary cuttings. However, few core samples could be obtained from depths less than about 2000 ft because shallower Santa Fe strata are poorly consolidated. Drill cuttings were also collected from these wells at ten foot intervals, but incompletely lithified samples were seldom preserved.

Thin-Section Preparation

Selected sidewall cores from sandy intervals were thin-sectioned by a commercial laboratory. All thin-sections were vacuum-impregnated with a blue-dyed epoxy to distinguish true porosity from porosity created during thin-section preparation. Most samples were stained for potassium feldspar, and many for plagioclase feldspar. Selected thin-sections were hand polished with aluminum oxide paste for microprobe analysis.

Sandstone Petrography

The modal composition of forty-nine thin-sections was determined using a Swift Model F automated point-counter. Counting was done under plane-polarized light with occasional use of cross-polarized light. Three hundred points were counted per sample using a modified version of the Gazzi-Dickinson method (Gazzi, 1966; Dickinson, 1970) that allowed simultaneous tracking of both the mineralogy of grains and the type of rock fragment within which they occur. This method helped assess the potential contribution of unstable minerals to pore solutions, as well as revealed subtle differences in the content of lithic fragments between samples from different wells. Authigenic mineral counts and diagenetic textures, such as framework grain dissolution and alteration, were also recorded.

Point-Count Parameters

Each thin-section point was assigned a category based on clast lithology, type of pore space, or authigenic mineralogy. These categories, and the recalculated parameters used in ternary classification (QFR) diagrams are outlined in Appendix A. Clast lithologies are discussed under Sandstone Petrology, and descriptions of porosity and authigenic mineralogy are presented in the Diagenesis section.

A separate count of 100 points was made of each sample that tallied only pore space. This tabulation, and the definition of porosity terms used, are located in Appendix B.

Point-count Error

The reliability of point-counting results is related to the total number of points counted, and is expressed in terms of the standard deviation (van der Plas and Tobi, 1965). At a 95% confidence level, modal compositions of the units sampled are within four- to six percent of the values reported in Appendix A (+/- 2σ). Because the Santa Fe Group is heterogeneous, the values reported cannot be reliably extrapolated to units outside the immediate vicinity of the sidewall cores.

Scanning Electron Microscopy

It became apparent early in the petrographic study that some important textural relationships and mineral identities could not be resolved using standard petrographic methods alone. Scanning electron microscopy, with its greater depth of field and significantly higher magnification, defined many fine-scale features not otherwise discernable.

Two different scanning electron microscopes were used: a Hitachi HHS-2R located at the electron microscopy facility of New Mexico Tech, and a Hitachi S-450 located at the University of New Mexico Institute of Meteoritics. Both machines were equipped with a Tracor Northern energy dispersive X-ray analysis system (EDS). Starting accelerating voltages ranged from 15 to 20 keV. Small chips of core material (5-10 mm in diameter) were cemented onto carbon stubs, and sputter-coated with a 200 to 500 angstrom-thick carbon coating under a 200 to 300 angstrom-thick gold/palladium coating. Total coating thicknesses are on the order of 700 angstroms. Coating materials

conduct electrical current away from the specimen, facilitating clearer imaging. Unfortunately, an inverse relationship exists between image clarity and EDS resolution. Thicker coatings produce sharper micrographs but mute the X-ray spectra of mineral constituents. The choice of coating materials and thickness was thus a compromise between two objectives.

Electron Microprobe Analysis

Chemical compositions of framework grains and selected authigenic minerals were determined using the University of New Mexico Institute of Meteoritics Jeol "Superprobe" Model 733.

Electron microprobe analysis determines elemental compositions by focusing an electron beam within a small area of polished sample. The Jeol Model 733 uses a tungsten filament and accelerating voltages of 10-30 keV. Beam diameter ranges from 1-5μm, and beam current from 10^{-9} to 10^{-7} amps. X-rays emitted from the sample are diffracted by spectrometer crystals within the probe, and collected in a wavelength dispersive (WDS) detection system. Comparing the emission spectra of the sample to the spectra of a standard of known composition determined the composition of the sample. Feldspar and volcanic rock fragment compositions are based on a rhyolite glass standard; clay compositions are from a biotite standard. Error associated with microprobe analysis is a function of element concentration and spectrometer count rate, and is given in Appendix D as weight percent of each element.

X-Ray Diffraction Analysis

Analyses of sidewall cores taken from clay-rich zones in Charles Wells 5, Thomas 5 and 7, SAF-1 and Cerro Colorado wells were done in the New Mexico Bureau of Mines and Mineral Resources clay laboratory. Results of these analyses were first reported by Mozley et al. (1992).

Mineralogy of the less-than-two micron clay fraction was determined from oriented clay mineral aggregates (i.e., with preferred c-axis orientations) sedimented onto glass slides. Oriented samples were analyzed on a Rigaku DMAXA diffractometer using monochromatic (Ni-filtered) CuKa radiation at a scanning rate of two degrees 2$\ominus$ per minute. Samples were solvated in ethylene glycol and then heated to 375° C as an aid to mineral identification. Such treatments result in the expansion of smectite or smectite-like interlayers within the material, and produce shifts in XRD patterns that are characteristic of the particular mineral species. The samples were analyzed only for the major clay minerals kaolinite, chlorite, illite, smectite and interlayered illite/smectite.

Zeolite mineralogy was determined using random powder mounts of air-dried material ground in a mortar and pestle. Random orientations obtain more complete diffraction data for comparison to standard powder diffraction files by maximizing the number of crystal reflections. Because of the low relative abundance of zeolite crystals, the scanning rate was reduced to 0.6 degrees 2$\ominus$ per minute.

Cathodoluminescence Microscopy

One problem encountered in routine petrographic work was distinguishing between authigenic sparry calcite and corroded carbonate lithoclasts. Differences in luminescence of authigenic and detrital carbonates provided a relatively quick and qualitative means of resolving carbonate identity. A Nuclide ELM Luminoscope, mounted on a Nikon petrographic microscope, was used with accelerating voltages ranging from about 10 to 15 keV. Only a small group of representative, carbonate-rich thin-sections were chosen for analysis. These samples were polished manually with an aluminum oxide paste.

SANDSTONE PETROLOGY

Primary Composition

The most abundant detrital grains are quartz, feldspar and various rock fragments, with lesser amounts of biotite, muscovite and various heavy minerals (Appendix A, Table A-1). Volcanic rock fragments are the most abundant and most petrographically varied lithic type, followed by granitic/gneissic fragments, sedimentary rock fragments and trace metamorphic rock fragments. Using Folk's (1974) mineralogical classification scheme, sidewall core samples classify as lithic arkose, feldsarenite, or feldspathic litharenite (Figure 2).

Quartz

Monocrystalline quartz in the sampled intervals is mainly of the common or plutonic variety (Folk, 1974), with straight to slightly undulose extinction, entrained inclusions and occasional microlites. Common quartz is believed to be characteristic of a granitic source area. Volcanic quartz, with straight extinction, almost no inclusions, and the preserved bipyramidal crystal habit of beta quartz, is also prevalent in some intervals. Volcanic grains typically have embayed margins.

Polycrystalline quartz varieties are mostly equigranular granoblastic types (quartzites), with straight grain boundaries that form triple-junctions with adjacent grains. Some stretched and schistose metamorphic types also occur, with granulated to crenulated grain boundaries, strong undulosity, and aligned muscovite, sillimanite or chlorite inclusions. No attempt was made to quantify quartz varieties on a genetic basis.

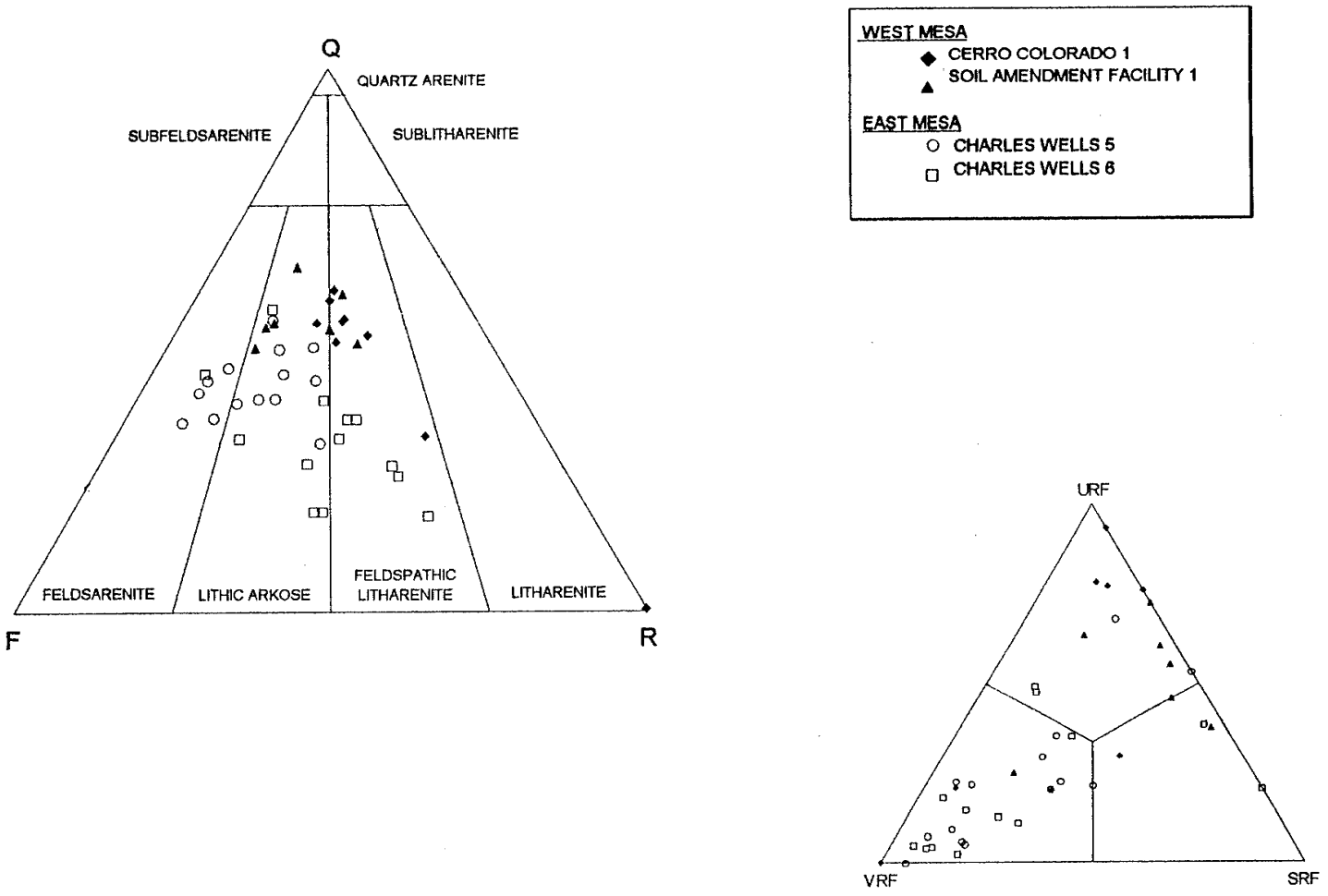

Figure 2. Ternary diagram of detrital modes (after Folk, 1974). Q = quartz; F = feldspar; R = rock fragments; URF = undifferentiated rock fragments; VRF = volcanic rock fragments; SRF = sedimentary rock fragments. Definition of parameters in Appendix A. Differences in sandstone composition between west mesa wells (CC1 and SAF1, solid symbols) and east mesa wells (CW5 and CW6, open symbols) is the result of differences in respective source area.

Feldspar

Plagioclase feldspars are typically monocrystalline, but also occur with quartz in granitic-gneissic rock fragments (discussed below). Within volcanic rock fragments, plagioclase occurs either as tabular microphenocrysts or as microlytic or felted lathwork within the groundmass. Polysynthetic lamellar twinning is diagnostic of plagioclase, but untwinned, anhedral grains are also common that are either of metamorphic origin or lie on the {010}cleavage. Concentric compositional zoning is evident in a number of microphenocrysts.

Microprobe results (Appendix D, Table D-1) show that a typical monocrystalline plagioclase from Charles Wells 5 has a composition ranging from $An_{13.7}$ (oligoclase) to $An_{28.2}$ (oligoclase-andesine), but may also contain up to 7% potassium. A small orthoclase content may account for the fact that many feldspar grains accept both plagioclase and alkali feldspar stains.

Alkali feldspars occur in both high temperature (disordered) and low temperature (ordered) forms, the latter being more prevalent. Discrete, monocrystalline grains are most often grid-twinned microcline or untwinned orthoclase, as are granitic-gneissic rock fragments that occur with quartz, +/- muscovite. A typical monocrystalline K-feldspar from Charles Wells 5 has a composition ranging from 3.1% to 13.4% sodium (Appendix D, Table D-1).

Granitic-gneissic rock fragments are polymineralic grains of muscovite, biotite, chlorite or sillimanite that occur with quartz and feldspar and are plotted together with feldspar at the F-pole on the QFL diagram (Figure 2). Perthitic or myrmekitic

intergrowths, while not abundant, are not uncommon within granitic-gneissic fragments, and are often associated with vacuolized feldspars. Vacuolization refers to minute gas or fluid inclusions incorporated within a mineral grain either during or after its formation. Some skeletal or microporous polycrystalline quartz grains were observed that may in fact be granitic rock fragments with perthitic intergrowths.

Lithic Fragments

Volcanic rock fragments are the most abundant and most varied lithic type, with compositions ranging from rhyolitic ash-flow tuffs (ignimbrites) to andesites to basalts. Silicic volcanics are typically fragmental, with microphenocrysts of sanidine or quartz embedded in an aphanitic to felsitic or glassy groundmass. Intermediate volcanics consist of plagioclase feldspar microphenocrysts (often with compositional zonation) +/- biotite, pyroxene or amphibole in a felted, or occasionally trachytic, groundmass. Mafic volcanics, with sphene or olivine microphenocrysts and microlitic plagioclase laths, are less common, and often display iddingsite or opaque Fe-Ti oxide alteration. Skeletal or ghost microphenocrysts within a coherent groundmass are common, reflecting selective dissolution of components during diagenesis.

Pumiceous fragments are typically rust-brown in plane light, display axiolitic or spherulitic devitrification, and are either isotropic or exhibit a "streaky" form of petrographic extinction. Microprobe analysis (Appendix D, Table D-1) of the groundmass of a vitroclast sample from Charles Wells 5 was found to have the general formula

$$(K_{.511}Na_{.200}Fe_{.017}Ca_{.007}Ti_{.005}Ba_{.002}Mg_{.001})Al_{.745}Si_{3.246}O_{8.000}$$

which has a similar composition and an Al/Si ratio similar to, but slightly lower than sanidine. Microprobe results indicate that pumiceous rock fragments were derived from a rhyolitic or latitic magma. Pumice fragments generally accept alkali feldspar stain.

Siliceous volcanic rock fragments are fine-grained and look very much like chert in cross-polarized light, but exhibit a combination of relict microphenocrysts, microlytic fabic and heavy minerals. These grains are distinguished from undifferentiated rock fragments (discussed below) by the presence of plagioclase and/or alkali feldspar stains over the entire grain surface.

Sedimentary rock fragments include sandstone/siltstone rock fragments, carbonate lithoclasts and chert. Sandstone/siltstone rock fragments, defined by fine-grained quartz and feldspar in a detrital clay matrix, have grain boundaries that are mostly ragged and indistinct. Siltstone abundance may be underestimated in fine-grained samples that contain abundant detrital clay. Intact fragments of quartz arenites were not found, though a number of well-rounded monocrystalline grains were observed to have partially rounded quartz overgrowths. If these overgrowths are remnants of an earlier generation cement, they represent clasts recycled from a texturally more mature sandstone (Folk, 1974).

Carbonate lithoclasts are nowhere abundant, and are essentially absent from west mesa wells. In most cases carbonate grains are comminuted and appear sparitic, perhaps as a result of weathering and transport rather than recrystallization. Intact foraminifera were found in two samples, both in Charles Wells 6, and were tentatively identified as nodosariids.

Chert consists of microcrystalline quartz (an aggregate of equidimensional grains that form a birefringent mosaic) and/or chalcedonic quartz (sheaf-like bundles of radiating fibers). Chert is differentiated from fine-grained siliceous rock fragments by the absence of feldspar staining.

Undifferentiated rock fragments are a fairly common and problematic rock type that could not be identified with certainty. These grains are siliceous, very fine-grained, have low birefringence and are apparently polycrystalline in a way resembling chert. Extinction boundaries of these clasts are more "feathery" and indistinct than chalcedonic quartz boundaries, and extinction undulosity is more irregular. Color in plane-polarized light ranges from pale yellow-gold to pale green. In a few samples, rock fragments with features otherwise characteristic of undifferentiated rock fragments were found to contain feldspar and amphibole microphenocrysts, clearly indicating a volcanic origin. Yet other samples were found to contain relict twinning and vacuolization--characteristics of monocrystalline plutonic feldspar. Only those grains that could not be classified as either feldspar or volcanic rock fragments were categorized as undifferentiated rock fragments. QFL diagrams will be skewed towards the lithics pole, should many of these grains be in fact altered feldspar.

Metamorphic rock fragments are extremely rare, with the exception of several quartzite fragments (counted as polycrystalline quartz). The few metamorphic grains encountered are granoblastic polycrystalline quartz + sericitized feldspar $\pm$ biotite, tabulated as granitic-gneissic rock fragments. Foliated rock fragments are not common

probably because of their inherent instability and because annealing of such grains would render them unrecognizable within the sand fraction (Blatt and Christie, 1963).

Heavy Minerals were defined for point-counting purposes as all mineral grains, excluding micas, having a specific gravity greater than that of quartz (specific gravity 2.89; Folk, 1974). Amphiboles, pyroxenes, olivines or sphene, occurring as members of volcanic lithic fragments, were identified on the basis of crystal habit and pleochroism. These grains were seldom pristine. Tourmaline, zircon, Al_2O_3 polymorphs, amphiboles and pyroxenes were also observed within granitic-gneissic lithic fragments. Unless heavy minerals occurred as discrete grains, they were recalculated using standard point counting methods as lithic fragments.

Allogenic Clay

Allogenic clay was differentiated from authigenic clay by particle morphology and distribution with respect to detrital sand-sized grains (Wilson and Pittman, 1977). Petrographically, detrital clays are variegated, occurring in patches or swaths of medium to dark reddish brown (plane-polarized light). High-order yellow interference colors are typically masked by the mineral color. Under high magnification and reduced opening of the iris diaphragm, the variable relief of numerous individual clay particles stands out in the form of multiple Becke lines. With the SEM, detrital clay flakes were seen to be preferentially aligned sub-parallel to the surfaces of sand grains, and to have ragged and irregular terminations.

Sidewall core samples are interpreted to contain both syndepositional and mechanically infiltrated clays (classification of Wilson and Pittman, 1977). Dispersed

matrix is probably the most common mode of occurrence, particularly where silt-sized grains are abundant. Thin, intercalated lamina occur in only a few of the thin-sectioned cores, and no biogenic or biogenically introduced clay was observed. Intraformational, or "rip-up" clasts are not common, but may not have been recognizable due to diagenetic or sampling-induced alterations. Detrital clays are ductile and easily deformed, and their origin could not always be determined with certainty. Furthermore, the coring process and possible desiccation during storage may have destroyed morphological and textural properties of some clay samples that would facilitate their identification.

DIAGENESIS

Authigenic Composition

Diagenetic minerals present in the samples are clays (smectite and interlayered illite/smectite), zeolites and calcite. Not all phases are present in all wells, and no systematic occurrence of any one phase is discernable with increasing depth. Most sidewall cores contain more than a single authigenic component, but typically contain only one, or perhaps two components in significant quantity. Samples were thus grouped in Appendix C according to dominant authigenic mineralogy. Thin-sections having more than one cement in excess of an arbitrary 10% of pre-cement porosity were placed in a two-cement category. Samples were considered "uncemented" if they contained no secondary minerals in excess of 10% of pre-cement porosity.

Smectite, Illite and Interlayered Illite/Smectite

All of the samples examined with SEM contained abundant clay, determined from particle morphology to consist of both authigenic and detrital varieties. In thin-section, authigenic clay was interpreted to occur where irregularly distributed patches of microporosity were observed. These patches or zones were seen to be uniformly colorless, have low birefringence, and to completely fill pore spaces (Plates 1A and 2A). Undeformed zones extend into narrow recesses where adjacent framework grains meet, but are absent at points of grain-grain contact (Plate 1). Microporous zones returned clay-like compositions when microprobed (Appendix D, Table 2).

Using the terms and identification criteria of Wilson and Pittman (1977), authigenic clay is identified as either a pore-filling phyllosilicate cement or a psuedomorphous replacement of framework grains. Pore-fillings are defined by these workers as clay that partially or completely plugs interstitial pore space, and displays no apparent alignment or preferred orientation of particles. Psuedomorphous replacement is defined as clay that replaces unstable detrital grains, or infills voids left by framework grain dissolution. The compositional purity of both modes of authigenic clay (Plates 1A and 2A) results in uniformity in color and texture (Wilson and Pittman, 1977), as well as a "clear transparency" (Dickinson, 1970). The concentric color zonation criteria of Dickinson (1970) was not observed in thin-section samples, but Wilson and Pittman (1977) state this is a relatively uncommon feature.

The irregular or spotty distribution of material and the absence of flame-like wisps or drapes about detrital grains, suggest it is not dispersed detrital matrix or mechanically infiltrated clay (Wilson and Pittman, 1977; Dickinson, 1970). The occurrence of undeformed patches of microporosity within narrow, angular recesses of grain contacts indicates in situ growth, rather than allogenic material squeezed between rigid grains. Where framework grain alteration is sufficiently advanced, psuedomorphous replacements may have extended into pore spaces and become indistinguishable from phyllosilicate cement. Clay was only point-counted as replacement where relict lithic fragments or microphenocrysts were observed (framework microporosity, Appendix C).

Chemical compositions of representative authigenic clay from Charles Wells 5 are shown in Appendix D, Table 2. Both Na^+- and non-Na^+ clay varieties were identified, which have the following average formulas:

$$(Na_{.52}K_{.31}Ca_{.28})(Al_{1.52}Fe_{.08}Mg_{.03})Si_{3.96}O_{11}$$

$$(K_{.08}Ca_{.06})(Al_{.66}Mg_{.30}Fe_{.27}Ti_{.16})Si_{4.51}O_{11.}$$

The analytical difficulty associated with hydrous minerals of characteristically high cation exchange capacity (Brindley, 1981) is reflected in the low totals in Appendix D. The results shown are considered semi-quantitative. The presence of octahedral magnesium and abundant tetrahedral silica in both clay species indicates that the samples belong to the dioctahedral group of (smectitic) phyllosilicate minerals. The non-Na^+ clays are also characterized by titanium substitution within the octahedral site.

Chemical compositions of morphologically similar clays vary, even at the scale of a thin-section, but at least some of this variability may result from interstratifications of different clay mineral species. Illite and smectite differ principally in the degree of cation substitution possible within their respective crystal unit cells, and in the variable hydration states of smectite. The similarity of unit cell allows illite and smectite structural sheets to stack on top of each other in any sequence from completely random to regularly ordered (Brindley, 1981). Microprobe analysis necessarily averages the chemical compositions of mixed-layer illite/smectite.

Morphology of Albuquerque samples observed with SEM suggests that smectite or smectite-like material are the dominant clay species (Plates 1, 2 and 3). The ragged-edged, crenulated or webby to flaky appearance, while not diagnostic in-and-of itself, is

characteristic of smectite or a smectite-dominated illite/smectite (Welton, 1984). The regularity of the illite/smectite layer stacking is not distinguishable with SEM. Based on XRD analyses, Mozley et al. (1992; their Table 5, Appendix G) report that selected core samples have a consistently greater abundance of smectite than of other phases. Illite, illite/smectite and kaolinite are of lesser abundance. XRD analysis does not, however, distinguish between authigenic and detrital clay species.

Kaolinite

Kaolinite is a common weathering product of feldspars and mafic volcanic rocks, but was not observed in thin section or with SEM in any of the Albuquerque cores. It is typical of environments with high permeability and large fluid volumes (so-called leaching environments) whereas smectites, which were observed, are characteristic alteration products in alkaline environments and drier climates (Carroll, 1970). An earlier study by Mozley et al. (1992) reported small amounts of kaolinite in Cerro Colorado 1 and SAF 1 using XRD techniques, but they did not identify it in thin section. The earlier XRD study located kaolinite only in clayey-silty cores, indicating its occurrence is limited to finer-grained sediments. Its absence in the sandier cores selected for petrographic work raises the possibility that kaolinite in clayey zones is detrital.

Zeolites

Zeolites were observed in a number of samples from Charles Wells 5 and Charles Wells 6, and in one sample from SAF 1. Where they occur, zeolites form in pore spaces as clusters of euhedral to subhedral crystals, and are often (but not always) associated with authigenic clay. Petrographically, zeolites are length-fast, have high relief and low birefringence (.006-.008), and are colorless in plane polarized light (Plate 2A). Crystal size is on the order of 20 to 30 microns.

With SEM, zeolites are seen to have prismatic habit, and to be flattened along the b-axis and elongated along the c-axis (Plate 4). Chemical composition of five zeolite samples from Charles Wells 5 (2992.1 feet) are shown in Appendix D, Table D-3. The crystal morphology visible with SEM, combined with microprobe and XRD analyses, identify the zeolite species as a calcium-rich, low silica variety of the heulandite group.

Oxide totals in Table D-3 are low--76% to 85%. However, microprobe results are given on an anhydrous basis. Idealized heulandite, $CaAl_2Si_7O_{18}\cdot 6H_20$ (Woods and Garrels, 1987), has a molecular weight of 686.79, of which water comprises 15.74%, by weight. Adding approximately six formula units of non-structural water to the results in Table D-3 brings the oxide totals up to acceptable values, and demonstrates that unbound water within the framework channelways of zeolites reasonably accounts for deficiencies in microprobe analytical results. Analysis number 1 (Table D-3) has an oxide total of 96.6%, which may reflect greater retention of structural water by this sample, at the expense of calcium and magnesium.

Some workers (e.g., Mason and Sand, 1960; Mumpton, 1960) consider heulandite as one end-member of a heulandite-clinoptilolite structural series, with clinoptilolite as the potassium-sodium, high silica end-member. However, Hay (1966) points out that the two species may be ion-exchange varieties of the same mineral. Inconsistencies in physical properties and extent of cation substitutions led Tschernich (1992) to argue for abandonment of the clinoptilolite nomenclature, reasoning that compositional and structural variations should be addressed using descriptive modifiers. For purposes of this report, zeolites are referred to simply as heulandite.

Mason and Sand (1960) defined heulandite according to the ratio $Ca^{2+}+Sr^{2+}+Ba^{2+}$: $Na^{+}+K^{+}$. On this basis, Albuquerque basin zeolites have less $Na^{+}+K^{+}$ and less $Ca^{2+}+Sr^{2+}+Ba^{2+}$ than the natural heulandite sample of Johnson, et al. (1985), but a similar value of $Al^{3+}+Si^{4+}$. Albuquerque samples also have less $Na^{+}+K^{+}$ than either the high or low silica heulandite varieties reported by Tschernich (1992), but similar ratios of Al^{3+} to Si^{4+} as varieties with similar $Ca^{2+}+Sr^{2+}+Ba^{2+}$. Some of the alkali cations in Albuquerque zeolites may have been evacuated by sample dehydration during storage and sample preparation. Also, chemical compositions reported in the literature are for large crystals (millimeters to centimeters), which tend toward high-calcium, low-silica content (Tschernich, 1992). Because all of the exchangeable cations (the alkali and alkaline earth metals) are located on two crystal lattice sites, sample compositions may deviate from published compositions because of differences in crystal size and cation exchange capacity.

In an earlier report (Mozley et al., 1992), Albuquerque zeolites were tentatively identified as the variety stilbite. This conclusion was based on preliminary XRD analyses of material present in relatively low abundance. Additional analyses and refinements to XRD techniques now confirm the zeolite species as heulandite.

According to Hay (1978), zeolite formation is associated with one of several processes: 1) hydrothermal alteration; 2) low-grade, regional metamorphism; 3) saline, alkaline lake (playa) or saline, alkaline soil deposition; and 4) percolation of meteoric water in open hydrologic systems. Of these, only the last two are pertinent to the Albuquerque Basin. Each of these two types of deposit has a characteristic mineral zonation associated with its occurrence. Arid-region lacustrine or playa deposits are characterized by a concentric, lateral zonation in facies inward from fresh tuffaceous material on the basin periphery, to alkalic zeolites, to analcime, and finally to authigenic alkali feldspar at the basin center (Sheppard and Gude,1968; Surdam and Sheppard, 1978). The distribution of facies is believed related to evaporative concentration of sodium carbonate-bicarbonate waters. In open hydrologic systems, downward-percolating meteoric waters react with detrital minerals and become progressively enriched in silica and alkaline metals, producing a vertical zonation in groundwater chemistry and authigenic minerals (Hay, 1978). Upper zones, typically consisting of fresh glass and smectite, are generally in sharp contact with underlying clinoptilolite/heulandite and analcime zones, indicating a significant increase in solution pH and ionic strength as descending pore waters react with volcanic materials.

Vertical zeolite zones were not detected over the depths sampled (heulandite is the single zeolite species observed) but the absence of vertical zonation does not rule out a hydrologic mechanism for zeolite precipitation. Zeolites precipitated preferentially in medium to coarse-grained, moderately to poorly sorted sands (discussed below), suggesting a correlation between zeolite occurrence and sediment with higher permeability. Greater fluid flux through permeable aquifer zones enhances dissolution of framework grains (Sullivan and McBride, 1991; Siebert et al., 1984) and ultimately impacts the saturation state of migrating fluids. Lateral zonation associated with playa deposits cannot be evaluated from bore-hole data.

Calcite

The Santa Fe Group is mostly uncemented in outcrop but commonly contains discontinuous bands and lenses of calcite-cemented, sediment-filled channels, cut-and-fill structures and concretionary sands. In thin section, micrite comprises most of the matrix of a few fine-grained samples or occurs as isolated poikilitic crystals in some coarser-grained samples (Plate1A and 1B). There is an apparent tendency for calcite to occur in finer grained, better sorted sands, but the correlation between the relative abundance of calcite and grain size is weak (discussed below).

Carbonate lithoclasts were nearly always brecciated, and thus easily mistaken for secondary sparite. Cathodoluminescence microscopy was useful in differentiating the two carbonate origins, but point-counting was done exclusively under plane polarized or cross polarized light. Cathodoluminescence was used only as a qualitative guide.

Core Depth and Secondary Mineralization

Secondary minerals observed in this study are essentially low temperature and pressure varieties, the occurrences of which are unsystematic with respect to depth of burial. Figure 3 illustrates the distribution of authigenic minerals by core depth, and indicates the absence of a discernable trend in mineralization over the intervals sampled.

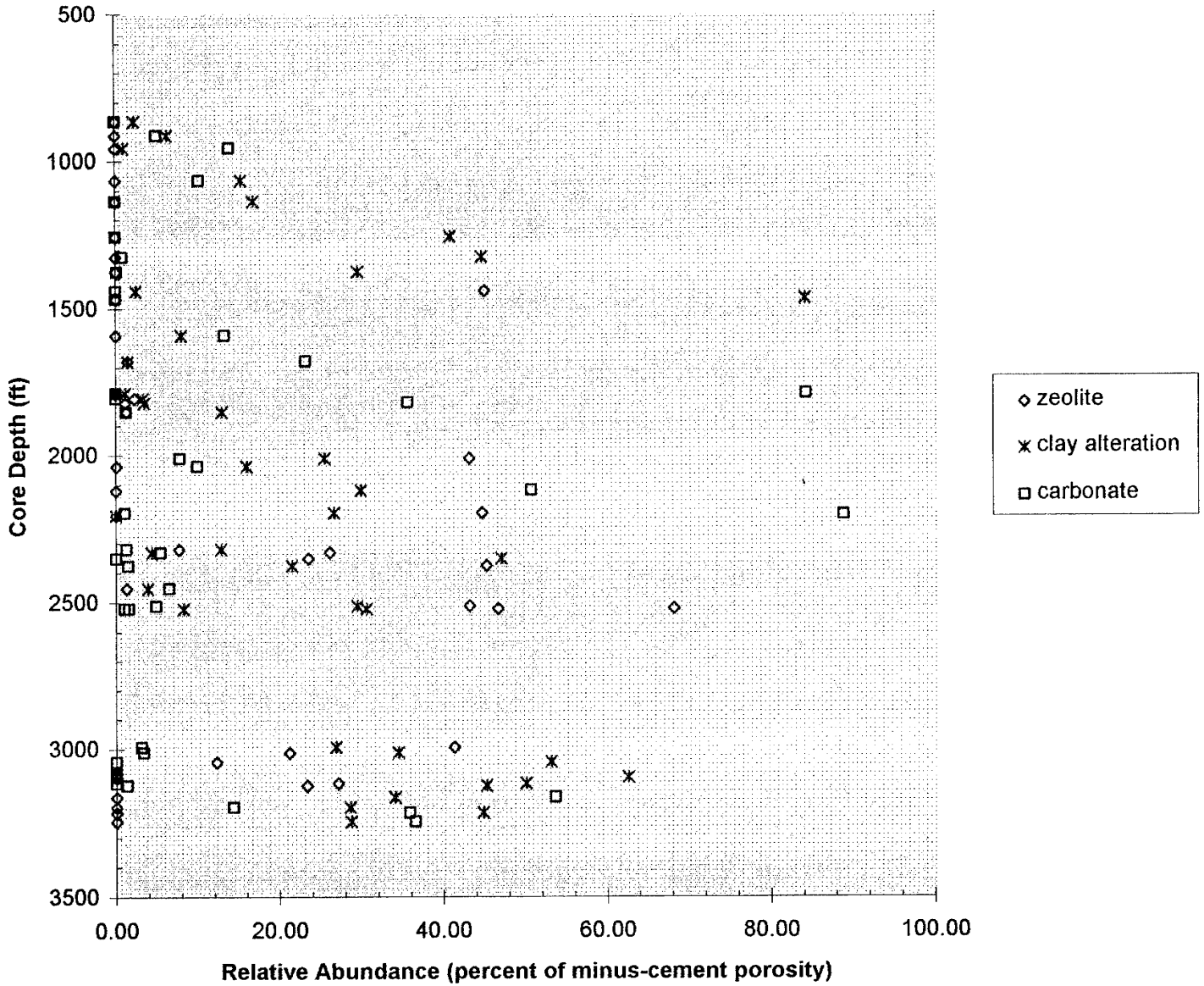

Figure 3. Distribution of authigenic minerals by depth of occurrence. Mineral abundance, expressed in terms of relative pore volume, is independent of burial depth.

Influence of Primary Mineralogy and Sedimentary Texture

The formation of secondary clay and zeolites is typically attributed to chemical decomposition of sediment containing abundant volcanic rock fragments and feldspars (e.g., Hay, 1966; Colella et al., 1978; Reeves, 1978), but the correlation of authigenic mineral suites to a specific sandstone composition is typically weak (Hay, 1966). The single West Mesa sample containing zeolites (SAF ; 1440 feet), for example, has no volcanic lithic fragments, has a relatively low plagioclase content, but does contain an abundance of undifferentiated rock fragments. No zeolites were observed in volcanic glasses of Cerro Colorado No. 1 (below 1500 feet), perhaps indicating some additional control on zeolite precipitation besides detrital composition.

The relationship between secondary mineral precipitation and sedimentary texture was evaluated by estimating the grain size and sorting of uncut sidewall core plugs using visual comparitors (Swanson, 1981; Tucker, 1982). These estimates are considered a first approximation of sedimentary texture.

The range in grain size in cored intervals covers the entire sand spectrum, extending from very fine lower- to very coarse upper sand (0.06 to 2.00 mm; Appendix A, Table 2). The most commonly occurring grain size (mode) is nearly as diverse, ranging from very fine upper- to medium lower sand. Mean grain size was calculated using the relation $\phi 16\% + \phi 50\% + \phi 84\%/3$; sorting, expressed as the standard deviation in grain size, was calculated using the relation $\phi 84\% - \phi 16\%/2$ (modified from Folk, 1974). Grain roundness varies from angular to subround.

Authigenic mineralization is evident throughout the observed range of sedimentary texture (Figure 4). Though occurrences may span a range in grain size and degree of sorting, the general trend is that zeolites and zeolites + clay form in coarse-grained, less sorted sediments; calcite and calcite + clay forms in medium to fine-grained, well sorted sediments; and clay replacements of framework grains develop in medium-grained, moderately sorted sediments. Uncemented samples may be either fine-grained or coarse-grained, but are generally better sorted than mineralized samples. The apparent preference of authigenic minerals for a specific grain-size class is not necessarily reflected in the relative abundance of that mineral, however. Correlation coefficients calculated for number of mineral occurrences and several primary sedimentological parameters are shown in Table 1. No strong relationships are seen in Table 1 between authigenic mineralization and sedimentary composition and texture, the highest correlations being between zeolite occurrence and sorting ($r = 0.56$), between zeolite occurrence and the ratio of standard deviation/mean grain size ($r = 0.58$), and between clay alteration and percent lithics ($r = 0.55$). Correlations indicate, in general, that zeolites are more likely to occur in coarser-grained, less sorted sediments containing volcanic rock fragments. Phyllosilicate and calcite cement abundance are less predictable from primary sedimentological considerations alone.

The quantity of authigenic minerals that precipitate is not appreciably affected by texture, but it is apparent that certain environmental conditions must be met before a particular authigenic suite can develop. Poor correlation between secondary mineral abundance and primary sedimentological composition is explained in part by the fact that

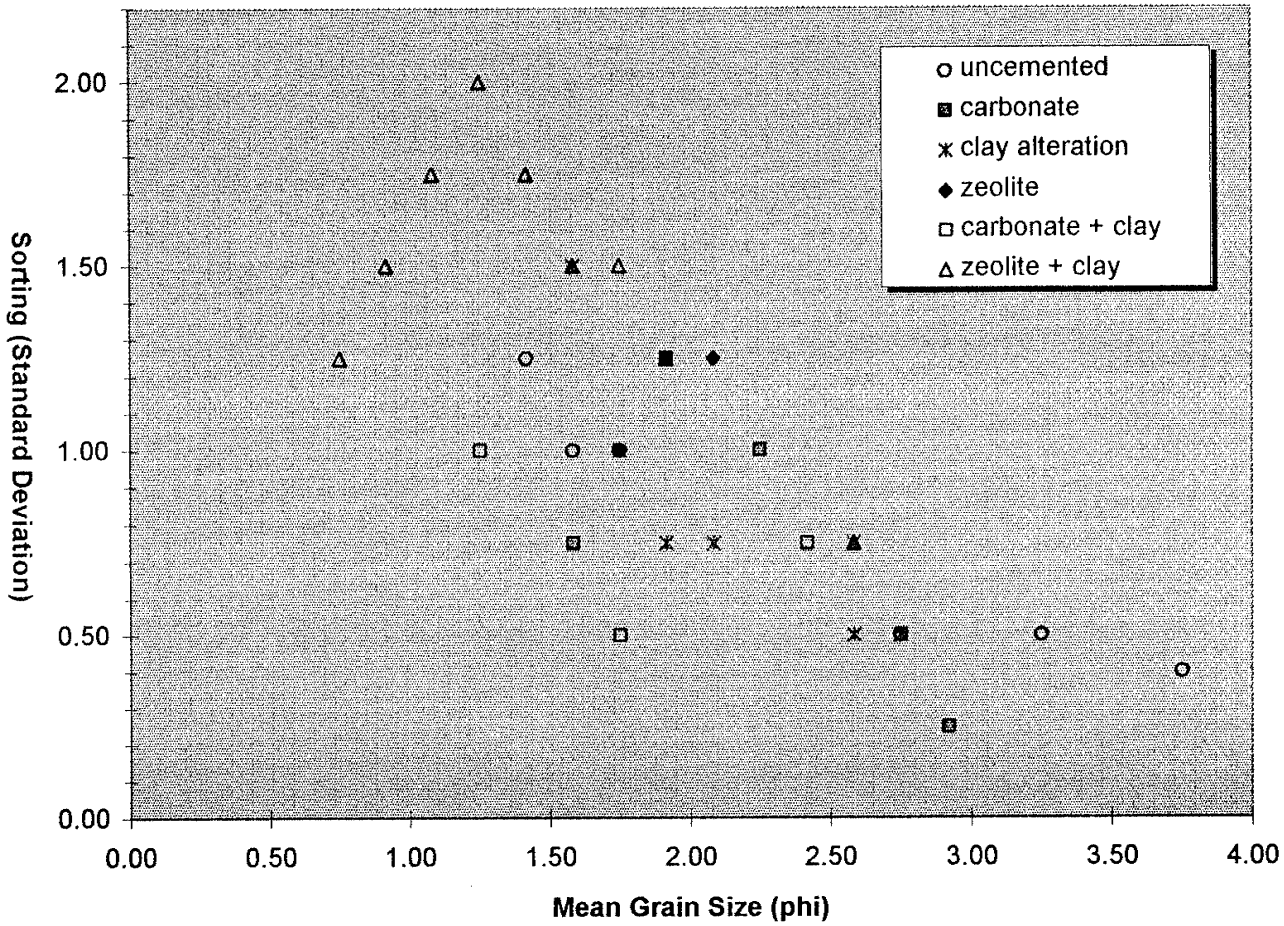

Figure 4. Cement groups plotted according to texture of host sediment. Zeolites and zeolites + clay occur in coarser grained, less sorted sands, whereas carbonate and carbonate + clay occur in finer grained, better sorted sands. Grain size and sorting from Appendix A, table 2; cement groups from Appendix C.

Table 1. Correlation coefficients calculated for authigenic mineral abundance and primary sedimentological parameters. Primary mineral percentages are based on point-count parameters recalculated using the Gazzi-Dickinson method, which emphasizes mineralogical content over lithic type. The ratio of sorting to grain size (std dev/mean phi) is a means of combining two textural parameters into a single variable.

Zeolite (%)	Clay Alteration (%)	Calcite (%)	
-0.42	0.02	0.03	Mean Phi
0.56	-0.01	-0.08	Std Deviation
0.58	0.02	-0.12	Std Dev/Mean Phi
0.38	0.55	-0.30	% Lithics
-0.15	-0.15	0.24	% Feldspar
-0.23	-0.39	0.08	% Quartz
-0.39	-0.33	-0.01	% URF
0.43	0.39	0.09	% VRF
-0.13	-0.15	-0.19	% SRF
-0.29	-0.44	-0.33	Intergranular Macroporosity

soluble feldspars and lithic fragments occur with such abundance throughout the Santa Fe Group that authigenesis is not limited by the absence of a necessary solute. In the geochemical modeling section of this report, each of the observed authigenic minerals was simulated by simply dissolving increased amounts of oligoclase: the specific chemical species released into model pore solutions remained the same. These observations suggest that the presence or absence of secondary minerals in sidewall cores is related more to the hydrologic properties of aquifer zones than to specific sediment composition. Sedimentary texture is important insofar as providing an environment conducive to nucleation and crystal growth, and in it's affect on the movement of groundwater .

Porosity and Framework Grain Dissolution

Variability in original porosity is related to grain sorting and to the abundance of fines within the primary sediment (Beard and Weyl, 1973). During diagenesis, porosity may be enhanced by dissolution of framework grains, occluded by precipitation of secondary minerals, or reduced by burial compaction (Beard and Weyl, 1973; Siebert et al., 1984; Houseknecht, 1987).

Porosity of Albuquerque core samples is shown in Figures 5 and 6. Total macroporosity, reported as a percentage of total sample volume, generally decreases with depth (Figure 5) though there is considerable scatter amongst data points. The implication of this decrease in total porosity is that porosity occlusion and compaction become more pronounced at depth. Secondary porosity also displays considerable

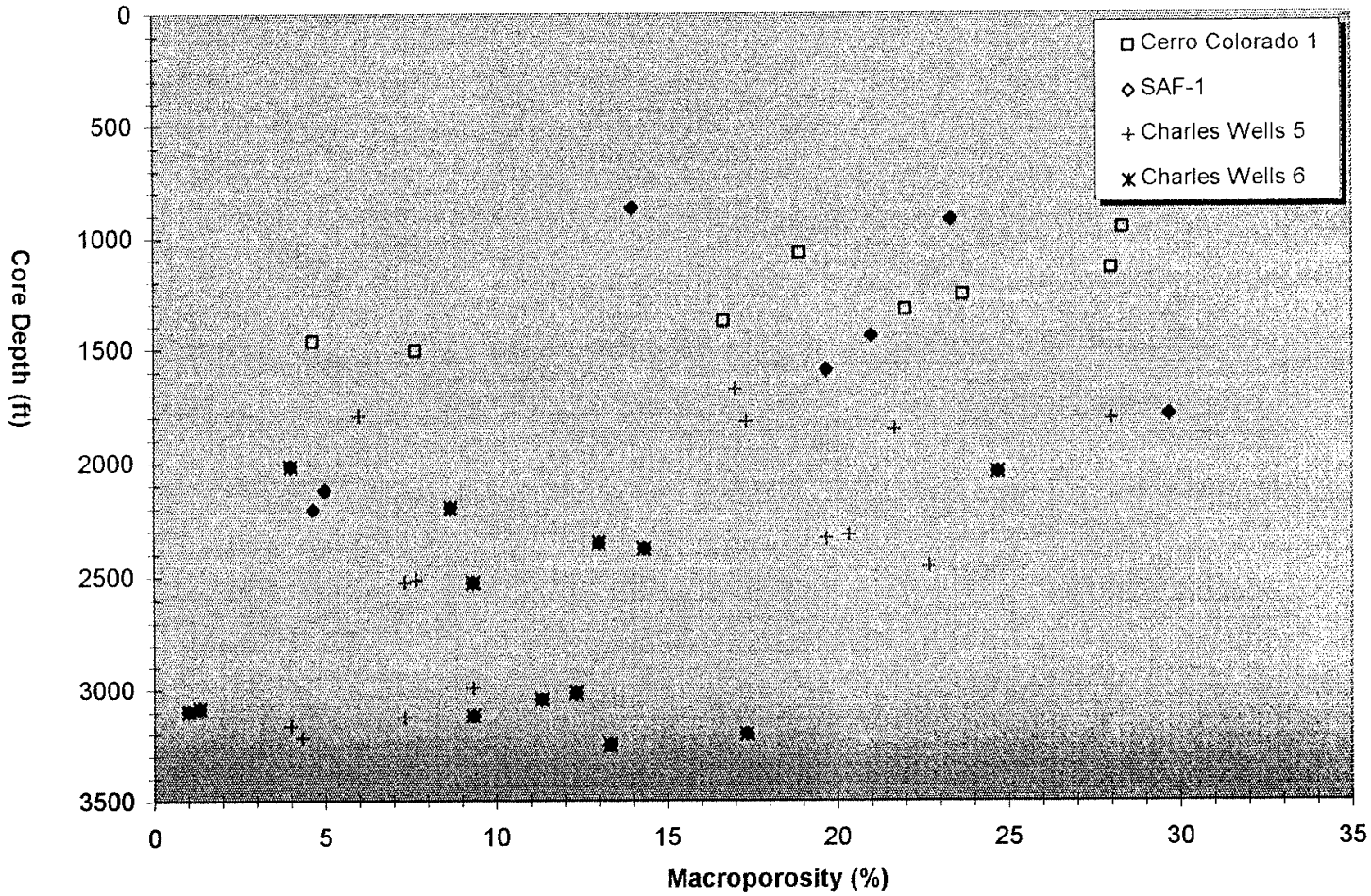

Figure 5. Total macroporosity of each core sample, as a percentage of 300 point counts. Porosity generally decreases with increasing well depth, suggesting porosity loss to compaction and occlusion by mineral cements. Wide differences in porosity of samples from similar depths reflect the heterogeneity in sedimentary texture.

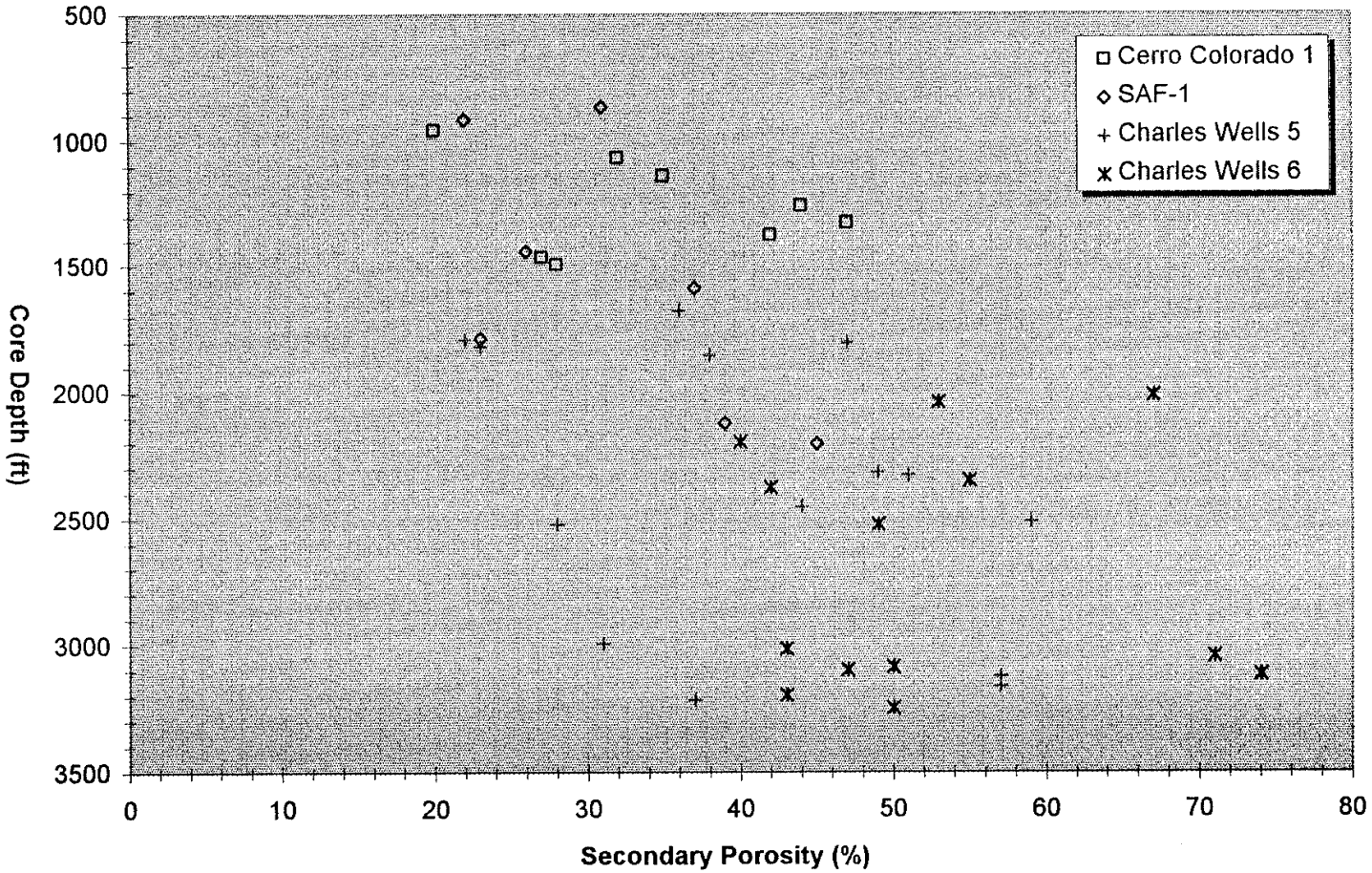

Figure 6. Secondary porosity resulting from framework grain dissolution, alteration and fracture, expressed as a percentage of 100 porosity point counts. Secondary porosity generally increases with depth, suggesting diagenetic modifications to original porosity are more pronounced in deeper aquifer zones.

variability, but in general increases with depth (Figure 6), supporting the notion that diagenetic modifications to original porosity become greater in deeper parts of the basin. The distribution of authigenic minerals, however, does not support this conclusion (Figure 3) because secondary mineral precipitation is inconsistent with depth.

Secondary porosity generated by intrastratal solution of framework grains results in skeletal grains with a remnant, identifiable structure (Plate 2D); ghost grains, identified by an insoluble clay or cement residue (Plate 4D); or oversized pores that suggest framework grain dissolution by conspicuous pore size. Selective dissolution of microphenocrysts produces euhedral or lath-shaped voids within volcanic rock fragments (Plate 1A). Skeletal grain content of Albuquerque samples ranges from 2.3 to 4.3 percent of total sandstone volume, and averages 3.08 percent (Appendix B; summarized below in Table 2). Nearly 50 percent of grains showing skeletal characteristics (i.e., with relict grain margins) are plagioclase, 25 percent are K-feldspar, and 18 percent are volcanic rock fragments (Appendix B, Table 2b). Skeletal grain content is slightly higher for East Mesa wells Charles Wells 5 and Charles Wells 6 than for West Mesa wells, but no trend in skeletal grain content is seen with depth.

Table 2. Average skeletal grain content (all mineralogies) for each well; percent of 300 point counts

	Cerro Colorado	SAF 1	Charles Wells 6	Charles Wells 5
mean	2.52	2.28	3.21	4.33
std dev	2.33	1.27	1.64	1.69

Processes commonly advanced for chemically aggressive pore fluids are dissociation of organic acids and the resulting generation of CO_2 during organic diagenesis (e.g., Surdam et al., 1984; Lundegard and Land, 1986; Kharaka et al., 1986), leaching of mineral matter in the shallow subsurface by meteoric water in equilibrium with atmospheric CO_2 (Bloch and Franks, 1993), hydrolysis reactions between minerals and groundwater (Bjørlykke, 1983) and microbial metabolic processes (e.g., Tan, 1980; Robert and Berthelin, 1986). Geochemical reactions in the CO_2-organic acid system of hydrocarbon reservoirs play an important role in the generation of secondary porosity. However, the organic carbon of oil-field waters is associated with kerogen-rich rocks not found in the Santa Fe Group, and may not be present in the Santa Fe except in relatively small concentrations. The second and third processes, hydrolysis reactions and mineral leaching, are similar processes that both impart an alteration to the silicate structure, but differ from each other in regard to the fate of chemical reaction products. In open hydrologic systems with relatively high fluid flow rates, soluble reaction products (such as aluminum hydroxides) are supposedly removed or leached from their site of formation rather than accumulated in intergranular pore spaces (Bloch and Franks, 1993). Physical

removal of products by groundwater flow facilitates the forward reaction and further dissolution, in accordance with LeChatelier's Principle. Hydrolysis differs from leaching in that it is in theory a reversible reaction that permits establishment of an equilibrium between reactant detrital grains and product minerals. If this equilibrium is reached, for example in constricted pore spaces with limited exposure to circulating fluids, dissolution of detrital grains will be significantly slowed or stopped. Factors influencing the rate of feldspar hydrolysis and silicate solubility are mineralogical composition of the sediment, grain size, fracturing and degree of alteration before deposition, acidity of porewaters and the duration of exposure to pore fluids (Bjørlykke, 1983).

The importance of microbial metabolism, the fourth process, in the synthesis of organic acids and production of CO_2 is well established (Stevenson, 1967; Tan, 1980), and those compounds most effective in dissolving aluminosilicate minerals are also strong chelating agents believed responsible for the mobilization and transport of decomposed mineral matter out of the soil profile (Stevenson, 1967; Stevenson and Fitch, 1986). Although qualitative estimates of microbial biomass and activity are difficult to obtain, arid and semiarid soils are known to contain most of the same major taxa of micro-organisms contained in less extreme climates (Kieft, 1991). The distribution of acid-generating microbial colonies is patterned about what has been termed "fertile islands" of low population density perennial plants. Microbial populations are most active in the upper 5-20 cm of the vertical soil profile, though some fungi populations are known to extend to depths of around 10 m (Kieft, 1991).

Microbial decomposition in the shallow subsurface of the Albuquerque Basin requires that skeletal grains have survived burial and the effects of burial compaction. Bloch and Franks (1993) determined that dissolution of plagioclase feldspars in the San Joaquin Basin of California was mostly generated in the shallow subsurface, and that delicate dissolution structures were protected from compaction by the high rigid-grain content of the sands. Burial depths of samples in the Albuquerque Basin are considerably less than the 2,900 feet to 13,000 feet sampled in the San Joaquin Basin, so it is feasible that skeletal structures produced in the shallow subsurface have survived to their present depths.

In order to evaluate possible dissolution mechanisms, the following calculations were made to estimate the amount of material released into solution, and to compare that estimate to the amount of material potentially dissolved by organic acid generation. Soluble minerals anorthite, Ca-glass, microcline, sanidine, K-glass, albite and Na-glass have molar volumes, in cm^3/mol, ranging from 100.07 for albite to 100.79 for anorthite to 116.50 for K-glass (Robie et al., 1979). The mean molar volume for these minerals is 106.88 cm^3/mol, or 9.4 $mmol/cm^3$. If 3% of Albuquerque Basin sediment exhibits framework grain dissolution (Table 2), then

$$(9.4\ mmol/cm^3)\ (0.03) = 0.28\ mmol\ mineral\ matter/cm^3\ sediment$$

has been released into pore solution. The amount of acid required to hydrolyze this sediment is given by the dissociation reaction of oligoclase, the most abundant detrital feldspar. Assuming no conservation of aluminum,

$$4\ NaAlSi_3O_8 \cdot CaAl_2Si_2O_8 + 16\ H_2O + 24\ H^+ \rightleftharpoons 4\ Na^+ + Ca^{2+} + 6\ Al^{3+} + 14\ H_4SiO_4$$

requires 24 mmol acid per mmol oligoclase dissolved. If 24 mmol acid are required per mmol of sediment dissolved, and there is 0.28 mmol of dissolved sediment per cm^3, then (24 mmol H^+/mmol Olig) (0.28 mmol dissolved Olig/cm^3 sediment) = 6.72 mmol H^+ is required per cm^3 sediment dissolved.

According to Tan (1986), acetic acid concentrations in temperate-region soils are on the order of 0.7 to 1.0 mmol/100 g. Assuming a perfectly efficient utilization of available H^- ions and a density of sediment approximately equal to that of quartz (the most abundant mineral),

$$(7.0 \times 10^{-3} \text{ to } 1.0 \times 10^{-2} \text{ mmol/g sediment}) (2.65 \text{ g/cm}^3) = 1.86 \times 10^{-2} \text{ to } 2.65 \times 10^{-2} \text{ mmol acid/cm}^3 \text{ sediment}$$

is available, two orders of magnitude less than necessary to account for the observed dissolution. The rate at which organic acids are replenished is highly variable, but the paucity of vegetation and low soil-moisture content of arid and semiarid region soils place constraints on the biotic contribution to framework grain dissolution possible in Albuquerque Basin sediments. The calculations above, though crude, suggest that dissolution is perhaps enhanced or initiated by soil microbial processes early in the sediment burial history, but that microbial metabolism alone is inadequate to generate sufficient quantities of acid. The effects of biochemical reactions in deeper parts of the basin are unknown.

The solubilities of aluminosilicate minerals such as oligoclase are strongly dependent on the partial pressure of CO_2 which, when dissolved in groundwater, equilibrates with carbonic acid (Freeze and Cherry, 1979). CO_2 in groundwater may be

derived from the atmosphere or generated by biochemical reaction. Unless CO_2 is available at constant partial pressure (so-called "open systems"), H_2CO_3 is consumed by mineral dissolution reactions. Carbonic acid consumption is particularly high in carbonate terranes. However, high pCO_2 may be preserved in groundwater if water-rock reactions in soil or vadose zones are minimal. It is probable that framework grain dissolution in Albuquerque Basin cores indicate pore water whose flow path was primarily through crystalline Precambrian rocks, rather than through Paleozoic limestones.

Compaction

There is no strong petrographic evidence for significant mechanical compaction in the middle to lower Santa Fe Group. What evidence there is exists in the form of biotite, muscovite or argillaceous rock fragments bent and distorted about rigid framework grains, and in the nature of framework grain contacts. Most samples have floating or tangential (point) contacts, but some samples have mostly longitudinal contacts.

To assess the relative importance of compaction to diagenesis and porosity reduction, a plot of minus-cement porosity versus total cement was constructed following the technique of Houseknecht (1987). The diagram (Figure 7) assumes an original, uncompacted porosity of about 44%, which is an estimate based on naturally and artificially packed sands that are well sorted or better (Beard and Weyl, 1973). The diagonal lines in Figure 7 are lines of equal intergranular macroporosity determined from 300 point-counts; samples are grouped by their dominant cement (Appendix C) and

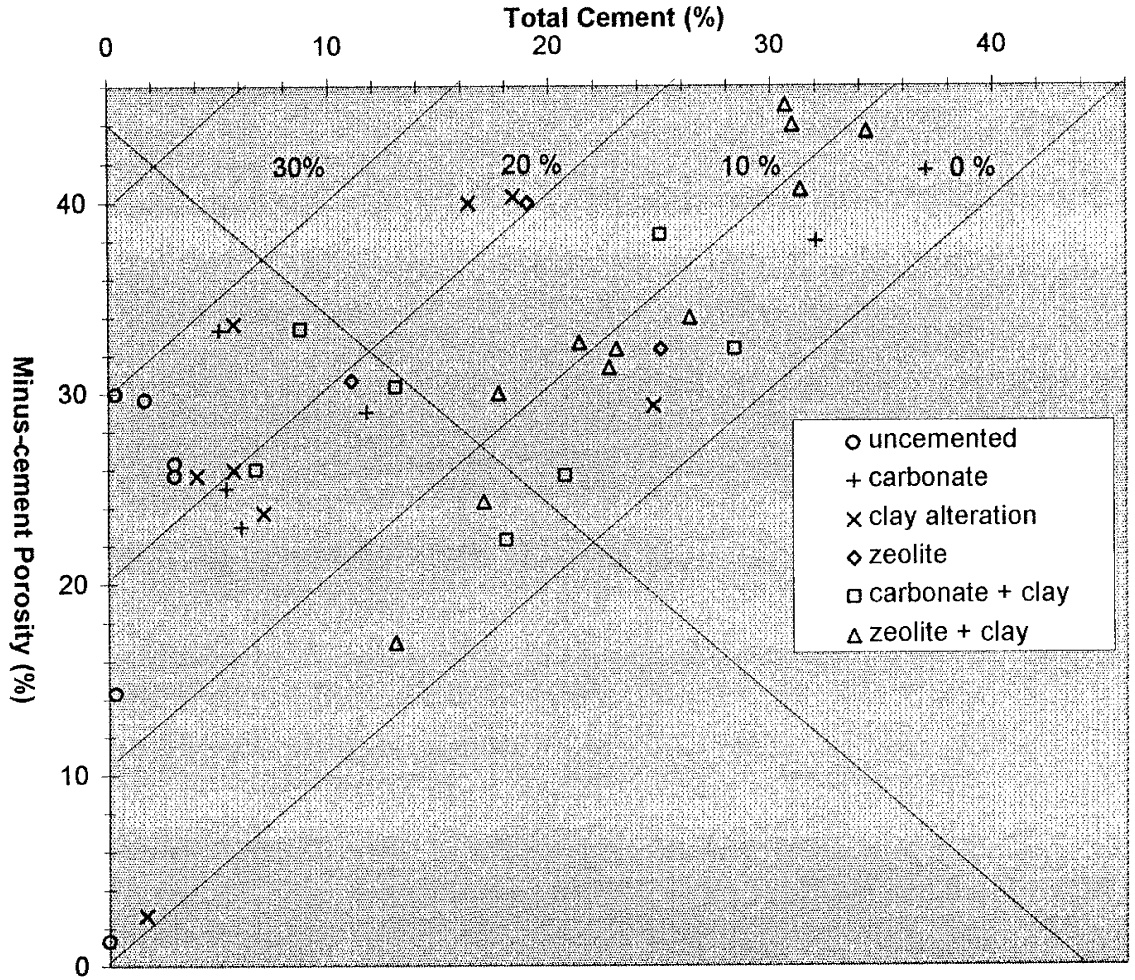

Figure 7. Minus-cement porosity versus total cement for each of the dominant cement types (after Houseknecht, 1987). NE-SW diagonal lines are lines of equal intergranular volume (post-cementation/compaction); NW-SE diagonal line separates graph into a cementation-dominated field (above) and a compaction-dominated field (below).

plotted as separate data series on the diagram. "Uncemented" samples contain less than about 4% cement, and cluster near the y-axis at around 25-30% minus-cement porosity (plus two outliers at 2 and 12%). The remaining samples are scattered across the diagram, plotting on either side of the dividing line between the cementation and compaction fields.

Because of their relatively large crystal size and tendency to encompass several grains, carbonate cements occupy the largest pore volume of any cement type, and are more capable than zeolites or clay of preserving original intergranular spacing upon burial. Though calcite-cemented samples are among the group of samples in Figure 7 with the highest minus-cement porosity, zeolite and clay samples are also present, suggesting porosity reduction by compaction has not been an active process. On the other hand, uncemented samples have less minus-cement porosity than most samples, possibly indicating moderate compaction of at least some of the cores.

A problem with Houseknecht's method of estimating porosity loss, pointed out by Pate (1989) and Ehrenberg (1989), is that there is a dynamic reduction in bulk sediment volume as compaction progresses. Point-counting can only address existing intergranular volume and relate it to an empirical estimate of original porosity. Porosity loss due to compaction will thus be slightly higher than indicated by Houseknecht's figure.

Houseknecht assumes for the diagram that sands are well-sorted or better, that grains are of similar sphericity, are nonductile, and have minimal secondary porosity. Ideally, only samples with similar textural characteristics will have been selected for compaction analysis. Because the Albuquerque sample set is relatively small, all sample

data was used in the construction of Figure 7 regardless of textural characteristics: restricting the sample set would result in too few data points for comparison. None-the-less, the exercise was largely inconclusive.

LITHOFACIES AND INDICATORS OF PROVENANCE

Lithofacies, as defined by Hawley and Haase (1992); Hawley et al. (1995), are shown for each sample on Table C, Appendix C. An underlying assumption in subdividing core samples into lithofacies is that volcanic rock fragments indicate fluvial deposition, due to the absence of an immediate source area. Thin sections provide no indication whether the fluvial system was a through-going, interbasinal system or a closed, internally drained system, but studies of regional sediment dispersal patterns (e.g., Ingersoll et al., 1990; Love and Young, 1983; Lozinsky and Tedford, 1991) suggest cores are from stratigraphic levels that pre-date a through-going axial Rio Grande. Regional volcanic centers capable of supplying volcaniclastics to the Albuquerque basin include the Latir-Questa volcanic field (Dungan et al., 1979), the older volcanic pile of the Jemez Mountains (Keres Group of Bailey et al., 1969), the Espinaso Formation (Smith et al., 1991), or the Mogollon-Datil field (Chamberlin et al., 1994).

Volcanic rock fragments, silicified rock fragments and feldspars from deep crustal sources are petrographically similar once they have become altered. These grains were collectively termed "undifferentiated rock fragments" where they could not be distinguished from one another. Because volcanic or undifferentiated rock fragments are present in all thin sections, a fluvial origin cannot be ruled out for any of the core. Fine-grained samples may indicate termination of the drainage system in a low energy basin floor or playa environment.

The occurrence within the same thin section of granitic-gneissic and volcanic rock fragments indicates considerable mixing of sediment from diverse source areas. Possible mechanisms for sediment mixing include 1) stream-channel integration of fluvially-derived volcaniclastics with piedmont alluvium delivered to the axial basin by up-stream arroyo systems, such as the ancestral Tijeras or Embudo; 2) fluvial transport of volcanic debris and plutonic-metamorphic rocks, both derived from an area to the north; 3) incision of pre-existing fluvial facies by piedmont arroyos that downcut into the footwall block of subsiding rift segments, reworking the volcanic component into prograding alluvial fans.

Granitic and metamorphic detritus within the Gabaldon Badlands section of the Sierra Ladrones Formation was interpreted by Lozinsky and Tedford (1991) to have originated in a source area to the northwest. Unless the Sandia block was sufficiently uplifted by early to mid Santa Fe time to expose Precambrian basement, sediment within the Albuquerque Basin would have come from the same plutonic-metamorphic source area as sediment in basins to the south, such as the Gabaldon section. A Sandia-Manzano source area for granitic-gneissic and sedimentary rock fragments in West Mesa cores is improbable because of the east-dipping structure of the north Albuquerque Basin.

Volcanic detritus in West Mesa wells is mostly pumiceous, displaying devitrification textures and a high degree of alteration to clay. Volcanic rock fragments occur below depths of 1300 feet in Cerro Colorado, and below 2000 feet in SAF 1. Though transport distances for these clasts are conceivably quite large, a likely source area for West Mesa volcanic rock fragments is the older volcanic pile of the Jemez

mountains (Keres Group of Bailey et al., 1969) or deposits of the Latir-Questa caldera system (Lipman and Reed, 1989; Dungan et al., 1989).

Although clast lithologies described earlier in the Sandstone Petrology section occur in virtually all core samples, there is a noticeable difference in the modal composition of samples from East and West Mesa wells (Figure 2). West Mesa samples Cerro Colorado 1 and SAF 1 are more quartzose and less feldspathic than East Mesa samples, and generally contain fewer volcanic rock fragments. Higher percentages of monocrystalline quartz, and the presence in some samples of recycled quartz overgrowths suggest a contribution to the West Mesa from an older sedimentary source, probably Mesozoic rocks of the Colorado Plateau region to the west and northwest.

In Figures 8 to 11, the relative abundance of framework grains is plotted against well depth for each of the four wells. East Mesa wells show a higher degree of variability in clast abundance across their depth profile (Figures 10 and 11) than do West Mesa wells (Figures 8 and 9). This implies a more dynamic sediment delivery system for East Mesa wells (both of which are located in a zone of inferred mixing of ancestral Rio Grande and Tijeras Arroyo fan deposits). The greater mineralogical maturity and consistency in grain abundance of West Mesa wells implies a more stable sediment supply.

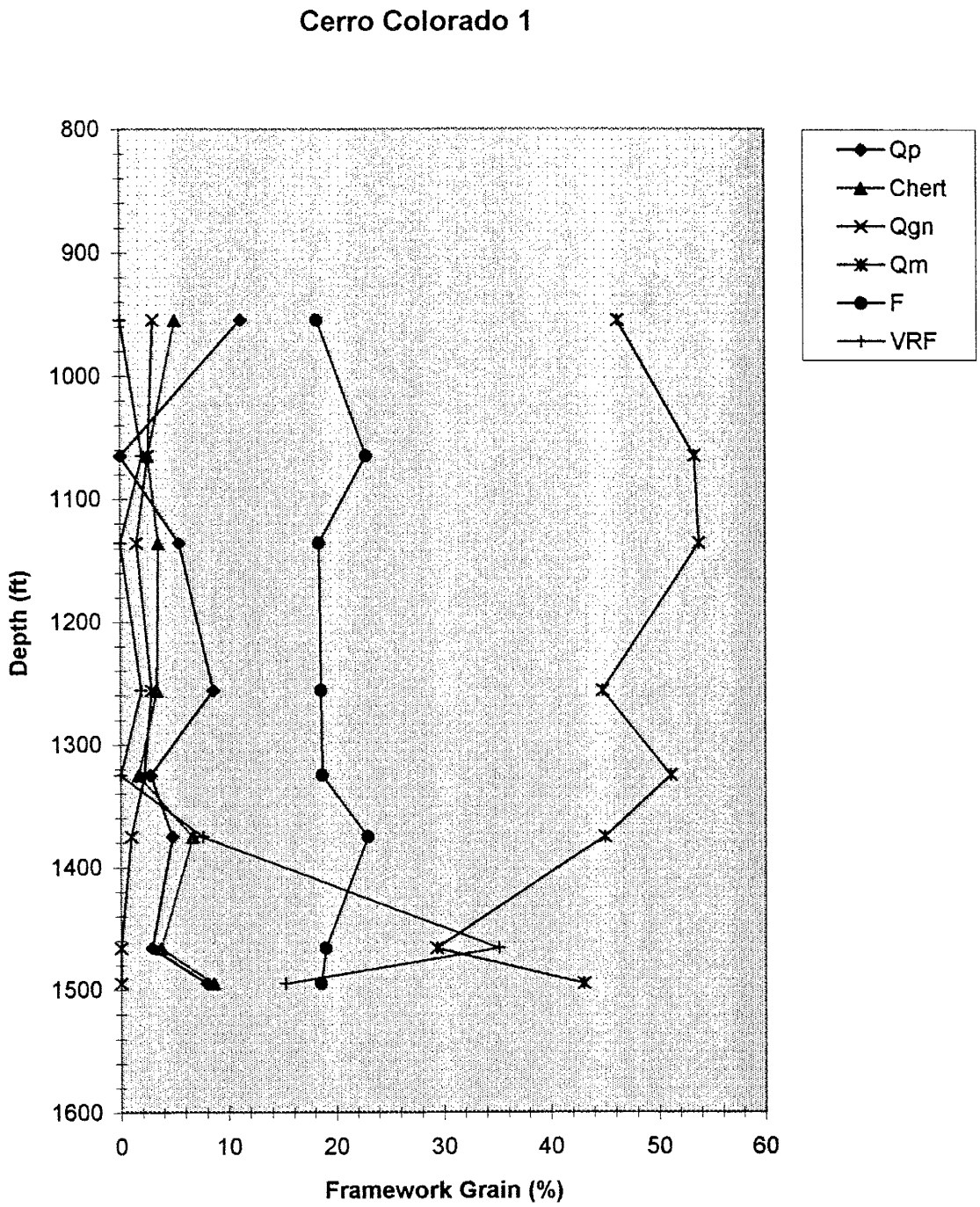

Figure 8. Relative abundance of framework grains versus well depth for Cerro Colorado 1. Definition of counted parameters in Appendix A.

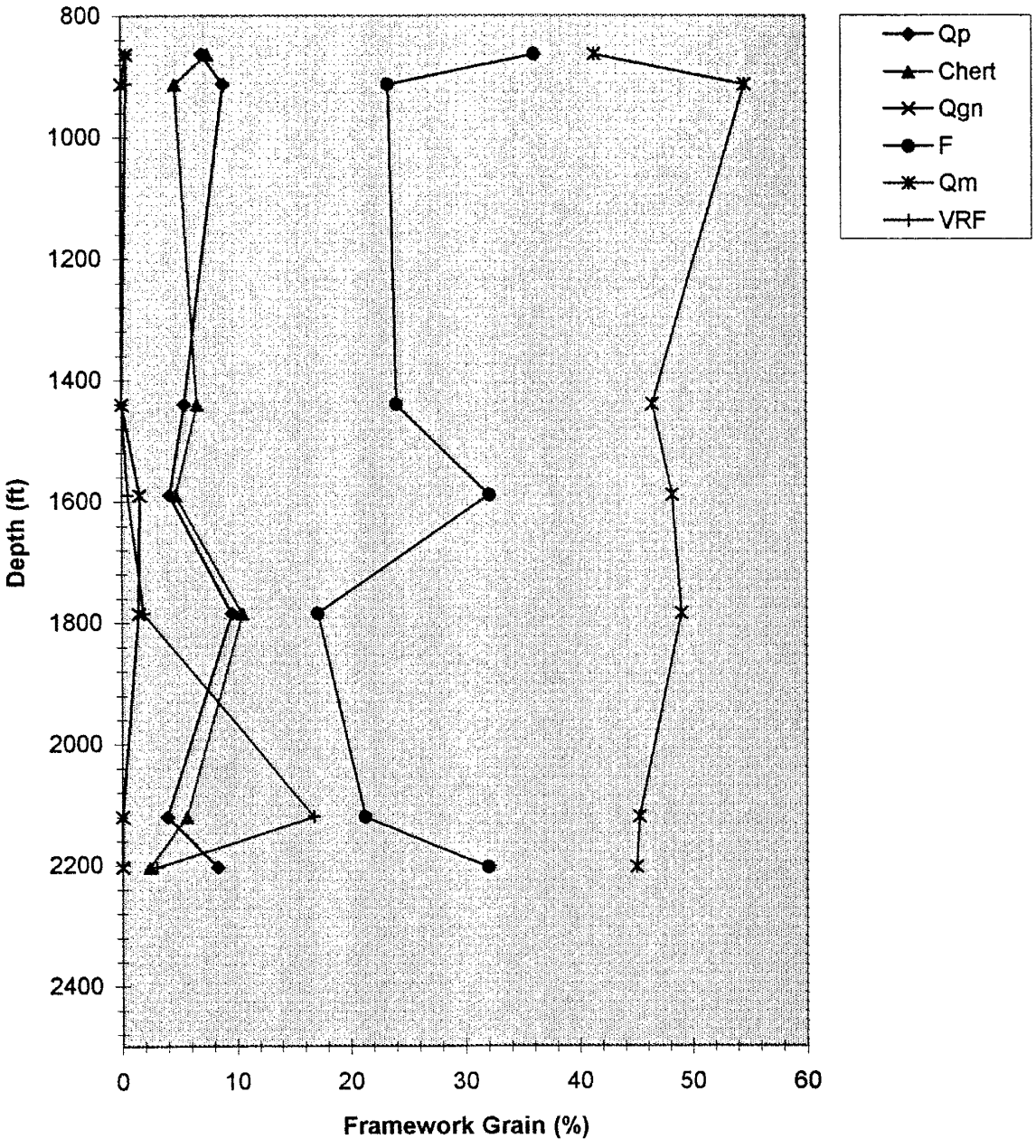

Figure 9. Relative abundance of framework grains versus well depth for SAF 1. Definition of counted parameters in Appendix A.

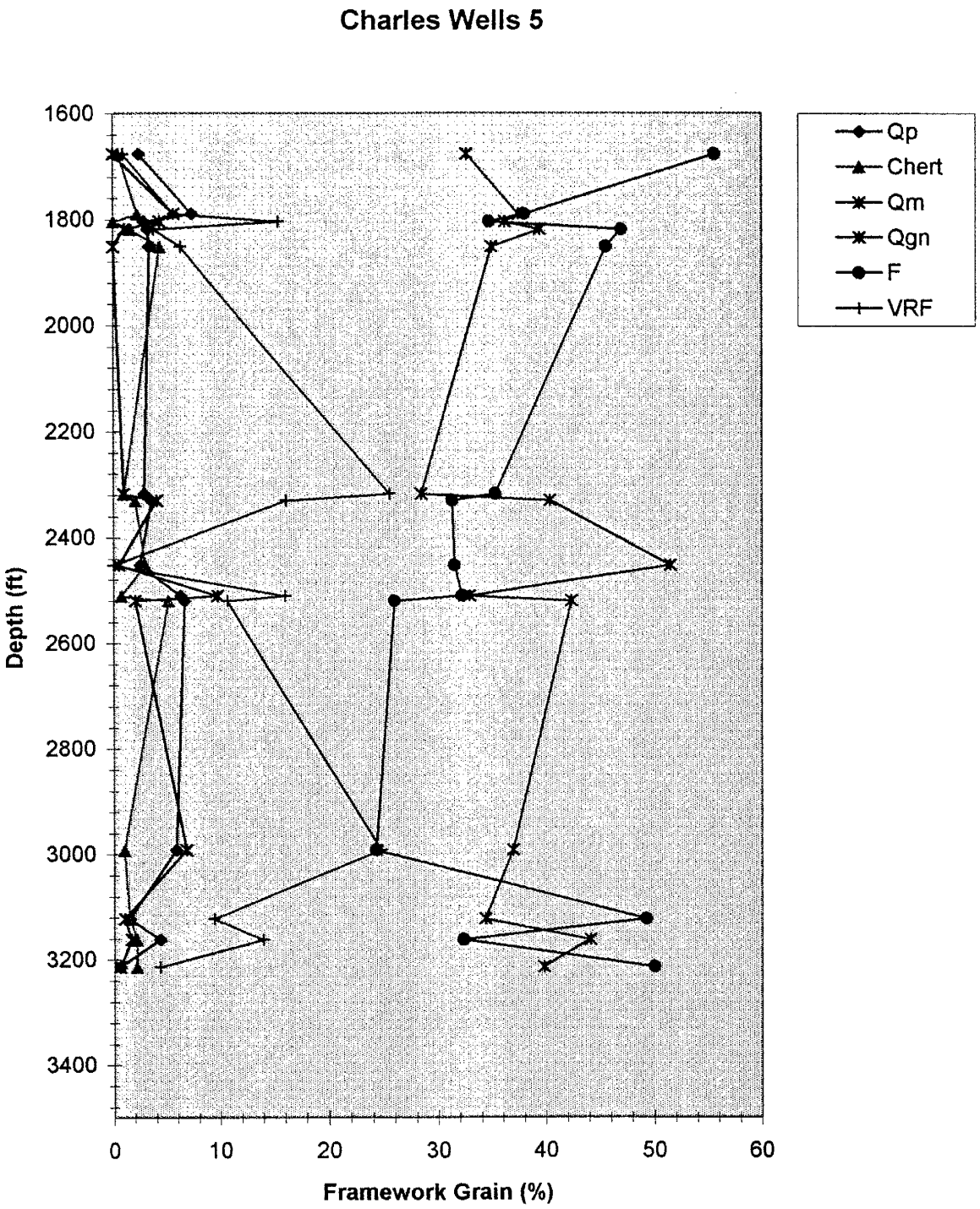

Figure 10. Relative abundance of framework grains versus well depth for Charles Wells 5. Definition of counted parameters in Appendix A.

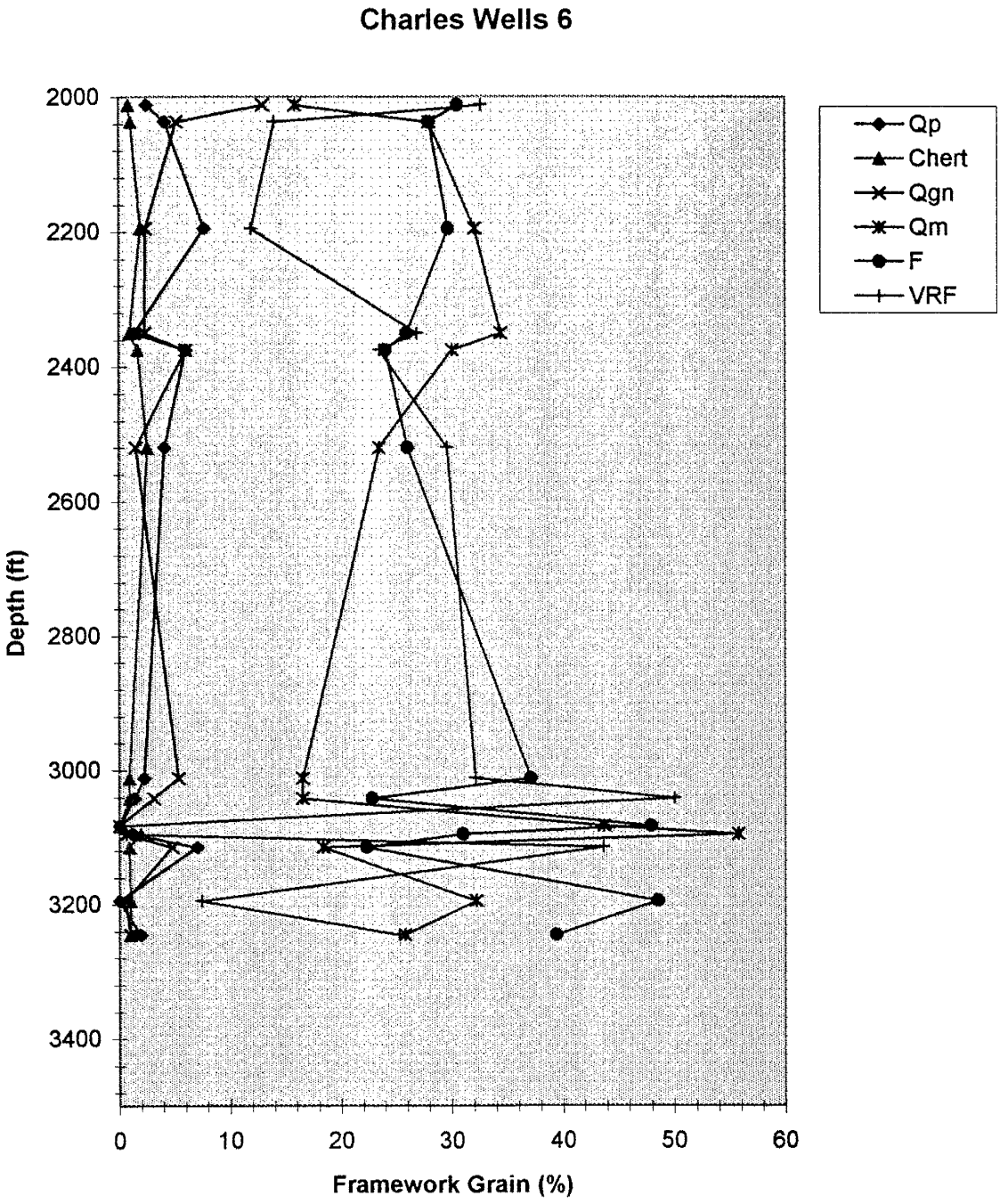

Figure 11. Relative abundance of framework grains versus well depth for Charles Well 6. Definition of counted parameters in Appendix A.

GEOCHEMICAL MODELING

Changes in pore water chemistry and mineral mass during low-temperature diagenesis were modeled using the FORTRAN IV program PHREEQE (Parkhurst et al., 1990). The purpose of modeling was to evaluate mineral phase coexistence and to determine whether those phases could be produced sequentially from a simple starting solution. PHREEQE, one of a series of programs developed by the United States Geological Survey to simulate geochemical equilibrium, calculates the pH, pe, ionic strength, and saturation state of a solution, and the mass transfer of minerals into or out of the aqueous phase.

Methods

Thermodynamic data for clay and zeolite species are not widely available, so data for minerals whose formulas are similar to, but simpler than the sample minerals were obtained from the literature. Microprobe results indicate clay species contain Na^+ and Ca^{2+} in approximately equal amounts and contain relatively lesser amounts of K^+. Zeolites are calcic heulandite. For simulation purposes, idealized Ca-smectite, Na-smectite, illite and calcite were modeled using mineral formula and free energies and enthalpies of formation from Woods and Garrels (1987); data for calcic heulandite is from Johnson et al. (1985). Equilibrium constants and free energies and enthalpies of reaction were calculated for mineral dissociation reactions and input to the program. Because the temperature of Albuquerque Basin waters is variable, the Van't Hoff

equation was used by the program to address the temperature dependence of equilibrium constants. Activity coefficients were calculated using the Debye-Hückel formula.

Two separate fluid evolution schemes were tried. In the first scheme, products of feldspar, aegerine, actinolite and biotite dissociation reactions were added to a pure-water starting solution and allowed to equilibrate with the simplified authigenic phases. In the second scheme, water quality data supplied by the City of Albuquerque Water Utilities Division for CW6, SAF1 and CC1 was input to the program and defined as the starting solution. Mean values for seventeen analytes, sampled during the period January 1992 to April 1994, were used. The addition of dissolved components was also required in the latter scheme to bring the solution to equilibrium with all the simulated phases. Reaction input in the second scheme was defined by dissolution of oligoclase.

Results

Each of the authigenic phases was successfully simulated in scheme 1 by dissolving sufficient quantities of detrital minerals into a pure water starting solution (Table 3). However, no paragenetic relationships could be defined: trials involving multiple phases always resulted in metastable or non-sensical solutions that had saturation indices greater than zero, or that dissolved non-existing authigenic phases. In contrast, trials using water quality data as a starting solution, the second scheme, simulated both paragenesis and mass transfer in the precipitation of each product mineral.

Table 3. Pore fluid composition and saturation state in the K_2O-Na_2O-CaO system: results of geochemical simulation using PHREEQE (Parkhurst et al., 1993) and a pure-water starting composition.

Equilibrium Mineral Phase	Solution pH	Solution Alkalinity ($x10^{-5}$)	Detrital Minerals Dissolved/kg H_2O (mol $x10^{-6}$)
heulandite	8.6366	4.4038	0.8468
Ca-smectite	8.7066	5.8446	1.1239
illite	8.8063	9.2807	1.7847
Na-smectite	8.8064	9.2860	1.7860
calcite	7.0466	6.2882E-3	1.1056E-3

Table 4 lists the results of simulations using water analyses from CW6, CC1 and SAF1. Shown are the mineral phase (or phases) maintained in equilibrium with the solution, the solution stability (defined by its saturation index) and the number of micro moles of each phase dissolved or precipitated in reaching equilibrium. Results of trials using water quality data (scheme 2) are discussed below by well-of-origin.

Charles Wells 6

The initial solution, using CW6 water analyses as a starting point, is supersaturated with respect to all model phases (Table 4). Trial number 9, a two-phase equilibria (point A, Table 4), is the first simulation to result in a stable solution. Each of the single-phase trials, and most multiphase trials are supersaturated in at least one other phase. Some trials produced non-sensical results. For example, trial 6 (Ca-smectite/heulandite) resulted in a stable solution (i.e., no saturation index greater than zero) but required destruction of 118 mmol authigenic smectite before any smectite had

yet been formed by the model. The only way that the model could produce phases other than heulandite and calcite was by hydrolyzing detrital oligoclase. Trial 23 (point B) introduces Ca-smectite into the system by dissolving 77.18 mmol oligoclase; 230 mmol heulandite precipitate in the reaction, and 3 mmol calcite dissolve (leaving 61.7 mmol calcite from point A). The mass value of 0.0 mmol for Ca-smectite means that the solution is just saturated with respect to smectite, but no smectite has yet formed. In trial 27 (point C), illite enters the system following the addition of 747 mmol oligoclase. Each of the existing phases continued to precipitate in this step, including a very large amount of calcite (1.6×10^6 μmol). A fraction of this calcite (73 mmol) was lost in the final step (trial 28, point D) to bring Na-smectite into the system. The pH, alkalinity and ionic strength of the pore fluid became progressively elevated as the fluid equilibrated with each additional phase.

Cerro Colorado 1

In trial number 1 (point A, Table 3) a very small amount of heulandite precipitates as the first equilibrium phase. No other phases could be generated without addition of dissolved oligoclase. Trial 12 (point B) resulted in the introduction of three additional phases to the system, calcite, Ca-smectite and illite, following addition of 575 mmol oligoclase. The final phase, Na-smectite, was introduced in trial 13 (point C, Table 3) after 1,936 mmol dissolved oligoclase were added to solution. Again, the pore fluid became increasingly alkaline with reaction progress, but less so than in CW6.

Soil Amendment Facility 1

The reaction path modeled for SAF1 is similar to that of CC1 in that heulandite equilibrated with the starting solution (trial 1, point A) and in that the second step in the reaction path was a multiphase equilibria (trial 12, point B). The SAF1 path differs from the CC1 and CW6 paths in its failure to introduce Na-smectite as a product phase, and in the relatively low amount of heulandite produced. No reactions beyond point B succeeded without consuming more product phases than were present in the system.

Discussion of Modeling Results

In the model, feldspar hydrolysis resulted in a step-wise progression in products where each new phase continued to precipitate as subsequent phases equilibrated with the solution. Heulandite, the first phase to precipitate in the model, was predicted to occur in abundance in all wells. However, a discrepancy exists between the model and the system it mimics. Heulandite was not observed with its projected frequency, and thin-section samples were seldom seen to possess more than one or two authigenic phases. This is explained in part by the simplifications used in constructing the model. Modeling illite and the calcium and sodium smectites as independent phases was a way to simulate interstratified clays of varying composition. Busenberg (1978) noted chemical compositions of clay precipitated from artificial feldspar weathering experiments (with high initial Ca, Mg and SiO_2 concentrations) were not only complex, but varied over time. Differences between the discrete product sequence predicted by the model and petrographic observation is diminished if clay phases are considered collectively. The

failure of the model to precipitate Na-smectite in SAF1 likely indicates clays formed in these waters are more calcic than their counterparts in the other wells. Zeolites, which can form from the same starting materials as clay, are favored by lower ratios of hydrogen to sodium, potassium and calcium, and by lower activities of magnesium (Hay, 1978).

Table 4 shows that heulandite precipitated from the starting solution without affecting the solution's ending pH, alkalinity or ionic strength (trial 1, all wells). The formation of additional phases, however, required dissolution of detrital minerals and produced a change in pore fluid chemistry. Water quality analyses (the starting solution) must therefore reflect either 1) the composition of the shallow aquifer only, and implies that total dissolved solids increase with depth; or 2) the average composition of water mixed from a number of relatively small aquifer compartments, some of which may equilibrate with secondary minerals. Water in middle and lower Santa Fe Group aquifer zones has had a longer residence time, relative to the shallow aquifer, within which to hydrolyize detrital grains. Deeper water is also less susceptible to dilution by recharge. However, there is no data to either confirm or deny the assertion that water quality data reflects only the shallow aquifer. Water analyses, collected at the wellhead, do not pertain to a specific depth, and sidewall cores were collected from depths below the screened interval. The alternate idea, that water chemistry varies across discrete aquifer zones, requires that pockets of more saline water be isolated from meteoric recharge. Such pockets are conceivable within fine-grained sediments that act as barriers to groundwater flow. But petrographic observations suggest authigenesis occurs in

"cleaner" sands lacking silt and detrital clay, with supposedly higher permeability. Low fluid flux through clean sandy zones, or restricted communication between sandy zones and meteoric recharge may result from impeding lenses or beds of fine-grained material (or cemented or gouge-filled faults in certain areas). Outcrop analogs of the Middle and Lower Santa Fe consist of discontinuous sandy lenses that are traceable for only several meters before pinching out against silty or clayey units (Galusha and Blick, 1971; Lozinsky, 1988; Lozinsky and Tedford, 1991). In all probability, both depth and small-scale aquifer compartmentalization may operate to promote diagenesis.

Though there is no apparent correlation between framework-grain dissolution and authigenesis, it is reasonable to assume, based on conservation of mass arguments, that precipitation is associated with dissolution. The low correspondence may indicate transport (dispersion) of dissolved constituents away from their grain of origin. The quantity of dissolved mineral matter, calculated from point-counts of intragranular macroporosity, is 0.28 moles per liter of water (Diagenesis/Dissolution Processes section). This is two orders of magnitude greater than required by the model to equilibrate with the last clay phase (Table 4). Many of the products of mineral hydrolysis must therefore have remained in solution, dispersed throughout the aquifer matrix.

CONCLUSIONS

Basic questions underlying this investigation concern the factors controlling diagenesis, and what effect these factors have had on water quality and availability. These questions were approached by examining both the allogenic and authigenic composition of the basin-fill, and by drawing certain inferences about the geochemical conditions that would account for the observed mineral species and textures. While the set of sidewall cores on which the study is based provided a unique glimpse into the geochemical environment of the lower Santa Fe Group, they were collected selectively from sandy intervals in only a few widely separated wells. Thin-sectioned samples display a high degree of textural and compositional variability, both between wells and within the same well. Over the course of the investigation, it proved difficult to group samples by common characteristics and to define consistent patterns or trends within the groupings. Framework grain types are not homogeneously distributed, nor are the products of their dissolution and alteration. Despite the small sample population, some generalizations may be drawn.

Provenance

Differences in clast composition between East and West Mesa wells suggest dissimilar provenance, and down-hole variations in clast abundance imply that a more dynamic sediment delivery system existed on the East Mesa. Plutonic and metamorphic sediments were probably derived from the northwest, while volcaniclastic sediments

originated in the Jemez, Espinaso or Latir volcanic fields to north. West Mesa wells CC1 and SAF1 have a west to northwest sedimentary source area (of predominantly Mesozoic rocks) not shared by East Mesa wells CW5 and CW6.

Dissolution

Skeletal grain content of Albuquerque samples ranges from 2 to 4 percent of total sandstone volume, and is slightly higher for East Mesa wells than for West Mesa wells. While dissolution of framework grains may be initiated or enhanced by microbial processes early in the sediment burial history, prolonged contact with groundwater (hydrolysis) is a more plausible mechanism for the generation of secondary porosity. Feldspar hydrolysis has released approximately 0.3 moles dissolved mineral matter per liter of water, far more than the $3x10^{-3}$ moles required by the geochemical model to equilibrate with the last phase in the paragenetic sequence. "Surplus" solutes are dispersed through deeper aquifer zones.

Cementation and Alteration

Diagenetic minerals present in the samples are clay (smectite and interlayered illite/smectite), zeolites and calcite. Zeolites are most often (but not always) associated with clay. Calcite occurs as both isolated, poikilitic crystals encompassing several adjacent pores, and micritic patches restricted to a single pore. Clay is interpreted petrographically to occur in microporous zones as a pore-filling or a psuedomorphous replacement of framework grains.

Results of geochemical simulations indicate the pH, alkalinity and ionic strength of pore waters become progressively elevated as feldspar dissolves to precipitate each phase in the system. A theoretical paragenesis of model phases, based on thermodynamic considerations alone, is heulandite-calcite-Ca smectite-illite-Na smectite. Though modeled as discrete species, clay phases are actually compositional variants of a more or less generic phyllosilicate structure.

Equilibrium conditions existing at a local scale control both the occurrence and speciation of diagenetic minerals. These conditions are in turn determined by aquifer heterogeneity and the hydrodynamic properties of groundwater within small-scale aquifer compartments.

REFERENCES

Aldrich, M. J., Jr., Chapin, C. E., and Laughlin, A. W., 1986, Stress history and tectonic development of the Rio Grande Rift, New Mexico: Journal of Geophysical Research, vol. 91, no. B6, pp. 6199-6211.

Allen, P. A. and Allen, J. R. L., 1990, Basin analysis-principles and applications: Blackwell Scientific, Oxford, England, pp. 228-238.

Bachman, G. O., and Mehnert, H. H., 1978, New K-Ar dates and the late Pliocene to Holocene geomorphic history of the central Rio Grande region, New Mexico: Geological Society of America Bulletin, vol. 89, pp. 283-292.

Bailey, R. A., Smith, R. L., and Ross, C. S.,1969, Stratigraphic nomenclature of volcanic rocks in the Jemez Mountains, New Mexico: United States Geological Survey Bulletin 1274-P, 19 pp.

Beard, D. C., and Weyl, P. K., 1973, Influence of texture on porosity and permeability of unconsolidated sand: American Association of Petroleum Geologists Bulletin, vol. 57, pp. 349-369.

Blatt, H. and Christie, J. M.,1963, Undulatory extinction in quartz of igneous and metamorphic rocks and its significance in provenance studies of sedimentary rocks: Journal of Sedimentary Petrology, vol. 33, pp. 559-579.

Bloch, S. and Franks, S. G., 1993, Preservation of shallow plagioclase dissolution porosity during burial: implications for porosity prediction and aluminum mass balance: AAPG Bulletin, vol. 77, no. 9, pp. 1488-1501.

Bjørlykke, K., 1983, Diagenetic reactions in sandstones in Parker, A. and Sellwood, B. W. (eds.), Sediment Diagenesis: Reidel Publishing Co., pp. 169-213.

Brindley, G. W., 1981, X-ray identification (with ancillary techniques) of clay minerals, in Longstaffe, F. J. (ed.), Clays and the resource geologist: Mineralogical Association of Canada Short Course Handbook, Vol. 7, pp. 22-35.

Bryan, K., 1938, The Ceja del Rio Puerco: a border feature of the basin and range province in New Mexico, II. Geomorphology: Journal of Geology, vol. 46, no. 1, pp. 1-16.

Bryan, K, and McCann, F. T., 1937, The Ceja del Rio Puerco: a border feature of the basin and range province in New Mexico, I. Stratigraphy and structure: Journal of Geology, vol. 45, no. 8, pp. 801-828.

Busenberg, E., 1978, The products of the interaction of feldspars with aqueous solutions at 25• C: Geochimica et Cosmochimica Acta, vol. 42, pp. 1679-1679.

Carroll, D., 1970, Clay minerals: a guide to their X-ray diffraction: Geological Society of America Special Paper 126, 80 pp.

Chamberlin, R. M.,1983, Cenozoic domino-style crustal extension in the Lemitar Mountains, New Mexico: a summary: New Mexico Geological Society Guidebook 34, pp. 111-118.

Chamberlin, R. M., Kues, B. D., Cather, S. M., Barker, J. M., and McIntosh, W. C., 1994, Mogollon Slope, West-Central New Mexico and East-Central Arizona: New Mexico Geological Society Guidebook 45, 335 pp.

Chapin, C. E., 1988, Axial basins of the northern and central Rio Grande rifts, in Sloss, L. L., ed., Sedimentary Cover--North American craton: U.S.; the Geology of North America vol. D-2: Boulder, Colorado, Geological Society of America, p. 165-170.

Chapin, C. E. and Cather, S., 1994, Tectonic setting of the axial basins of the northern and central Rio Grande rift: Geological Society of America, Special Paper 291, pp. 5–25.

Colella, C., Aiello, R. and Porcelli, C., 1978, Hydration as an early stage in the zeolitization of natural glass, in Sand, L. B. and Mumpton, F. A. (eds.), Natural zeolites: occurrence, properties, use: Pergamon Press Ltd., Oxford, pp. 345-350.

Darton, N. H., 1922, Geologic structure of parts of New Mexico: United States Geological Survey Bulletin 726, pp. 173-275.

Denny, C. S., 1940, Santa Fe Formation in the Espanola Valley, New Mexico: Geological Society of America Bulletin vol. 51, pp. 677-694.

Dickinson, W. R., 1970, Interpreting detrital modes of graywacke and arkose: Journal of Sedimentary Petrology, vol. 40, no. 2, pp. 695-707.

Dungan, M. A., Thompson, R. A., and Stormer, J. S., 1989, Rio Grande rift volcanism: northeastern Jemez zone, New Mexico: New Mexico Bureau of Mines and Mineral Resources Memoir 46, pp. 435-483.

Ehrenberg, S. N., 1989, Assessing the relative importance of compaction processes and cementation to reduction of porosity in sandstones: Discussion; compaction and porosity evolution of Pliocene sandstones, Ventura Basin, California: Discussion: American Association of Petroleum Geologists Bulletin, vol. 73, no. 10, pp. 1274-1276

Faure, G., 1991, Principles and applications of inorganic geochemistry: Macmillan Publishing Company, New York, NY, variously paginated.

Freeze, R. A., and Cherry, J. A., 1979, Groundwater: Prentice-Hall, Inc., Englewood Cliffs, N. J., p. 95.

Folk, R. L., 1974, Petrology of Sedimentary Rocks: Hemphill Publishing Company, Austin, 182 pp.

Galusha, T., 1966, The Zia Sand Formation, new early to medial Miocene beds in New Mexico: American Museum Novitates 2271, 12 pp.

Galusha, T., and Blick, J. C., 1971, Stratigraphy of the Santa Fe Group, New Mexico: American Museum of Natural History Bulletin, vol. 144 article 1, 128 pp.

Gazzi, P., 1966, Le arenarie del flysch sopracretaceo dell'Appennino modenese; correlazioni con il flysch di Monghidoro: Mineralogica e Petrografica Acta, vol. 12, pp. 69-97.

Hawley, J. W., compiler, 1978 Guidebook to the Rio Grande rift in New Mexico and Colorado: New Mexico Bureau of Mines and Mineral Resources, Circular 163, 241 pp.

Hawley, J. W., and Haase, C. S., 1992, Hydrogeologic framework of the northern Albuquerque basin: New Mexico Bureau of Mines and Mineral Resources Open-File Report 387

Hawley, J. W. and Love, D. W., 1991, Quaternary and Neogene landscape evolution: A transect across the Colorado Plateau and Basin and Range provinces in west-central and central New Mexico, in Julian, B., and Zidek, J., eds., Field guide to geologic excursions in New Mexico and adjacent areas of Texas and Colorado: New Mexico Bureau of Mines & Mineral Resources, Bulletin 137, pp. 105-148 (130-133).

Hawley, J. W., Haase, C. S., and Lozinsky, R. Pp., 1995, An underground view of the Albuquerque Basin, in Ortega-Klett, C., ed., Proceedings of the 39th Annual New Mexico Water Conference, "The water future of Albuquerque and Middle Rio Grande Basin": New Mexico Water Resources Research Institute Report 290, pp. 37-55.

Hay, R. L., 1978, Geologic occurrence of zeolites, in Sand, L. B. and Mumpton, F. A. (eds.), Natural zeolites: occurrence, properties, use: Pergamon Press Ltd., Oxford, pp. 135-143.

Hay, R. L., 1966, Zeolites and zeolitic reactions in sedimentary rocks: Geological Society of America Special Paper No. 85.

Hayden, F. V., 1869, Preliminary field report of the United States Geological Survey of Colorado and New Mexico: U. S. Government Printing Office, Washington, D. C., 155 pp.

Henry, C. D., and Price, J. G., 1986, Early basin and range development in trans-Pecos Texas and adjacent Chihuahua: magmatism and orientation, timing, and style of extension: Journal of Geophysical Research, vol. 91, no. B6, pp. 6213-6224.

Houseknecht, D. W., 1987, Assessing the relative importance of compaction processes and cementation to reduction of porosity in sandstones: American Association of Petroleum Geologists Bulletin, vol. 71, pp. 633-642.

Ingersoll, R. V., Cavazza, W., Baldridge, W. S., and Shafiqullah, M., 1990, Cenozoic sedimentation and paleotectonics of north-central New Mexico: Implications for initiation and evolution of the Rio Grande rift: Geological Society of America Bulletin, vol. 102, pp. 1280-1296.

Johnson, G. K., Flowtow, H. E., and O'Hare, P. A. G., 1985, Thermodynamic studies of zeolites: heulandite: American Mineralogist, vol. 70, pp. 1065-1071.

Kelley, V. C.,1977, Geology of Albuquerque basin, New Mexico: New Mexico Bureau of Mines and Mineral Resources Memoir 33, 60 pp.

Kharaka, Y. K., Law, L. M., Carothers, W. W., and Goerlitz, D. F., 1986, Role of organic species dissolved in formation waters from sedimentary basins in mineral diagenesis, in Gautier, D. L. (ed.), Roles of organic matter in sediment diagenesis: Society of Economic Paleontologists and Mineralogists Special Publication 38, pp. 111-112.

Kieft, T. L., 1991, Soil microbiology in reclamation of arid and semiarid lands, in Skujins, J. (ed), Semiarid lands and deserts: soil resource and reclamation: Marcel Dekker, Inc., New York, pp. 209-256.

Kottlowski, F. E., 1953, Tertiary-Quaternary sediments of the Rio Grande valley in southern New Mexico: New Mexico Geological Society Guidebook 4, pp. 144-148.

Lambert, P. W., 1968, Quaternary stratigraphy of the Albuquerque area, New Mexico: unpublished Ph.D. dissertation, University of New Mexico, 329 pp.

Lambert, P. W., Hawley, J. W., and Wells, S. G., 1982, Supplemental road-log segment III-S: Urban and environmental geology of the Albuquerque area: New Mexico Geological Society, Guidebook 333, pp. 977-124.

Love, D. W. and Young, J. D., 1983, Progress report on the late Cenozoic geologic evolution of the lower Rio Puerco, in Chapin, C. E. and Callender, J. F. (eds), Socorro II: New Mexico Geological Society 34th Field Conference Guidebook, pp. 277-284.

Lozinsky, R. P., 1988, Stratigraphy, sedimentology, and sand petrology of the Santa Fe Group and pre-Santa Fe Tertiary deposits in the Albuquerque basin, central New Mexico: Unpublished Ph.D. dissertation, New Mexico Institute of Mining and Technology, 298 pp.

Lozinsky, R. P., 1994, Cenozoic stratigraphy, sandstone petrology, and depositional history of the Albuquerque Basin, central New Mexico: Geological Society of America, Special Paper 291, pp. 73-81.

Lozinsky, R. P. and Tedford, R. H., 1991, Geology and paleontology of the Santa Fe Group, southwestern Albuquerque basin, Valencia County, New Mexico: New Mexico Bureau of Mines and Mineral Resources Bulletin 132, pp. 8-24.

Lundegard, P. D. and Land, L. S., 1986, Carbon dioxide and organic acids: their role in porosity enhancement and cementation, Paleogene of the Texas Gulf Coast, in Gautier, D. L. (ed.), Roles of organic matter in sediment diagenesis: Society of Economic Paleontologists and Mineralogists Special Publication 38, pp. 129-146.

Machette, M. N., 1985, Calcic soils of the southwestern United States, in Weide, D. L., ed., Quaternary soils and geomorphology of the American Southwest: Geological Society of America Special Paper 203, pp. 1–21.

Mack, G. H., and Grigsby, J. D.,1985, Mechanical and chemical diagenesis of the Haynor Ranch and Rincon Valley formations (Santa Fe Group, Miocene), San Diego Mountain, New Mexico: New Mexico Geology, vol. 7 no. 3, pp. 45-48.

Mason, B. and Sand, L. B., 1960, Clinoptilolite from Patagonia. The relationship between clinoptilolite and heulandite: American Mineralogist, vol. 45, pp. 341-350

May, S. J. and Russell, L. R., 1994, Thickness of the syn-rift Santa Fe Group in the Albuquerque Basin and its relation to structural style: Geological Society of America, Special Paper 291, pp. 113-123.

McIntosh, W. C., Sutter, J. F., Chapin, C. E., Osburn, G. R., and Ratte, J. C., 1986, A stratigraphic framework for the eastern Mogollon-Datil volcanic field based on paleomagnetism and high-precision $^{40}Ar/^{29}Ar$ dating of ignimbrites--a progress report: New Mexico Geological Society Guidebook 37, pp. 183-195.

Mozley, P. S., Chamberlin, R., Gillentine, J. M., and Lozinsky, R. P., 1992, Petrologic date, in Hydrogoeologic framework of the northern Albuquerque Basin; New Mexico Bureau of Mines and Mineral Resources, Open-File Report 387, pp. IV-1 to IV-17.

Mumpton, F. A., 1960, Clinoptilolite redefined: American Mineralogist, vol. 45, pp. 351-369

Nelson, R. A., Patton, T. L. and Morley, C. K., 1992, Rift-segment interaction and its relation to hydrocarbon exploration in continental rift systems: American Association of Petroleum Geologists Bulletin, vol. 76, no. 8, pp. 1153-1169.

Ogilvie, I. H.,1905, The high-altitude conoplane; a topographic form illustrated in the Ortiz Mountains: American Geologist, vol. 36, pp. 27-34.

Olsen, K. H, Baldridge, W. S., and Callender, J. F., 1987, Rio Grande rift: an overview: Tectonophysics, vol. 143, pp. 119-139.

Osburn, G. R., and Chapin, C. E.,1983, Ash-flow tuffs and cauldrons in the northeast Mogollon-Datil volcanic field: a summary: New Mexico Geological Society Guidebook 34, pp. 197-204.

Pate, C. R., 1989, Assessing the relative importance of compaction processes and cementation to reduction of porosity in sandstones: Discussion: American Association of Petroleum Geologists Bulletin, vol. 73, no. 10, pp. 1270-1273.

Parkhurst, D. L., Thorstenson, D. C., and Plummer, L. N.,1993, PHREEQE: a geochemical reaction model based on an ion-pairing aqueous model, version 2.1: International Ground Water Modeling Center, Colorado School of Mines, Golden, Colorado.

Plas, L. van der, and Tobi, A. C., 1965, A chart for judging the reliability of point counting results: American Journal of Science, vol. 263, pp. 87-90.

Reeves, C. C., Jr., 1978, Economic significance of playa lake deposits, in Matter, A. and Tucker, M. E. (eds.), Modern and ancient lake sediments: International Association of Sedimentologists Special Publication 2, pp. 279-290.

Robert, M. and Berthelin, J., 1986, Role of biological and biochemical factors in soil mineral weathering, in Huang, P. M. and Schnitzer, M. (eds), Interactions of soil minerals with natural organics and microbes: Soil Science Society of America Special Publication No. 17, pp. 453-495.

Robie, R. A., Hemingway, B. S., and Fisher, J. R., 1979, Thermodynamic properties of minerals and related substances at 298.15∞ K and 1 bar pressure and at higher temperatures: U. S. Geological Survey Bulletin 1452.

Rosendahl, B. R., Reynolds, K. J., Lorber, P. M., Burgess, C. F., McGill, J., Scott, D., Lambiase, J. J., and Derksen, S. J., 1986, Structural expressions of rifting: lessons from Lake Tanganyika, Africa, in Frostick, L. E., et al., eds., Sedimentation in the African Rifts: Special Publications of the Geological Society of London 25, pp. 29-43.

Sheppard, R. A. and Gude, A. J., 1968, Distribution and genesis of authigenic silicate minerals in tuffs of Pleistocene Lake Tecopa, Inyo County, California: United States Geological Survey Professional Paper 597, 38p.

Siebert, R. M., Moncure, G. K., and Lahann, R. W., 1984, A theory of framework grain dissolution in sandstones, in McDonald, D. A., and Surdam, R. C., (eds.), Clastic Diagenesis: AAPG Memoir 37, pp. 163-175.

Smith, G. A., Larsen, D., Harlan, S. S., McIntosh, W. C., Erskine, D. W., and Taylor, S., 1991, A tale of two volcaniclastic aprons: field guide to the sedimentology and physical volcanology of the Oligocene Espinaso Formation and Miocene Peralta Tuff, north-central New Mexico, in Julian, B. and Zidek, J. (eds.) Field guide to geologic excursions in New Mexico and adjacent areas of Texas and Colorado: New Mexico Bureau of Mines and Mineral Resources Bulletin 137, pp. 87-103.

Spiegel, Z., and Baldwin, B., 1963, Geology and water resources of the Santa Fe area, New Mexico: United States Geological Survey Water-Supply Paper 1525, 258 pp.

Stevenson, F. J., 1967, Organic Acids in Soils, in McLaren, A. D. and Peterson, G. H. (eds), Soil Biochemistry: Marcel Dekker, Inc., New York, pp. 119-146.

Stevenson, F. J., and Fitch, A., 1986, Chemistry of complexation of metal ions with soil solution organics, in Huang, P. M. and Schnitzer, M. (eds), Interactions of soil minerals with natural organics and microbes: Soil Science Society of America Special Publication No. 17, pp. 29-58.

Sullivan, K. B. and McBride, E. F., 1991, Diagenesis of sandstones at shale contacts and diagenetic heterogeneity, Frio Formation, Texas: AAPG Bulletin, vol. 75 no. 1, pp. 121-138.

Surdam, R. C., Boese, S. W., and Crossey, L. J., 1984, The chemistry of secondary porosity, in McDonald, D. A., and Surdam, R. C., (eds.), Clastic Diagenesis: AAPG Memoir 37, pp. 127-149.

Surdam, R. C., and Sheppard, R. A., 1978, Zeolites in saline, alkaline-lake deposits, in Sand, L. B. and Mumpton, F. A. (eds.), Natural zeolites: occurrence, properties, use: Pergamon Press Ltd., Oxford, pp. 145-174.

Swanson, A. G., 1981, Sample examination manual, American Association of Petroleum Geologists Methods in Exploration Series, Tulsa, Oklahoma.

Tan, K. H., 1986, Degradation of soil minerals by organic acids, in Huang, P. M. and Schnitzer, M. (eds), Interactions of soil minerals with natural organics and microbes: Soil Science Society of America Special Publication No. 17, pp. 1-27.

Tan, K. H., 1980, The release of silicon, aluminum, and potassium during decomposition of soil minerals by humic acid: Soil Science, vol. 129 no. 1, pp. 5-11.

Tedford, R. H, 1981, Mammalian biochronology of the late Cenozoic basins of New Mexico: Geological Society of America Bulletin, Part I, v. 92, pp. 1008–1022.

Tedford, R. H., 1982, Neogene stratigraphy of the northwestern Albuquerque basin: New Mexico Geological Society 33, pp. 273-278.

Thorn, C. R., McAda, D. P., and Kernodle, J. M., 1993, Geohydrologic framework and hydrologic conditions in the Albuquerque Basin, central New Mexico, U.S. Geological Survey, Water-Resources Investigations Report 93-4149, 106 pp.

Tschernich, R. W., 1992, Zeolites of the world: Geoscience Press, Inc. Phoenix, Az., pp. 246-273.

Tucker, M. E., 1982, The field description of sedimentary rocks: Geological Society of London Handbook Series, Open University Press, Buckinghamshire; Halsted Press, New York, 112 p.

Walker, T. R., Waugh, B., and Crone, A. J., 1978, Diagenesis in first-cycle desert alluvium of Cenozoic age, southwestern United States and northwestern Mexico: Geological Society of America Bulletin, vol. 89, pp. 19-32.

Welton, J. E., 1984, SEM petrology atlas: American Association of Petroleum Geologist Methods in Exploration Series, No. 4, variously paginated.

Wilson, M. D., and Pittman, E. D., 1977, Authigenic clays in sandstones: recognition and influence on reservoir properties and paleoenvironmental analysis: Journal of Sedimentary Petrology, vol. 47, no. 1, pp. 3-31.

Woods, T. L. and Garrels, R. M., 1987, Thermodynamic values at low temperature for natural inorganic materials: an uncritical summary: Oxford University Press, New York, variously paginated.

Plate 1. Sidewall core sample from Charles Wells 6 at a depth of 2037 ft. **(A)** Microporosity (mp), lower left and left center, completely fills the space between framework grains (blue coloration is vacuum-impregnated epoxy). Birefringent microlites and sanidine microphenocryst (equant crystal, lower left) suggest microporosity resulted from dissolution of volcanic rock fragment. A coherent grain boundary is no longer evident, further suggesting that authigenic clay is partly responsible for the microporosity seen in thin-section through replacement of framework grains. Poikilitic calcite cement is visible along lower left edge of photo. Framework grains are quartz (Q), carbonate lithoclasts (CRF), and granitic-gneissic rock fragment (GRF). Thin-section photomicrograph, plane-polarized light; scale bar=1mm. **(B)** Same view as 1A under cross-polarized light. **(C)** Coarse surface texture of volcanic tuff fragment produced by framework grain dissolution and precipitation of authigenic clay; skeletal microphenocryst at apex of grain (upper right) is calcic plagioclase (P). Grain in foreground is illite-coated quartz. SEM photomicrograph; scale bar=33.3μm. **(D)** Enlargement of rectangle in Plate 1C showing interconnecting meshwork of authigenic illite/smectite. SEM photomicrograph; scale bar=5μm.

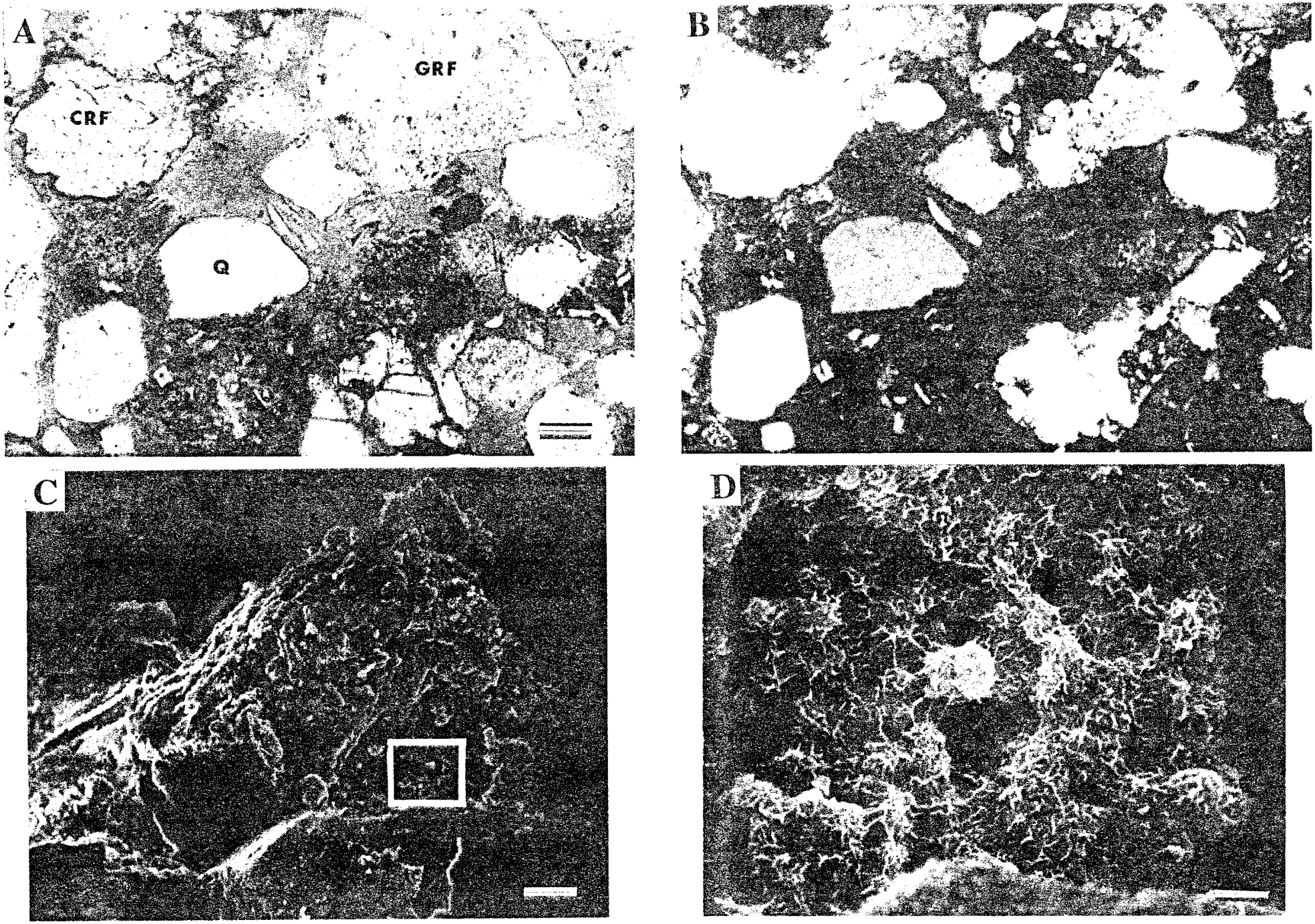
A
GRF
CRF
Q
B
C
D

Plate 2. Sidewall core sample from Charles Wells 5 at a depth of 2510.3 ft. **(A)** Authigenic heulandite (H; small euhedral crystals within intergranular pore spaces) and pore-filling clay (arrows; upper center and lower right). Volcanic rock fragments (VRF; center and right-center) exhibit dissolution microporosity and intrastratal solution of lath-shaped microphenocrysts. Spherulitic devitrification of volcanic glass (gls) at left. Thin-section photomicrograph, plane polarized light; scale bar=1mm. **(B)** Alkali feldspar grain (K) at left with coating of authigenic clay (flakes and discontinuous ribbons standing perpendicular to grain surface). At right is biotite grain (B) ductily deformed about framework grains, also with authigenic clay coating. Heulandite crystals (H) have precipitated on and between both grains. SEM photomicrograph; scale bar=40μm. **(C)** Volcanic glass altered to authigenic clay; relict shards visible upper right. Plagioclase in center field-of-view has undergone extensive framework grain dissolution. SEM photomicrograph; scale bar=33.3μm. **(D)** Enlargement of Plate 2C showing fluted surface of detrital plagioclase, and incipient clay formation between flutes. Dissolution and clay authigenesis within the surrounding glass fragment is credited with the microporosity seen in thin-section, such as in Plate 2A. SEM photomicrograph; scale bar=1000μm.

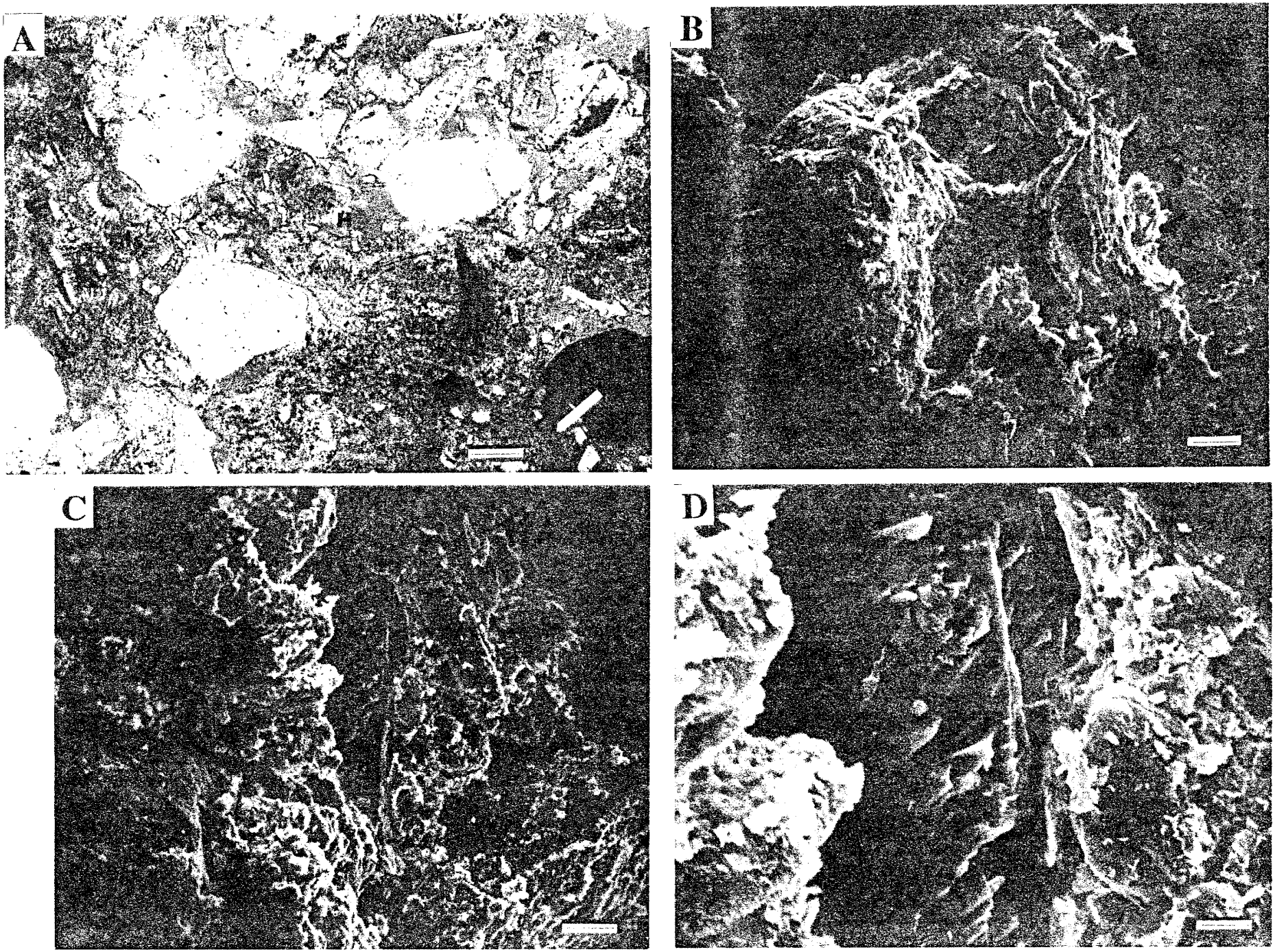
A
B
C
D

Plate 3. Particle morphology of authigenic clay. **(A)** Crenulated ribbons of smectite coating a detrital quartz grain. SEM photomicrograph from Cerro Colorado (1256 ft.); scale bar=5μm. **(B)** Enlarged view of smectite ribbon standing perpendicular to underlying grain surface. SEM photomicrograph from Cerro Colorado (1256 ft.); scale bar=5μm. **(C)** Individual illite flakes, some with characteristic needle-like projections, developed on detrital K-feldspar grain (lower right-hand corner). Crenulated ribbons of smectite or illite-smectite are also visable. SEM photomicrograph from SAF-1 (1590 ft.); scale bar=5μm. **(D)** Fine-textured, webby morphology of smectite developed on detrital grains (quartz at lower right) and progressively coarser crenulated ribbons towards the pore center. SEM photomicrograph from Cerro Colorado (1325 ft.); scale bar=50μm.

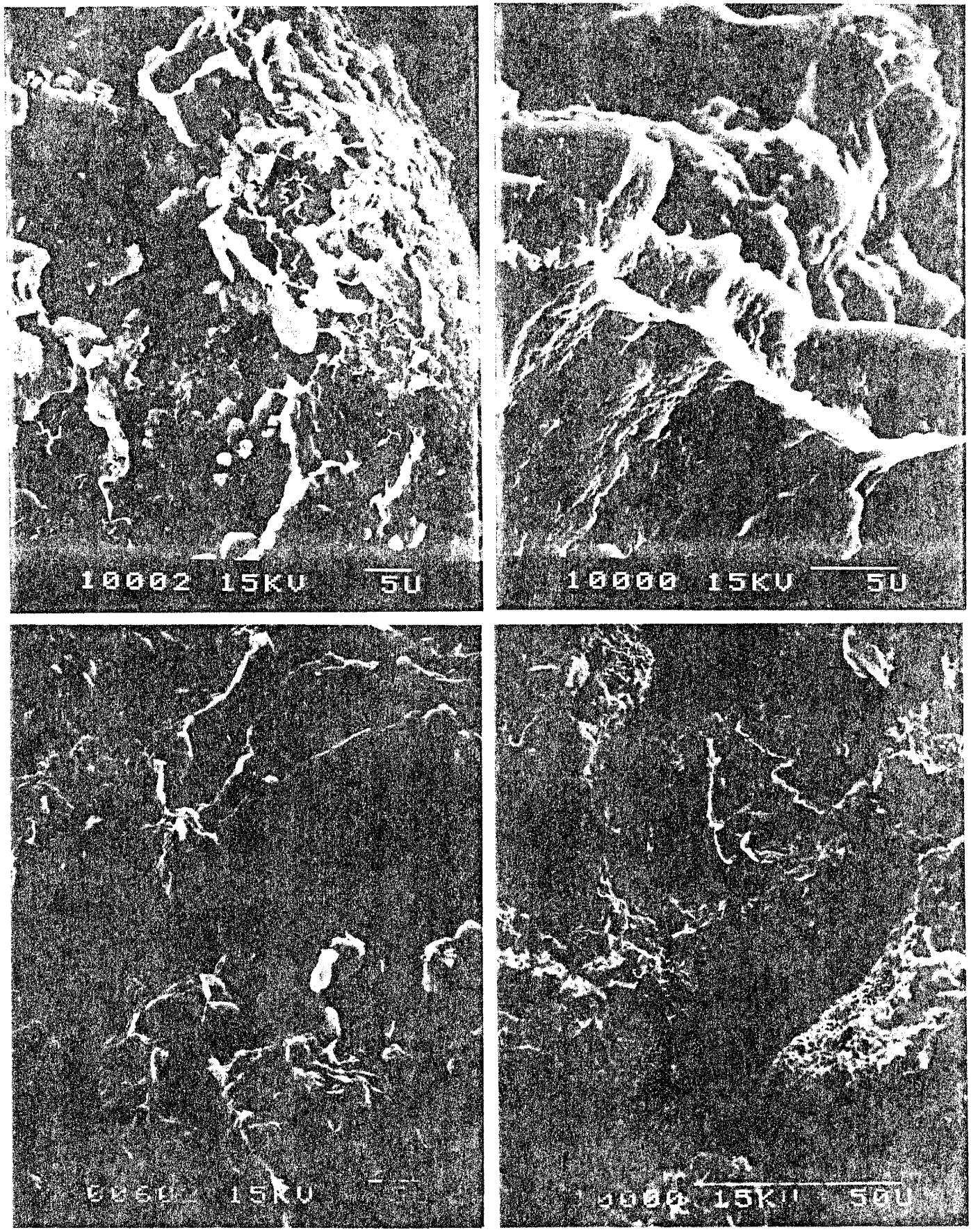
10002 15KV 5U
10000 15KV 5U

Plate 4. Framework grain dissolution and authigenic clay and zeolite precipitation. **(A)** Prismatic crystal habit and c-axis elongation of heulandite (center) on surface of detrital grain from SAF-1 (1440 ft.). Zeolites were found in no other West Mesa samples. SEM photomicrograph; scale bar=5μm. **(B)** Heulandite development within dissolution-etched cavity of K-feldspar grain; framework grain dissolution preceded zeolite precipitation. SEM photomicrograph from Charles Wells 6 (2520 ft.); scale bar=20μm. **(C)** Resorbed calcic plagioclase feldspar encapsulated within a crust of authigenic clay. SEM photomicrograph from Charles Wells 6 (2037 ft.); scale bar=20μm. **(D)** Dissolution and in-situ alteration of framework grain. SEM photomicrograph from Charles Wells 5 (2510.3 ft.); scale bar=20μm.

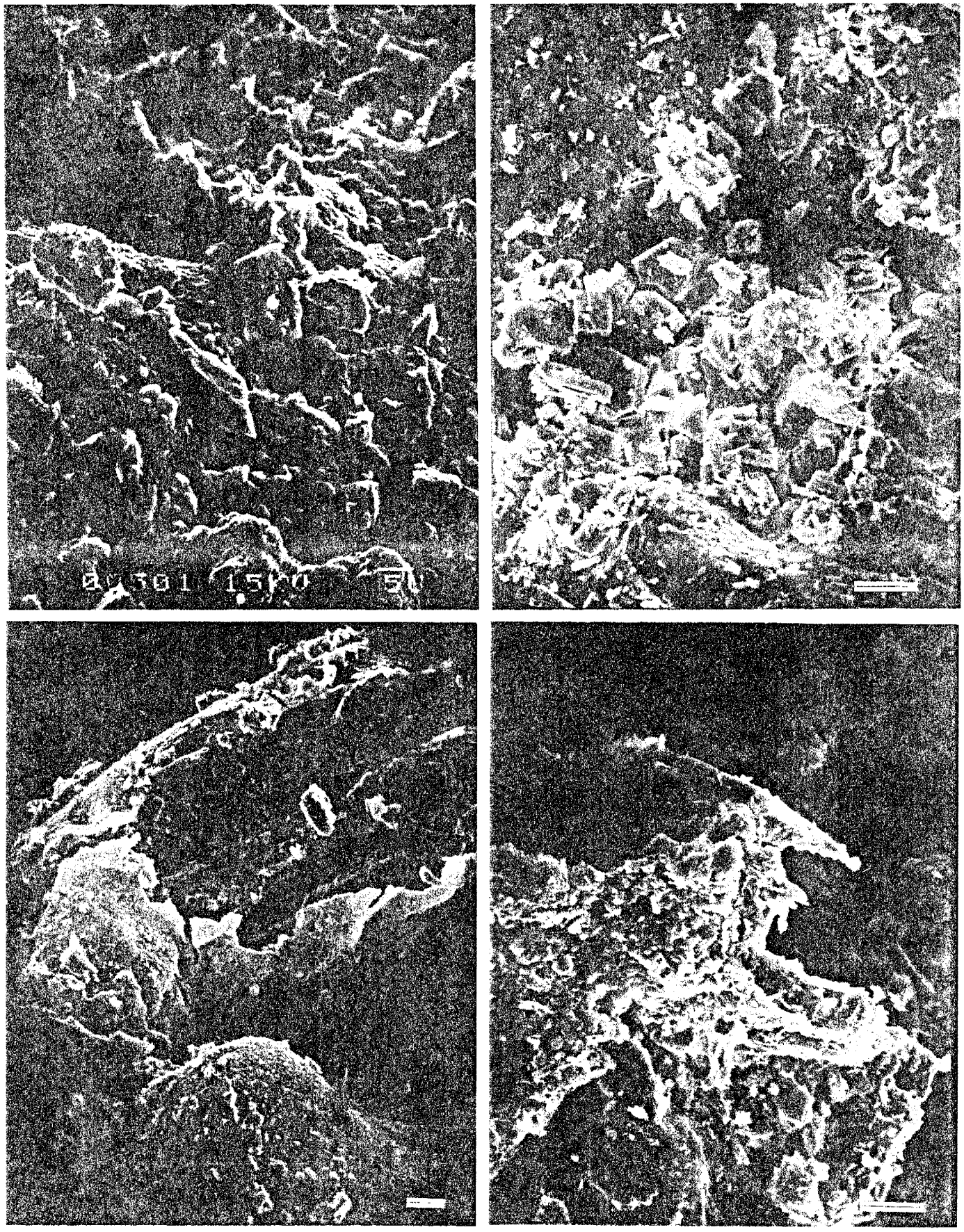

APPENDIX A

Counted Parameters

Framework Grains

Qm: monocrystalline quartz
Qp: polycrystalline quartz
P: monocrystalline plagioclase feldspar
K: monocrystalline alkali feldspar
gn: polymineralic rock fragment of granitic or gneissic origin
Q_v: quartz phenocryst within volcanic rock fragment
P_v: plagioclase phenocryst within volcanic rock fragment
K_v: alkali feldspar phenocryst within volcanic rock fragment
V_g: groundmass of volcanic rock fragment
V_s: fine-grained, siliceous volcanic rock fragment
V_p: pumice or pumiceous volcanic rock fragment
Q_s: quartz within sedimentary rock fragment
Q_c: chert
F_s: feldspar within sedimentary rock fragment
S_m: fine-grained matrix of sandstone or siltstone sedimentary rock fragment
S_c: carbonate rock fragment (limestone)
U: undifferentiated rock fragment

Non-framework Grains

M: biotite, muscovite or chlorite
HM: heavy mineral
Opq: opaque mineral
DC: allogenic (detrital) clay
Cmt: pore-filling mineral growth (zeolite, calcite or phyllosilicate cement)
MP: intergranular macroporosity

Recalculated Parameters

Standard Method

% Q: $(Q_m + Q_p)$/total framework grains
% F: (P + K + gn)/total framework grains
% R: (Qv + Pv + Kv + Vg + Vs + Vp + Qs + Qc + Fs + Sm + Sc + U)/total framework grains
% U: U/total lithic fragments
% V: (Qv + Pv + Kv + Vg + Vs + Vp)/total lithic fragments
% S: (Qs + Qc + Fs + Sm + Sc)/total lithic fragments

Modified Gazzi-Dickinson Method

% Q: (Qm + Qp + Qgn + Qv + Qs + Qc)/total framework grains
% F: (P + K + gn + Pv + Kv + Fs + Fgn)/total framework grains
% L: (Vg + Vs + Vp + Sm + Sc + U)/total framework grains
% U: U/total lithic fragments
% V: (Vg + Vs + Vp)/total lithic fragments
% S: (Sm + Sm + Sc)/total lithic fragments
C/Q: (Qp + Qgn + Qv + Qs + Qc)/Q
P/F: (P + Pv + Ps)/F

Cerro Colorado No. 1

TABLE 1

Counted Parameters

Depth (ft)	Q_m	Q_p	P	K	gn	Q_v	P_v	K_v	V_g	V_s	V_p	Q_s	Q_c	F_s	S_c	S_m	U	M	HM	Opq	DC	Cmt	MP
955	91	22	12	19	11	0	0	0	0	0	0	0	10	0	0	0	32	0	0	0	3	15	85
1065	105	7	20	22	8	0	1	0	3	0	0	1	5	0	0	0	32	0	3	0	18	17	58
1136	108	11	9	22	9	0	0	0	0	0	0	0	7	0	3	0	32	0	1	0	6	8	84
1256	94	18	11	27	7	0	1	0	0	0	3	0	7	0	0	1	41	1	0	0	4	14	71
1325	93	5	10	21	7	0	0	0	0	0	0	0	3	0	0	0	43	1	0	0	34	17	66
1375	94	10	19	24	7	1	0	1	0	0	14	0	14	0	0	9	16	1	0	0	34	6	50
1466	71	7	20	22	4	0	9	3	0	0	73	0	9	0	0	0	24	1	1	0	22	20	14
1495	65	12	13	15	0	1	0	0	0	0	22	0	13	0	0	1	9	2	0	0	96	28	23
1516	1	0	0	0	0	0	7	14	0	0	234	0	0	0	0	0	0	5	0	0	0	0	39
1556	0	0	1	0	0	0	10	1	0	0	94	0	0	3	0	0	1	3	0	0	156	0	31
1575	0	0	0	0	0	0	15	1	0	0	238	0	0	0	0	0	0	3	0	0	0	0	43
1592	0	0	0	0	0	0	9	11	0	0	250	0	0	0	0	0	0	5	0	0	0	0	25
1605	0	0	0	0	0	0	5	5	0	0	244	0	0	0	0	0	0	3	0	0	0	0	43
1626	0	0	0	0	0	0	26	8	0	0	229	0	0	0	0	0	0	3	1	0	0	0	33
1635	0	0	0	0	0	0	18	5	0	0	245	0	0	0	0	16	0	5	0	0	0	0	11

Recalculated Parameters

	Standard Method							Modified Gazzi-Dickinson Method							
Depth (ft)	% Q	% F	% R	% U	% V	% S		%Q	%F	%L	%U	%V	%S	C/Q	P/F
955	57.36	21.32	21.32	76.19	0	23.81		65.48	18.78	15.74	100	0	0	0.29	0.32
1065	54.9	24.51	20.59	76.19	9.52	14.29		59.9	22.77	17.33	91.43	8.57	0	0.13	0.46
1136	59.2	19.9	20.9	76.19	0	23.81		64.18	18.41	17.41	91.43	0	8.57	0.16	0.24
1256	53.33	21.43	25.24	77.36	7.55	15.09		59.52	19.05	21.43	91.11	6.67	2.22	0.25	0.3
1325	53.85	20.88	25.27	93.48	0	6.52		57.69	18.68	23.63	100	0	0	0.11	0.29
1375	49.76	23.92	26.32	29.09	29.09	41.82		57.89	23.44	18.66	41.03	35.9	23.08	0.22	0.39
1466	32.23	19.01	48.76	20.34	72.03	7.63		35.95	23.97	40.08	24.74	75.26	0	0.18	0.5
1495	50.99	18.54	30.46	19.57	50	30.43		60.26	18.54	21.19	28.13	68.75	3.13	0.29	0.46
1516	0.39	0	99.61	0	100	0		0.39	8.2	91.41	0	100	0	0	0.33
1556	0	0.91	99.09	0.92	96.33	2.75		-	-	-	-	-	-		
1575	0	0	100	0	100	0		-	-	-	-	-	-		
1592	0	0	100	0	100	0		-	-	-	-	-	-		
1605	0	0	100	0	100	0		-	-	-	-	-	-		
1626	0	0	100	0	100	0		-	-	-	-	-	-		
1635	0	0	100	0	94.37	5.63		-	-	-	-	-	-		
mean	45.78	18.94	61.17	52.15	76.42	17.18		51.25	19.09	22.6	70.98	49.19	9.25	0.21	0.37
s.d.	18.73	7.05	37.99	34.11	37.41	12.6		20.92	4.69	9.05	33.38	38.15	9.64	0.07	0.09

TABLE 1, cont

Charles Wells 5

Counted Parameters

Depth (ft)	Qm	Qp	P	K	gn	Q_v	P_v	K_v	V_g	V_s	V_p	Q_s	Q_c	F_s	S_c	S_m	U	M	HM	Opq	DC	Cmt	MP
1677	67	5	63	50	1	0	0	0	1	1	0	0	1	0	3	0	13	7	12	7	0	18	51
1789.8	66	13	29	27	21	0	0	0	8	1	1	0	4	0	2	0	4	2	5	2	1	96	18
1804	75	6	38	29	14	0	4	0	27	1	0	0	0	0	2	1	10	4	2	1	0	2	84
1818.2	73	6	41	37	11	0	0	0	7	0	0	0	3	0	0	1	6	4	7	5	13	34	52
1851.4	72	7	49	39	6	0	0	0	11	1	1	0	9	0	0	4	7	0	10	4	6	9	65
2318.2	59	6	35	28	12	0	5	1	45	2	0	1	2	0	6	1	4	2	6	4	10	10	61
2330	80	7	31	22	17	0	1	0	27	3	1	0	4	0	0	3	2	1	2	1	8	31	59
2452.1	103	4	25	36	3	0	0	0	0	0	0	0	6	1	5	1	15	3	7	3	11	9	68
2510.3	47	9	17	16	27	0	0	0	16	4	3	0	1	0	0	1	2	5	0	2	56	71	23
2519.9	83	13	19	25	11	0	0	0	13	8	0	0	10	0	1	3	10	0	4	3	4	71	22
2992.1	76	12	23	17	24	0	3	1	40	5	2	0	2	0	0	1	0	2	7	3	4	50	28
3123.1	69	3	59	34	8	0	2	0	16	1	0	0	3	0	0	0	6	3	8	6	13	47	22
3162.1	82	8	37	17	9	0	1	0	25	0	0	0	4	0	0	0	3	5	1	7	17	72	12
3214.1	74	1	51	40	3	0	0	0	7	1	0	0	4	0	0	0	5	4	7	8	31	51	13

Recalculated Parameters

	Standard Method							Modified Gazzi-Dickinson Method							
Depth (ft)	% Q	% F	% R	% U	% V	% S		% Q	% F	% L	% U	% V	% S	C/Q	P/F
1677	35.12	55.61	9.27	68.42	10.53	21.05		35.44	55.83	8.74	72.22	11.11	16.67	0.08	0.56
1789.8	44.89	43.75	11.36	20	50	30		52.84	38.07	9.09	25	62.5	12.5	0.29	0.43
1804	39.13	39.13	21.74	22.22	71.11	6.67		43.48	36.71	19.81	24.39	68.29	7.32	0.17	0.55
1818.2	42.7	48.11	9.19	35.29	41.18	23.53		45.41	47.03	7.57	42.86	50	7.14	0.13	0.47
1851.4	38.35	45.63	16.02	21.21	39.39	39.39		42.72	45.63	11.65	29.17	54.17	16.67	0.18	0.52
2318.2	31.4	36.23	32.37	5.97	79.1	14.93		33.65	37.98	28.37	6.78	79.66	13.56	0.14	0.51
2330	43.94	35.35	20.71	4.88	78.05	17.07		50	31.82	18.18	5.56	86.11	8.33	0.19	0.51
2452.1	53.77	32.16	14.07	53.57	0	46.43		57.5	32	10.5	71.43	0	28.57	0.1	0.39
2510.3	39.16	41.96	18.88	7.41	85.19	7.41		49.31	31.94	18.75	7.41	88.89	3.7	0.34	0.37
2519.9	48.98	28.06	22.96	22.22	46.67	31.11		56.12	26.02	17.86	28.57	60	11.43	0.25	0.37
2992.1	42.72	31.07	26.21	0	94.44	5.56		50.49	26.21	23.3	0	97.92	2.08	0.27	0.48
3123.1	35.82	50.25	13.93	21.43	67.86	10.71		38.31	50.25	11.44	26.09	73.91	0	0.1	0.6
3162.1	48.39	33.87	17.74	9.09	78.79	12.12		52.15	32.8	15.05	10.71	89.29	0	0.15	0.62
3214.1	40.32	50.54	9.14	29.41	47.06	23.53		43.01	50	6.99	38.46	61.54	0	0.08	0.55
mean	41.76	40.84	17.4	24.7	60.72	20.68		46.46	38.73	14.81	29.9	67.95	11.63	0.18	0.5
s.d.	6.02	8.43	6.95	18.76	23.66	12.54		7.41	9.47	6.45	22.04	22.68	7.39	0.08	0.08

Charles Wells 6

TABLE 1, cont

Counted Parameters

Depth (ft)	Qm	Qp	P	K	gn	Q_v	P_v	K_v	V_g	V_s	V_p	Q_s	Q_c	F_s	S_c	S_m	U	M	HM	Opq	DC	Cmt	MP
2012	38	6	17	7	80	0	3	2	47	22	4	1	2	2	1	3	4	4	10	0	4	31	12
2037	54	8	29	23	12	0	2	0	22	0	3	0	2	0	0	4	34	2	1	1	18	11	74
2195	67	16	33	21	13	0	2	0	19	2	2	0	4	0	0	0	30	2	8	2	2	51	26
2350	73	3	30	17	13	0	0	1	46	6	4	0	2	0	4	2	11	2	2	4	1	40	39
2375	55	11	29	11	15	0	1	0	36	5	1	0	3	0	0	8	8	4	1	6	0	63	43
2520	46	8	19	20	15	0	2	1	44	3	8	0	5	0	2	13	10	4	2	2	4	64	28
3012	37	5	17	27	51	1	1	0	43	22	5	0	2	0	0	11	2	5	1	2	7	24	37
3042	37	3	14	27	17	0	7	0	83	10	12	0	2	0	0	7	5	3	8	11	7	13	34
3083	52	0	17	40	0	0	0	0	0	0	0	0	0	0	7	1	2	2	1	9	165	0	4
3095	88	2	18	29	3	0	0	0	1	0	0	0	3	0	6	0	8	1	3	4	131	0	3
3115	42	15	21	20	21	0	3	0	94	0	3	1	2	0	0	1	5	4	2	1	3	34	28
3195	65	2	47	46	6	0	1	0	14	0	0	0	2	0	7	0	14	4	7	12	1	20	52
3245	53	4	51	27	5	0	2	0	50	0	0	0	2	0	0	0	12	0	2	6	4	42	40

Recalculated Parameters

Standard Method

Modified Gazzi-Dickinson Method

Depth (ft)	% Q	% F	% R	% U	% V	% S		% Q	% F	% L	% U	% V	% S	C/Q	P/F
2012	18.41	43.51	38.08	4.4	85.71	9.89		32.64	33.47	33.89	4.94	90.12	4.94	0.51	0.25
2037	32.12	33.16	34.72	50.75	40.3	8.96		38.34	29.02	32.64	53.97	39.68	6.35	0.27	0.55
2195	39.71	32.06	28.23	50.85	42.37	6.78		44.02	30.62	25.36	56.6	43.4	0	0.27	0.55
2350	35.85	28.3	35.85	14.47	75	10.53		39.15	26.42	34.43	15.07	76.71	8.22	0.12	0.54
2375	36.07	30.05	33.88	12.9	69.35	17.74		43.72	24.59	31.69	13.79	72.41	13.79	0.31	0.67
2520	27.55	27.55	44.9	11.36	65.91	22.73		31.63	27.55	40.82	12.5	68.75	18.75	0.26	0.39
3012	18.75	42.41	38.84	2.3	82.76	14.94		25.45	37.5	37.05	2.41	84.34	13.25	0.35	0.21
3042	17.86	25.89	56.25	3.97	88.89	7.14		21.88	25.89	52.23	4.27	89.74	5.98	0.24	0.36
3083	43.7	47.9	8.4	20	0	80		43.7	47.9	8.4	20	0	80	0	0.3
3095	56.96	31.65	11.39	44.44	5.56	50		59.49	31.01	9.49	53.33	6.67	40	0.06	0.37
3115	25	27.19	47.81	4.59	91.74	3.67		31.14	23.68	45.18	4.85	94.17	0.97	0.41	0.44
3195	32.84	48.53	18.63	36.84	39.47	23.68		33.66	49.01	17.33	40	40	20	0.04	0.48
3245	27.67	40.29	32.04	18.18	78.79	3.03		30.81	41.92	27.27	7.41	92.59	0	0.13	0.64
mean	31.73	35.27	33	21.16	63.82	19.93		36.59	32.97	30.45	22.24	66.55	19.3	0.25	0.44
s.d.	11.17	8.14	13.77	18.19	26.34	21.91		9.76	8.59	12.94	20.88	27.87	22.78	0.14	0.14

SAF No. 1

TABLE 1, cont

Counted Parameters

Depth (ft)	Qm	Qp	P	K	gn	Q_v	P_v	K_v	V_g	V_s	V_p	Q_s	Q_c	F_s	S_c	S_m	U	M	HM	Opq	DC	Cmt	MP
864	94	16	10	69	4	0	0	0	1	0	0	0	17	0	0	2	12	0	1	6	26	0	42
913	117	19	12	38	0	0	0	0	0	0	1	0	10	0	0	0	17	0	0	0	9	7	70
1440	85	10	7	37	0	0	0	0	0	0	0	0	12	0	0	0	32	0	0	0	0	54	63
1590	93	8	33	29	3	0	0	0	1	0	0	0	9	0	2	0	15	0	1	0	36	11	59
1785	103	20	5	28	6	0	0	0	4	0	0	0	22	0	0	0	22	0	0	0	1	0	89
2120	81	7	19	17	2	0	2	0	19	0	9	0	10	0	0	0	13	0	1	0	57	48	15
2203	76	14	5	49	0	0	0	0	5	0	0	0	4	0	0	0	16	0	0	6	0	111	14

Recalculated Parameters

	Standard Method							Modified Gazzi-Dickinson Method							
Depth (ft)	% Q	% F	% R	% U	% V	% S		% Q	% F	% L	% U	% V	% S	C/Q	P/F
864	48.89	36.89	14.22	37.5	3.13	59.38		56.89	36.44	6.67	80	6.67	13.33	0.27	0.12
913	63.55	23.36	13.08	60.71	3.57	35.71		67.91	23.26	8.84	89.47	10.53	0	0.2	0.24
1440	51.91	24.04	24.04	72.73	0	27.27		58.47	24.04	17.49	100	0	0	0.21	0.16
1590	52.33	33.68	13.99	55.56	3.7	40.74		58.55	32.12	9.33	83.33	5.56	11.11	0.18	0.53
1785	58.57	18.57	22.86	45.83	8.33	45.83		70.48	17.14	12.38	84.62	15.38	0	0.3	0.14
2120	49.16	21.23	29.61	24.53	56.6	18.87		54.75	22.35	22.91	31.71	68.29	0	0.17	0.53
2203	53.25	31.95	14.79	64	20	16		55.62	31.95	12.43	76.19	23.81	0	0.19	0.09
mean	53.95	27.1	18.94	51.55	15.89	34.83		60.38	26.76	12.86	77.9	21.71	12.22	0.22	0.26
s.d.	5.31	6.99	6.5	16.65	20.95	15.41		6.22	6.85	5.62	21.75	23.78	1.57	0.05	0.19

Table A-2. Visual estimate in phi units of grain size and sorting from sidewall core plugs. Mean calculated from relation (ø16% + ø50% + ø84%)/3; standard deviation calculated from relation (ø84% - ø16%)/2 (Folk, 1974).

WELL	DEPTH	84% is coarser than	50% is	16% is coarser than	calculated mean	mean equates to	observed mode	calculated std dev	std dev equates to	estimated sorting
CC-1	955	2.00	2.25	0.50	1.58	mL	mL	0.75	moderate	very well
CC-1	1028	3.00	2.25	1.50	2.25	fU	fU	0.75	moderate	very well
CC-1	1065	3.00	2.25	0.50	1.92	mL	fU	1.25	poor	poor
CC-1	1136	2.50	2.25	1.00	1.92	mL	fU	0.75	moderate	very well
CC-1	1256	2.50	2.25	1.00	1.92	mL	mL	0.75	moderate	well
CC-1	1325	3.00	3.25	2.00	2.75	fL	fL	0.50	well-mod	very well
CC-1	1375	2.50	2.25	0.50	1.75	mL	fU-mL	1.00	mod-poor	poor
CC-1	1466	3.00	2.75	2.00	2.58	fL	fL	0.50	well-mod	very well
CC-1	1495	pumice								
CW-5	1677	3.00	3.25	2.50	2.92	fL	vfU	0.25	very well	very well
CW-5	1789.8	3.00	2.25	0.50	1.92	mL	fU	1.25	poor	poor
CW-5	1804	2.50	1.75	0.00	1.42	mU	mL	1.25	poor	poor
CW-5	1818.2	3.00	2.75	1.00	2.25	fU	fL	1.00	mod-poor	moderate
CW-5	1851.4	2.50	2.75	1.00	2.08	fL	fL	0.75	mod	poor
CW-5	2318.2	3.00	1.75	0.00	1.58	mL	fU	1.50	poor	poor
CW-5	2330	3.00	2.25	0.50	1.92	mL	fU	1.25	poor	poor
CW-5	2452.1	3.00	3.25	2.00	2.75	fL	vfU	0.50	well-mod	very well
CW-5	2510.3	2.50	1.75	-1.00	1.08	mU	mL-mU	1.75	poor	poor
CW-5	2519.9	n/a								
CW-5	2558.2	3.00	2.75	1.50	2.42	fU	vfU	0.75	moderate	very well
CW-5	2952.1	3.00	3.75	2.50	3.08	vfU	vfL	0.25	very well	very well
CW-5	2992.1	2.00	1.75	-1.00	0.92	cL	fU-mL	1.50	poor	poor
CW-5	3079.1	mudrock								
CW-5	3123.1	3.00	3.25	1.50	2.58	fL	vfU	0.75	moderate	well
CW-5	3162.1	2.00	1.75	0.00	1.25	mU	fU-mL	1.00	mod-poor	poor
CW-5	3214.1	3.00	3.25	2.00	2.75	fL	vfU	0.50	well-mod	well

Table A-2. Visual estimate in phi units of grain size and sorting from sidewall core plugs. Mean calculated from relation (ø16% + ø50% + ø84%)/3; standard deviation calculated from relation (ø84% - ø16%)/2 (Folk, 1974).

WELL	DEPTH	84% is coarser than	50% is	16% is coarser than	calculated mean	mean equates to	observed mode	calculated std dev	std dev equates to	estimated sorting
CW-6	2012	2.00	0.75	-0.50	0.75	cL	cL	1.25	poor	poor
CW-6	2037	2.00	1.75	0.00	1.25	mU	mL	1.00	mod-poor	moderate
CW-6	2113	mudrock								
CW-6	2195	3.00	1.75	-0.50	1.42	mU	mL	1.75	poor	moderate
CW-6	2350	3.00	2.25	0.50	1.92	mL	mL	1.25	poor	moderate
CW-6	2375	3.00	1.75	0.00	1.58	mL	mU	1.50	poor	moderate
CW-6	2485	mudrock								
CW-6	2570	mudrock								
CW-6	2520	3.00	2.25	0.50	1.92	mL	mL	1.25	poor	poor
CW-6	2870	3.00	3.75	2.00	2.92	fL	vfL	0.50	well-mod	very well
CW-6	3012	3.00	1.75	-1.00	1.25	mU	vfU/mU	2.00	poor-v poor	poor
CW-6	3042	3.00	2.25	0.00	1.75	mL	mL	1.50	poor	poor
CW-6	3083	mudrock								
CW-6	3095	3.00	3.25	1.50	2.58	fL	vfU	0.75	moderate	very well
CW-6	3115	3.00	1.75	0.00	1.58	mL	vfU/mU	1.50	poor	poor
CW-6	3195	3.00	3.25	2.50	2.92	fL	vfU	0.25	very well	very well
CW-6	3245	2.00	2.25	1.00	1.75	mL	fU	0.50	well-mod	moderate
SAF-1	913	n/a								
SAF-1	1440	3.00	2.75	0.50	2.08	fU	fL	1.25	poor	well
SAF-1	1558	3.00	2.75	2.00	2.58	fL	fL	0.50	well-mod	very well
SAF-1	1590	3.00	2.25	0.50	1.92	mL	fU	1.25	poor	moderate
SAF-1	1785	2.50	1.75	0.50	1.58	mL	fU	1.00	mod-poor	moderate
SAF-1	2120	3.00	2.75	1.50	2.42	fU	vfL	0.75	moderate	poor
SAF-1	2203	3.00	2.25	0.50	1.92	mL	mL	1.25	poor	moderate

APPENDIX B

Definitions of Porosity Terms

Total macroporosity: the percentage of each thin-section, based on 300 point-counts, represented by macroporosity (relatively large, open pores impregnated with blue-dyed epoxy).

Intergranular macroporosity: the percentage of pore space, based on 100 point counts, occurring between framework grains that consists of residual primary porosity, oversized pores and through-going fractures.

Residual primary porosity--that fraction of original porosity remaining after precipitation of authigenic minerals.

Oversized pores--pore spaces that are unusually large with respect to surrounding pore space, implying dissolution of framework grains; no grain remnants or relict clay rims are present.

Through-going fracture--epoxy-filled fractures that bisect two or more framework grains.

Intragranular macroporosity: the percentage of pore space, based on 100 point counts, occurring within framework grains that consists of framework grain dissolution and confined fractures.

Framework grain dissolution--includes both pore space within a remnant, identifiable framework grain ("skeletal grain"), and pore space outlined by a remnant grain boundary or relict clay rim ("ghost grain").

Confined fracture--epoxy-filled fracture that does not extend beyond an individual grain.

Intergranular microporosity: the percentage of pore space, based on 100 point counts, occurring between framework grains; diameters of micropores are on the order of several microns, and appear in thin-section as minute sponge-like areas of blue-dyed epoxy.

Clay--microporosity interpreted as resulting from intergranular growths of authigenic clay.

Cement--microporosity interpreted as resulting from intergranular growths of non-clay pore-filling minerals.

Intragranular microporosity: the percentage of pore space, based on 100 point counts, occurring within identifiable framework grains, that is interpreted as the result of framework alteration to a clay product.

Secondary porosity: the percentage of pore space, based on 100 point counts, consisting of the sum of oversized pores, framework grain dissolution, confined fractures and intragranular microporosity. Although intragranular microporosity is equated with the precipitation of secondary minerals (resulting in a solid-phase volume increase), it represents higher porosity relative to the framework grain it replaces, so it is included in this category. Through-going fractures are of uncertain origins, so they are excluded.

Minus-cement porosity: the percentage of each thin-section, based on 300 point-counts, consisting of the sum of intergranular cement (carbonate, zeolite and authigenic clay) and total macroporosity.

Table 1. Porosity distribution within Cerro Colorado 1 cores determined from 100 point counts per sample.

	INTERGRANULAR MACROPOROSITY				INTRAGRANULAR MACROPOROSITY			INTERGRANULAR MICROPOROSITY			INTRA-GRANULAR MICRO-POROSITY	SECNDARY POROSITY
Well Depth (ft)	Primary	Oversize pore	Fracture through-going	Total	Frmwrk grain dissoln	Fracture confined	Total	Clay	Cement	Total	Total	Total
Cerro Colorado												
955	77	15	0	92	1	1	2	3	0	3	3	16
1065	57	2	0	59	10	0	10	11	0	11	20	12
1136	62	10	1	73	8	0	8	2	0	2	17	18
1256	56	13	0	69	10	1	11	0	0	0	20	23
1325	44	4	0	48	16	1	17	9	0	9	26	20
1375	47	4	0	51	16	3	19	11	0	11	19	20
1466	24	0	3	27	4	2	6	45	1	46	21	4
1495	24	0	8	32	8	1	9	40	0	40	19	8

Table 1, cont. Porosity distribution within Charles Wells 5 cores determined from 100 point counts per sample.

	INTERGRANULAR MACROPOROSITY				INTRAGRANULAR MACROPOROSITY			INTERGRANULAR MICROPOROSITY			INTRA-GRANULAR MICRO-POROSITY	SECNDARY POROSITY
Well Depth (ft)	Primary	Oversize pore	Fracture through-going	Total	Frmwrk grain dissoln	Fracture confined	Total	Clay	Cement	Total	Total	Total
Charles Wells 5												
1677	52	0	0	52	5	0	5	6	6	12	31	5
1789.8	19	2	0	21	4	7	11	59	0	59	9	6
1804	52	12	0	64	21	0	21	1	0	1	14	33
1818.2	39	1	1	41	4	0	4	34	2	36	18	5
1851.4	38	1	0	39	10	1	11	23	1	24	26	11
2318.2	38	5	0	43	19	4	23	10	3	13	21	24
2330	45	3	0	48	20	3	23	4	0	4	25	23
2452.1	36	2	1	39	14	0	14	19	0	19	28	16
2510.3	17	4	0	21	7	1	8	15	9	24	47	11
2519.9	43	7	0	50	2	3	5	7	22	29	16	9
2992.1	28	0	0	28	6	3	9	19	22	41	22	6
3123.1	14	0	0	14	8	5	13	29	0	29	44	8
3162.1	5	1	5	11	11	9	20	28	5	33	36	12
3214.1	8	0	2	10	2	2	4	53	0	53	33	2

Table 1, cont. Porosity distribution within Charles Wells 6 cores determined from 100 point counts per sample.

	INTERGRANULAR MACROPOROSITY				INTRAGRANULAR MACROPOROSITY			INTERGRANULAR MICROPOROSITY			INTRA-GRANULAR MICRO-POROSITY	SECNDARY POROSITY
Well Depth (ft)	Primary	Oversize pore	Fracture through-going	Total	Frmwrk grain dissoln	Fracture confined	Total	Clay	Cement	Total	Total	Total
CW 6												
2012	17	1	1	19	19	1	20	6	9	15	46	20
2037	41	9	0	50	27	1	28	6	0	6	16	36
2195	37	4	0	41	9	3	12	0	23	23	24	13
2350	36	0	0	36	14	4	18	1	8	9	37	14
2375	34	1	0	35	6	1	7	0	24	24	34	7
2520	16	0	0	16	7	2	9	0	35	35	40	7
3012	37	0	0	37	12	8	20	5	15	20	23	12
3042	27	6	0	33	19	5	24	0	2	2	41	25
3083	2	2	0	4	19	5	24	48	0	48	24	21
3095	11	1	0	12	22	4	26	42	0	42	20	23
3115	21	0	0	21	13	4	17	0	5	5	57	13
3195	43	3	0	46	11	0	11	14	0	14	29	14
3245	33	1	1	35	13	8	21	10	6	16	28	14

Table 1, cont. Porosity distribution within Soil Amendment Facility 1 cores determined from 100 point counts per sample.

	INTERGRANULAR MACROPOROSITY				INTRAGRANULAR MACROPOROSITY			INTERGRANULAR MICROPOROSITY			INTRA-GRANULAR MICRO-POROSITY	SECNDARY POROSITY
Well Depth (ft)	Primary	Oversize pore	Fracture through-going	Total	Frmwrk grain dissoln	Fracture confined	Total	Clay	Cement	Total	Total	Total
SAF 1												
864	59	0	0	59	4	15	19	10	0	10	12	4
913	70	6	0	76	5	4	9	8	0	8	7	11
1440	59	2	0	61	13	3	16	15	0	15	8	15
1590	33	3	0	36	16	2	18	29	1	30	16	19
1785	70	5	0	75	11	0	11	7	0	7	7	16
2120	16	1	1	18	22	2	24	40	4	44	14	23
2203	22	1	13	36	11	23	34	20	0	20	10	12

Table 2a. Host mineralogy of intragranular macroporosity and microporosity. Skeletal framework grains are interpreted as resulting from dissolution processes, whereas shattered feldspar grains are interpreted as introduced by the coring process. Intragranular microporosity is interpreted as the product of framework grain alteration. Values are number of points counted out of 300 point counts per thin section.

Cerro Colorado 1

depth (ft)	skeletal framework grains					shattered feldspar	intragranular microporosity				
	qtz	plag	kspar	VRF	URF		qtz	plag	kspar	VRF	URF
955	0	0	1	0	0	0	0	0	0	0	0
1065	0	4	0	0	0	0	1	1	0	0	1
1136	0	2	2	0	2	0	2	1	4	0	2
1256	0	4	2	3	9	0	10	4	4	3	15
1325	2	4	0	0	19	0	8	4	1	0	25
1375	2	5	1	0	2	0	1	6	0	3	2
1466	0	11	1	2	0	0	2	5	0	48	0
1495	0	3	0	1	0	0	0	0	0	7	0
1516	0	0	0	0	0	14	1	4	5	73	0
1556	0	3	0	0	0	8	0	0	0	85	0
1575	0	3	0	0	0	10	0	3	0	68	0
1592	0	2	1	0	0	13	0	2	4	128	0
1605	0	1	0	0	0	5	0	0	0	142	0
1626	0	6	1	0	0	0	0	0	0	97	0
1635	0	6	1	0	0	0	0	0	0	96	0
sum	4	54	10	6	32	50	25	30	18	750	45
percent of category	3.77	50.94	9.43	5.66	30.19		2.88	3.46	2.07	86.41	5.18
category total	106					50	868				

Table 2a continued

SAF 1

depth (ft)	skeletal framework grains					shattered feldspar	intragranular microporosity				
	qtz	plag	kspar	VRF	URF		qtz	plag	kspar	VRF	URF
864	1	2	1	0	0	7	0	0	0	0	1
913	0	3	2	0	1	7	0	0	0	0	2
1440	0	0	0	0	0	0	0	0	2	0	1
1590	0	7	5	1	0	0	2	2	0	1	0
1785	0	0	4	0	0	0	1	0	0	0	0
2120	0	0	0	10	0	0	0	0	1	13	0
2203	0	0	0	1	3	18	0	0	0	0	0
sum	1	12	12	12	4	32	3	2	3	14	4
percent of category	2.44	29.27	29.27	29.27	9.76		11.54	7.69	11.54	53.85	15.38
category total					41	32					26

Table 2a continued

Charles Wells 6

depth (ft)	skeletal framework grains					shattered feldspar	intragranular microporosity				
	qtz	plag	kspar	VRF	URF		qtz	plag	kspar	VRF	URF
2012	1	5	0	5	2	0	0	0	0	21	0
2037	0	4	0	1	0	0	2	2	1	19	1
2195	1	3	1	4	0	0	1	0	1	13	2
2350	1	8	3	0	0	0	1	2	1	49	0
2375	0	6	0	6	0	0	0	0	0	28	1
2520	1	2	2	4	0	0	1	0	0	38	0
3012	0	1	0	2	0	0	0	2	0	27	0
3042	0	5	2	0	0	0	0	1	0	50	0
3083	0	2	2	0	0	0	0	0	0	0	0
3095	0	4	2	0	0	0	0	0	5	0	0
3115	0	8	1	0	0	0	1	1	1	60	0
3195	0	13	9	0	0	0	0	4	4	11	0
3245	0	7	3	4	0	0	2	1	0	30	0
sum	4	68	25	26	2	0	8	13	13	346	4
percent of category	3.2	54.4	20	20.8	1.6		2.08	3.39	3.39	90.1	.04
category total					125	0					384

Table 2a continued

Charles Wells 5

depth (ft)	skeletal framework grains					shattered feldspar	intragranular microporosity				
	qtz	plag	kspar	VRF	URF		qtz	plag	kspar	VRF	URF
1677	1	4	11	0	0	0	0	0	0	0	0
1789.8	0	2	1	3	0	3	0		0	0	0
1804	0	6	6	2	0	3	0	0	0	3	0
1818.2	0	7	3	1	0	0	0	1	0	0	0
1851.4	0	3	6	3	0	0	0	0	0	3	0
2318.2	1	5	3	2	0	8	0	0	0	7	0
2330	0	3	3	2	0	0	0	0	0	2	0
2452.1	2	5	4	0	0	0	0	0	0	0	0
2510.3	0	3	2	5	0	0	0	0	0	8	0
2519.9	0	2	1	6	0	0	0	0	0	4	0
2992.1	3	9	4	5	0	7	1	1	1	16	0
3123.1	0	12	10	3	0	8	0	0	0	4	0
3162.1	1	9	1	2	0	2	0	0	0	13	0
3214.1	0	6	8	1	0	0	0	0	0	3	0
sum	8	76	63	35	0	31	1	2	1	63	0
percent of category	4.4	41.76	34.62	19.23	0		1.49	2.99	1.49	94.03	0
category total					182	31					67

Table 2b. Host mineralogy of intragranular pore space: total of all wells.

well	skeletal framework grains					shattered feldspar	intragranular microporosity				
	qtz	plag	kspar	VRF	URF		qtz	plag	kspar	VRF	URF
CC 1	4	54	10	6	32	50	25	30	18	750	45
CW 5	8	76	63	35	0	31	1	2	1	63	0
CW 6	4	68	25	26	2	0	8	13	13	346	4
SAF 1	0	10	11	11	1	7	3	2	3	14	3
sum	16	208	109	78	35	88	37	47	35	1173	52
category total					446	88					1344
percent of category	3.59	46.64	24.44	17.49	7.85	100	2.75	3.50	2.60	87.28	3.87

APPENDIX C

Table C. Abundance and distribution of authigenic mineral cements (pore-filling mineral growths; Dickinson, 1970) determined from 300 point counts per sample. Samples are grouped by prevalent cement, defined as that cement occupying the highest volume of the pre-cement porosity. The percent of pre-cement porosity occupied by each cement is tabulated in the right-hand columns, and the number of points counted for each cement are tabulated in the left-hand columns. Samples with more than one cement in excess of an arbitrary 10% of pre-cement porosity are placed in a two-cement category. Point counts of intergranular and framework microporosity (center columns) are interpreted as dissolution and subsequent alteration of framework aluminosilicates to secondary clay minerals.

well	depth	zeolite	carbonate	inter-granular micro-porosity	framework micro-porosity	inter-granular macro-porosity	pre-cement porosity	%zeo	%clay	$\%CO_3$	litho-facies
UNCEMENTED											
CW 5	1804	2	0	0	3	84	89	2.25	3.37	0.00	3
CW 5	2452.1	1	5	3	0	68	77	1.30	3.90	6.49	9
CW 6	3083	0	0	0	0	4	4	0.00	0.00	0.00	2
SAF 1	864	0	0	0	1	42	43	0.00	2.33	0.00	4
SAF 1	913	0	4	3	2	70	79	0.00	6.33	5.06	4
SAF 1	1785	0	0	0	1	89	90	0.00	1.11	0.00	4
CARBONATE											
CC 1	955	0	14	1	0	85	100	0.00	1.00	14.00	9
CW 5	1677	1	16	1	0	51	69	1.45	1.45	23.19	3
CW 5	1789.8	0	96	0	0	18	114	0.00	0.00	84.21	3
CW 5	1818.2	1	31	2	1	52	87	1.15	3.45	35.63	3
SAF 1	1590	0	10	1	5	59	75	0.00	8.00	13.33	4
SAF 1	2203	0	111	0	0	14	125	0.00	0.00	88.80	4

well	depth	zeolite	carbonate	inter-granular micro-porosity	framework micro-porosity	inter-granular macro-porosity	pre-cement porosity	%zeo	%clay	$\%CO_3$	litho-facies
CLAY ALTERATION											
CC 1	1136	0	0	8	9	84	101	0.00	16.83	0.00	9
CC 1	1256	0	0	14	35	71	120	0.00	40.83	0.00	9
CC 1	1325	0	1	16	38	66	121	0.00	44.63	0.83	9
CC 1	1375	0	0.1	6	15	50	71	0.00	29.54	0.14	9
CC 1	1466	0	0	19	55	14	88	0.00	84.09	0.00	4
CC 1	1495	0	0	28	7	23	58	0.00	60.34	0.00	4
CC 1	1516	0	0	0	73	39	112	0.00	65.18	0.00	4
CC 1	1556	0	0	0	85	31	116	0.00	73.28	0.00	4
CW 5	1851.4	1	1	7	3	65	77	1.30	12.99	1.30	3
CW 5	2318.2	6	1	3	7	61	78	7.69	12.82	1.28	9
CW 6	3095	0	0	0	5	3	8	0.00	62.50	0.00	2
ZEOLITE											
CW 5	2330	24	5	2	2	59	92	26.09	4.35	5.43	9
CW 5	2519.9	66	1	4	4	22	97	68.04	8.25	1.03	9
SAF 1	1440	54	0	0	3	63	120	45.00	2.50	0.00	4
CLAY + CARBONATE											
CC 1	1065	0	8	9	3	58	78	0.00	15.38	10.26	9
CW 5	3162.1	0	52	20	13	12	97	0.00	34.02	53.61	3
CW 5	3214.1	0	24	27	3	13	67	0.00	44.78	35.82	3
CW 6	2037	0.1	10	1	15	74	100	0.10	15.98	9.99	3
CW 6	3195	0	13	7	19	52	91	0.00	28.57	14.29	2
CW 6	3245	0	42	0	33	40	115	0.00	28.70	36.52	2
SAF 1	2120	0	39	9	14	15	77	0.00	29.87	50.65	4

well	depth	zeolite	carbonate	inter-granular micro-porosity	framework micro-porosity	inter-granular macro-porosity	pre-cement porosity	%zeo	%clay	$\%CO_3$	litho-facies
					ZEOLITE + CLAY						
CW 5	2510.3	44	5	22	8	23	102	43.14	29.41	4.90	9
CW 5	2992.1	40	3	7	19	28	97	41.24	26.80	3.09	3
CW 5	3123.1	17	1	29	4	22	73	23.29	45.21	1.37	3
CW 6	2012	22	4	5	8	12	51	43.14	25.49	7.84	3
CW 6	2195	42	1	8	17	26	94	44.68	26.60	1.06	9
CW 6	2350	31	0	9	53	39	132	23.48	46.97	0.00	4
CW 6	2375	61	2	0	29	43	135	45.19	21.48	1.48	4
CW 6	2520	61	2	1	39	28	131	46.56	30.53	1.53	9
CW 6	3012	19	3	2	29	37	90	21.11	34.44	3.33	2
CW 6	3042	12	0	1	51	34	98	12.24	53.06	0.00	2
CW 6	3115	33	0	1	60	28	122	27.05	50.00	0.00	2

APPENDIX D

Table D-1. Chemical composition of representative detrital feldspars from Charles Wells 5; results of analysis by electron microprobe methods against rhyolite glass standard. Elements are omitted from totals column if their concentration is less than the error.

Analysis No. 1, grain 1: Oligoclase feldspar $An_{27.2}$

	Na	Mg	Al	Si	K	Ba	Ca	Ti	Mn	Fe	O	Total
% element	5.552	0.014	12.652	27.878	0.998	0.054	4.010	0.009		0.209	46.832	98.208
error (+/-)	0.047	0.004	0.090	0.133	0.025	0.020	0.083	0.008		0.024		
weight % oxide	7.485	0.024	23.907	59.637	1.202	0.060	5.610	0.015		0.269		98.208
formula	0.660	0.002	1.282	2.713	0.070	0.001	0.273	0.001		0.010	8.000	5.011

Analysis No. 2, grain 1: Oligoclase feldspar $An_{27.5}$

	Na	Mg	Al	Si	K	Ba	Ca	Ti	Mn	Fe	O	Total
% element	5.578	0.012	12.578	28.142	1.030	0.059	4.083			0.213	47.105	98.800
error (+/-)	0.047	0.004	0.089	0.133	0.025	0.020	0.083			0.024		
weight % oxide	7.520	0.020	23.767	60.201	1.240	0.066	5.713			0.274		98.800
formula	0.659	0.001	1.267	2.722	0.072	0.001	0.277			0.010	8.000	5.010

Analysis No. 3, grain 1: Oligoclase-andesine feldspar $An_{30.0}$

	Na	Mg	Al	Si	K	Ba	Ca	Ti	Mn	Fe	O	Total
% element	5.410	0.007	12.526	27.933	0.855	0.074	4.399			0.266	46.866	98.335
error (+/-)	0.046	0.004	0.089	0.133	0.023	0.020	0.086			0.025		
weight % oxide	7.293	0.011	23.669	59.753	1.030	0.083	6.155			0.342		98.336
formula	0.643	0.001	1.268	2.716	0.060	0.001	0.300			0.013	8.000	5.001

Analysis No. 1, grain 2: Alkali feldspar 94.23% K

	Na	Mg	Al	Si	K	Ba	Ca	Ti	Mn	Fe	O	Total
% element	0.385	0.013	9.708	29.539	10.700	0.426		0.016		0.044	44.691	95.523
error (+/-)	0.014	0.003	0.069	0.132	0.075	0.025		0.008		0.020		
weight % oxide	0.519	0.022	18.344	63.190	12.889	0.476		0.026		0.057		95.523
formula	0.048	0.002	1.031	3.012	0.784	0.009		0.001		0.002	8.000	4.888

Analysis No. 2, grain 2: Alkali feldspar 96.63% K

	Na	Mg	Al	Si	K	Ba	Ca	Ti	As	Fe	O	Total
% element	0.248		9.611	29.632	12.205	0.444			0.018		44.946	97.104
error (+/-)	0.012		0.068	0.132	0.080	0.025			0.012			
weight % oxide	0.334		18.160	63.388	14.703	0.496			0.023			97.104
formula	0.031		1.014	3.004	0.889	0.009			0.001		8.000	4.948

Analysis No. 1, grain 3: Alkali feldspar 95.92% K

	Na	Mg	Al	Si	K	Ba	Ca	Cl	Mn	Fe	O	Total
% element	0.245		9.574	30.172	9.692	0.206		0.027			44.981	94.898
error (+/-)	0.012		0.068	0.133	0.072	0.023		0.011				
weight % oxide	0.331		18.090	64.545	11.675	0.230		0.027				94.898
formula	0.030		1.010	3.057	0.705	0.004		0.002			8.000	4.809

Analysis No. 2, grain 3: Alkali feldspar 86.63% K

	Na	Mg	Al	Si	K	Ba	Ca	Ti	Mn	Fe	O	Total
% element	0.956		9.693	30.252	10.567	0.278				0.096	45.640	97.483
error (+/-)	0.020		0.069	0.134	0.075	0.024				0.022		
weight % oxide	1.288		18.315	64.716	12.729	0.311				0.124		97.483
formula	0.117		1.008	3.020	0.758	0.006				0.005	8.000	4.913

Analysis No. 1, grain 4: Alkali feldspar 96.86% K

	Na	Mg	Al	Si	K	Ba	Ca	Ti	As	Fe	O	Total
% element	0.231		9.657	29.938	11.945	0.219			0.017	0.058	45.268	97.332
error (+/-)	0.012		0.069	0.132	0.079	0.023			0.012	0.021		
weight % oxide	0.311		18.247	64.044	14.389	0.244			0.022	0.075		97.332
formula	0.028		1.012	3.014	0.864	0.005			0.001	0.003	8.000	4.926

Analysis No. 1, grain 5: Oligoclase feldspar $An_{15.9}$ (fresh area)

	Na	Mg	Al	Si	K	Ba	Ca	Ti	Mn	Fe	O	Total
% element	6.546		11.606	30.766	0.057		2.162			0.057	48.541	99.735
error (+/-)	0.050		0.082	0.138	0.010		0.067			0.021		
weight % oxide	8.824		21.929	65.814	0.069		3.025			0.074		99.735
formula	0.751		1.134	2.888	0.004		0.142			0.003	8.000	4.922

Analysis No. 2, grain 5: Oligoclase feldspar $An_{11.5}$ (cloudy interior)

	Na	Mg	Al	Si	K	Ba	Ca	Ti	Mn	Fe	O	Total
% element	6.754	0.009	10.993	30.740	0.060		1.525		0.020	0.524	47.931	98.557
error (+/-)	0.051	0.004	0.078	0.138	0.010		0.060		0.016	0.031		
weight % oxide	9.105	0.015	20.772	65.759	0.072		2.134		0.026	0.674		98.557
formula	0.785	0.001	1.088	2.922	0.004		0.102		0.001	0.025	8.000	4.928

Analysis No. 1, grain 6: Groundmass of volcanic rock fragment

	Na	Mg	Al	Si	K	Ba	Ca	Ti	Cl	Fe	O	Total
% element	1.608	0.009	7.050	31.979	7.010	0.076	0.095	0.078	0.021	0.331	51.744	100.000
error (+/-)	0.026	0.004	0.050	0.134	0.061	0.020	0.054	0.009	0.010	0.026		
weight % oxide	2.168	0.015	13.321	68.410	8.444	0.085	0.133	0.130	0.021	0.426		93.151
formula	0.025	0.000	0.093	0.406	0.064	0.000	0.001	0.001	0.000	0.002	1.153	0.592

Analysis No. 2, grain 6: Groundmass of volcanic rock fragment

	Na	Mg	Al	Si	K	Ba	Ca	Ti	Cl	Fe	O	Total
% element	1.979	0.013	7.217	31.759	6.767	0.055	0.107	0.061	0.036	0.287	51.718	100.000
error (+/-)	0.029	0.04	0.052	0.134	0.060	0.019	0.054	0.009	0.011	0.025		
weight % oxide	2.668	0.022	13.637	67.939	8.152	0.061	0.150	0.103	0.036	0.369		93.136
formula	0.031	0.000	0.095	0.403	0.062	0.000	0.001	0.000	0.000	0.002	1.153	0.595

Table D-2. Chemical composition of representative clay samples from Charles Wells 5; results of analysis by electron microprobe methods against biotite standard. Mineral formulas are calculated on an anhydrous basis of eleven oxygen atoms. Elements are omitted from totals column if their concentration is less than the error.

Analysis No. 1: $(Na_{.44}K_{.22}Ca_{.12})(Al_{1.16}Fe_{.11}Mg_{.06})Si_{4.33}O_{11}$

	Na	Mg	Al	Si	K	Ba	Ca	Ti	Mn	Fe	O	Total
% element	1.767	.235	5.427	21.132	1.521		.839	.058		1.047	30.617	62.585
error (+/-)	.056	.044	.072	.123	.063		.059	.068		.120		
weight % oxide	2.381	.390	10.254	45.206	1.832		1.174			1.347		62.585
formula	.442	.056	1.156	4.325	.224		.120			.108	11.00	6.430

Analysis No. 2: $(Ca_{.10}K_{.08})(Al_{.90}Mg_{.54}Fe_{.44}Ti.03)Si_{4.23}O_{11}$

	Na	Mg	Al	Si	K	Ba	Ca	Ti	Mn	Fe	O	Total
% element	.045	1.299	2.398	11.740	.306		.385	.162		2.397	17.374	36.061
error (+/-)	.044	.047	.058	.094	.046		.048	.061		.149		
weight % oxide		2.153	4.531	25.115	.368		.539	.270		3.084		36.061
formula		.541	.900	4.234	.079		.097	.034		.435	11.00	6.321

Analysis No. 3: $(Ca_{.62}Na_{.57}K_{.06})(Al_{1.46}Mg_{.03}Fe_{.09})Si_{3.54}Al_{.46}O_{11}$

	Na	Mg	Al	Si	K	Ba	Ca	Ti	Mn	Fe	O	Total
% element	2.585	.138	10.234	19.752	.445		4.923	.130		.953	34.924	73.954
error (+/-)	.060	.046	.091	.125	.053		.096	.068		.124		
weight % oxide	3.485	.229	19.338	42.252	.536		6.889			1.226		73.954
formula	.567	.029	1.912	3.544	.057		.619			.086	11.00	6.813

Analysis No. 4: $(K_{.08}Ca_{.02})(Al_{.41}Mg_{.06}Fe_{.11}Ti.29)Si_{4.78}O_{11}$

	Na	Mg	Al	Si	K	Ba	Ca	Ti	Mn	Fe	O	Total
% element	.041	.399	3.004	36.306	.884		.218	3.762		1.606	47.537	93.717
error (+/-)	.049	.043	.064	.152	.059		.055	.119		.149		
weight % oxide		.661	5.677	77.667	1.065		.305	6.275		2.066		93.717
formula		.061	.412	4.785	.084		.020	.291		.106	11.00	5.760

Analysis No. 5: $(K_{.64}Na_{.56}Ca_{.09})(Al_{1.49}Fe_{.05})Si_{4.02}O_{11}$

	Na	Mg	Al	Si	K	Ba	Ca	Ti	Mn	Fe	O	Total
% element	2.325	.015	7.234	20.373	4.515		.641	.121		.461	31.765	67.315
error (+/-)	.061	.045	.080	.124	.089		.062	.068		.103		
weight % oxide	3.134		13.670	43.582	5.439		.897			.593		67.315
formula	.560		1.486	4.019	.640		.089			.046	11.00	6.839

Table D-3. Chemical compositions of representative zeolite samples from Charles Wells 5; results of analysis by electron microprobe methods against rhyolite glass standard.

Analysis No. 1: $(Ca_{.55}Mg_{.20}Na_{.07}K_{.04}Ba_{.02}Fe_{.01})Al_{1.98}Si_{7.10}O_{18}$

	Na	Mg	Al	Si	K	Ba	Ca	Ti	Mn	Fe	O	Total
% element	.269		9.429	29.178	12.808	.327		.029		.117	44.432	96.588
std dev	.012		.067	.131	.082	.024		.009		.022		
weight % oxide	.362		17.816	62.417	15.429	.366		.048		.150		96.588
formula	.076		2.265	6.733	2.123	.015		.004		.014	18.00	11.230
Ca + Sr + Ba/Na + K:			5.153									
Si + Al:			9.081									

Analysis No. 2: $(Ca_{.60}Mg_{.17}Na_{.08}K_{.04}Ba_{.02})Al_{2.09}Si_{7.01}O_{18}$

	Na	Mg	Al	Si	K	Ba	Ca	Ti	Mn	Fe	O	Total
% element	.251	.559	7.447	26.035	.179	.375	3.201				38.098	76.145
std dev	.012	.009	.053	.123	.013	.024	.076					
weight % oxide	.338	.928	14.072	55.694	.215	.419	4.478					76.145
formula	.083	.174	2.087	7.007	.035	.021	.604				18.00	10.009
Ca + Sr + Ba/Na + K:			5.297									
Si + Al:			9.094									

Analysis No. 3: $(Ca_{.54}Mg_{.17}K_{.03}Na_{.03}Ba_{.02})Al_{1.95}Si_{7.16}O_{18}$

	Na	Mg	Al	Si	K	Ba	Ca	Ti	Mn	Fe	O	Total
% element	.080	.574	7.417	28.275	.163	.396	3.018	.012		.021	40.513	80.490
std dev	.008	.009	.053	.128	.012	.024	.076	.008		.019		
weight % oxide	.108	.952	14.015	60.487	.196	.442	4.223	.021		.027		80.490
formula	.025	.168	1.954	7.156	.030	.020	.535	.002		.003	18.00	9.896

Ca + Sr + Ba/Na + K: 10.091

Si + Al: 9.110

Analysis No. 4: $(Ca_{.57}Mg_{.17}Na_{.06}K_{.04}Ba_{.03}Fe_{.01})Al_{2.05}Si_{7.05}O_{18}$

	Na	Mg	Al	Si	K	Ba	Ca	Ti	Mn	Fe	O	Total
% element	.192	.606	8.155	29.256	.214	.586	3.380	.012	.019	.057	42.539	85.015
std dev	.010	.009	.058	.131	.013	.026	.076	.008	.016	.020		
weight % oxide	.259	1.005	15.410	62.583	.257	.654	4.729	.020	.025	.073		85.015
formula	.057	.169	2.046	7.051	.037	.029	.571	.002	.002	.007	18.00	9.971

Ca + Sr + Ba/Na + K: 6.383

Si + Al: 9.097

Analysis No. 5: $(Ca_{.56}Mg_{.18}K_{.06}Na_{.05}Ba_{.02})Al_{2.04}Si7_{.07}O_{18}$

	Na	Mg	Al	Si	K	Ba	Ca	Ti	Mn	Fe	O	Total
% element	.150	.630	7.821	28.272	.307	.296	3.207				41.009	81.690
std dev	.010	.009	.056	.128	.015	.023	.075					
weight % oxide	.202	1.045	14.779	60.479	.369	.330	4.487					81.690
formula	.046	.182	2.036	7.068	.055	.015	.562				81.690	9.964

Ca + Sr + Ba/Na + K: 5.713

Si + Al: 9.104

Table 4. Pore-fluid composition, saturation state and mineral mass transfer in the K_2O-Na_2O-CaO system upon equilibration with authigenic mineral phases: results of geochemical simulation using PHREEQE (Parkhurst et al., 1993) and water quality data supplied by Albuquerque Water Utilities Division. Thermodynamic data for clays from Woods and Garrels (1987) and for zeolites from Johnson et al. (1985). Upper-case letters identify the reaction path that allows each phase to enter the system.

CHARLES WELLS 6

Trial No.		Equilibrium Mineral Phase	Saturation Index + supersaturation - undersaturation					Mass µmol/kg H_2O + dissolution - precipitation					Solution Chemistry			
			heulandite	Ca-smectite	Na-smectite	illite	calcite	heulandite	Ca-smectite	Na-smectite	illite	calcite	pH	alk (10^{-3})	I (10^{-3})	oligoclase dissolved/kg H_2O (mol)
1		initial solution	11.2033	5.3706	4.6332	4.0120	0.2894						7.675	1.856	9.0	0.0
2		heulandite	0.0	-7.6630	-8.4004	-8.8532	0.2894	-0.7415					7.6751	1.85	9.0	0.0
3		Ca-smectite	6.5958	0.0	-0.7375	-1.2849	0.2952		-0.6333				7.6806	1.85	9.0	0.0
4		Na-smectite	7.2288	0.7375	0.0	-0.5569	0.2952			-0.6299			7.6806	1.85	9.0	0.0
5		illite	7.7124	1.3049	0.5674	0.0	0.2929				-0.6331		7.6784	1.85	9.0	0.0
6		calcite	11.1945	5.8720	5.1358	4.3109	0.0					-64.726	7.4197	1.72	8.9	0.0
7		Ca-smec/heul	0.0	0.0	-0.7351	-1.5949	-0.4008	-138.128	+118.107				7.0492	1.615	8.7	0.0
8		Na-smec/heul	0.0	0.7307	0.0	-0.8591	-0.4119	-140.203		+120.356			7.0422	1.615	8.7	0.0
9	A	illite/heul	0.0	1.2405	0.5060	0.0	-0.2134	-139.726			+123.803		7.2189	1.728	8.8	0.0
10		calcite/heul	0.0	-7.1512	-7.8874	-8.5441	0.0	-0.74153				-64.680	7.4197	1.720	8.9	0.0
11		illite/Ca-smec	8.2117	0.0	-0.7333	0.0	1.3621		-376.896		+381.205		8.7988	2.150	9.1	0.0
12		Na-smec/Ca-smec	4.1333	0.0	0.0	-0.7312	-2.6216		-1.867E+4	+1.867E+4			7.7516	1.850	6.3	0.0
13		calcite/Ca-smec	6.1475	0.0	-0.7362	-1.4850	0.0		-0.6346			+65.7749	7.4200	1.720	8.9	0.0
14		illite/Na-smec	7.9668	0.7409	0.0	0.0	0.7650			-117.053	+117.953		8.1493	1.943	9.1	0.0
15		calcite/Na-smec	6.7795	0.7362	0.0	-0.7583	0.0			-0.6325		-65.774	7.4200	1.719	8.9	0.0
16		calcite/illite	7.4403	1.5059	0.7697	0.0	0.0				-0.6361	-65.347	7.4199	1.720	8.9	0.0
17		Ca-smec/Na-smec/heul	0.0	0.0	0.0	-1.1152	-3.3189	-1.201E+2	-1.795E+4	+1.805E+4			7.1242	1.645	6.1	0.0
18		Ca-smec/illite/heul	0.0	0.0	-0.7315	0.0	+0.9623	-143.491	-379.170		+527.868		8.3833	2.155	9.0	0.0
19		Ca-smec/heul/calcte	0.0	0.0	-0.7380	-1.3340	0.0	-139.974	+120.045			+141.111	7.3683	1.897	9.0	0.0
20		illte/heul/calc	0.0	1.0959	0.3601	0.0	0.0	-141.075			+126.233	+66.921	7.3945	1.871	9.0	0.0
21		illte/heul/calc/Ca-smec	0.0	0.0	-0.6966	0.0	0.0	-92.703	-1.515E+3		+1.618E+3	-1.036E+3	7.9512	0.899	7.0	0.0
22		Nasm/heu/calc/Casm/il	0.0	0.0	0.0	0.0	0.0	-496.981	-3.3615E+4	+3.4529E+4	-120.589	+2.9734E+3	9.6587	9.555	12.1	0.0
23	B	calcte/heul/Ca-smec	0.0	0.0	-0.7380	-1.3340	0.0	-139.974	+120.045			+141.111	7.3683	1.897	9.1	0.0
24		Ca-smec/heul/calcte	0.0	0.0	-0.7046	-1.2704	0.0	-230.773	0.0			+2.972	7.4384	1.733	8.7	7.718E-5
25		Na-smec/heul/calcte	0.0	0.7036	0.0	-0.5561	0.0	-236.527		0.0		2.959	7.4389	1.748	8.7	7.976E-5
26		illte/heul/calcite	0.0	1.2511	0.5492	0.0	0.0	-246.796			0.0	+2.8878	7.4397	1.785	8.7	8.473E-5
27	C	Nasm/Casm/heu/calc	0.0	0.0	0.0	1.2743	0.0	-6.228E+3	-581.215	0.0		+93.484	10.1591	25.30	13.6	3.228E-3
28	D	illte/Ca-smec/heul/calc	0.0	0.0	-0.4880	0.0	0.0	-1.102E+3	-894.679		0.0	-1.644E+3	8.8771	0.987	5.6	7.466E-4
		Nasm/il/Casm/heu/calc	0.0	0.0	0.0	0.0	0.0	-6.235E+3	-507.694	0.0	-124.347	+73.199	10.1566	25.11	13.5	3.243E-3

Table 4, continued.

CERRO COLORADO 1

Trial No.		Equilibrium Mineral Phase	Saturation Index + supersaturation - undersaturation					Mass µmol/kg H_2O + dissolution - precipitation					Solution Chemistry			
			heulandtite	Ca-smectite	Na-smectite	illite	calcite	heulandite	Ca-smectite	Na-smectite	illite	calcite	pH	alk (10^{-3})	I (10^{-3})	oligoclase dissolved per kg H_2O (mol)
		initial solution	10.1107	5.3816	4.9559	4.0161	-0.2638						7.180	3.094	18.4	0.0
1	A	heulandite	0.0	-6.3833	-6.8090	-7.5969	-0.2640	-0.7421					7.180	3.095	18.4	0.0
2		calcite	10.1494	4.9967	4.5658	3.7868	0.0					+126.539	7.3815	3.354	18.7	0.0
3		Ca-smectite	5.4886	0.0	-0.4257	-1.2948	-0.2621		-0.6338				7.1816	3.096	18.4	0.0
4		illite	6.6146	1.3128	0.8870	0.0	-0.2628				-0.6337		7.1809	3.096	18.4	0.0
5		Na-smectite	5.8541	0.4257	0.0	-0.8746	-0.2621			-0.6322			7.1816	3.096	18.4	0.0
6		heul/Ca-smec	0.0	0.0	-0.4188	-1.3660	-0.6507	-180.045	+154.103				6.8772	2.789	18.0	0.0
7		heul/calcite	0.0	-6.8136	-7.2444	-7.8709	0.0	-0.7420				+126.621	7.3817	3.348	18.6	0.0
8		Ca-smec/heul/calcte	0.0	0.0	-0.4350	-1.0047	0.0	-184.759	+158.923			+391.323	7.3304	3.569	18.9	0.0
9		Ca-smec/heul/calcte	0.0	0.0	-0.4172	-0.9163	0.0	-305.648	0.0			+18.195	7.4249	3.396	18.6	1.024E-4
10		Na-smec/heul/calcte	0.0	0.4169	0.0	-0.4927	0.0	-310.797		0.0		+18.430	7.4256	3.411	18.6	1.047E-4
11		illte/heul/calcite	0.0	0.9013	0.4849	0.0	0.0	-321.338			0.0	+18.869	7.4269	3.447	18.6	1.097E-4
12	B	illte/Ca-smec/heul/calc	0.0	0.0	-0.2564	0.0	0.0	-888.508	-694.275		0.0	-1.106E+3	8.3957	2.751	17.4	5.752E-4
13	C	Nasm/il/Casm/heu/calc	0.0	0.0	0.0	0.0	0.0	-3.497E+3	-545.602	0.0	-382.764	-103.575	9.6707	14.57	22.4	1.936E-3

SOIL AMENDMENT FACILITY 1

Trial No.		Equilibrium Mineral Phase	Saturation Index + supersaturation - undersaturation					Mass µmol/kg H_2O + dissolution - precipitation					Solution Chemistry			
			heulandite	Ca-smectite	Na-smectite	illite	calcite	heulandite	Ca-smectite	Na-smectite	illite	calcite	pH	alk (10^{-3})	I (10^{-3})	oligoclase dissolved per kg H_2O (mol)
		initial solution	8.9366	3.0945	2.6739	2.1637	-0.0040						8.2730	1.541	8.5	0.0
1	A	heulandite	0.0	-7.2949	-7.7155	-8.0903	-0.0034	-0.7416					8.2742	1.541	8.5	0.0
2		calcite	8.9363	3.0872	2.6665	2.1591	0.0					+0.4618	8.2765	1.548	8.5	0.0
3		Ca-smectite	6.2875	0.0	-0.4206	-0.8830	0.0057		-0.6058				8.2829	1.543	8.5	0.0
4		illite	7.0542	0.8997	0.4791	0.0	0.0017				-0.5697		8.2788	1.542	8.5	0.0
5		Na-smectite	6.6485	0.4207	0.0	-0.4680	0.0055			-0.5899			8.2826	1.543	8.5	0.0
6		heul/Ca-smec	0.0	0.0	-0.4068	-1.5306	-1.1505	-105.071	+89.824				7.2449	1.364	8.3	0.0
7		heul/calcite	0.0	-7.3009	-7.7215	-8.0938	0.0	-0.7416				+0.3931	8.2773	1.542	8.5	0.0
8		Ca-smec/heul/calcte	0.0	0.0	-0.4330	-0.8010	0.0	-116.875	+107.248			+190.524	8.1525	1.778	8.7	0.0
9		Ca-smec/heul/calcte	0.0	0.0	-0.3876	-0.5442	0.0	-221.042	0.0			+0.8635	8.4261	1.706	8.5	8.046E-5
10		Na-smec/heul/calcte	0.0	0.3806	0.0	-0.1315	0.0	-268.567		0.0		+3.501	8.4537	1.899	8.5	1.041E-4
11		illte/heul/calcite	0.0	0.4959	0.1191	0.0	0.0	-293.831			0.0	+5.020	8.4689	2.002	8.6	1.167E-4
12	B	illte/Ca-smec/heul/calc	0.0	0.0	-0.2864	0.0	0.0	-485.600	-99.619		0.0	-116.778	9.0008	2.424	8.6	2.387E-4
13		Nasm/il/Casm/heu/calc	0.0	0.0	0.0	0.0	0.0	-4.138E+3	+141.404	0.0	-102.375	+1.612E+3	9.9864	20.54	16.3	2.027E-3
14		Nasm/Casm/heu/calc	0.0	0.0	0.0	0.9227	0.0	-4.135E+3	+80.244	0.0		+1.630E+3	9.9892	20.71	16.3	2.017E-3